AD-A040 671 PENNSYLVANIA STATE UNIV UNIVERSITY PARK APPLIED RESE--ETC F/G 21/5
THE DESIGN AND EVALUATION OF SCREENS TO PROVIDE MULTI-CYCLE 20%--ETC(U)
JAN 74 E P BRUCE N00017-73-C-1418
UNCLASSIFIED TM-74-16 NL

1 OF 1
AD
A040671

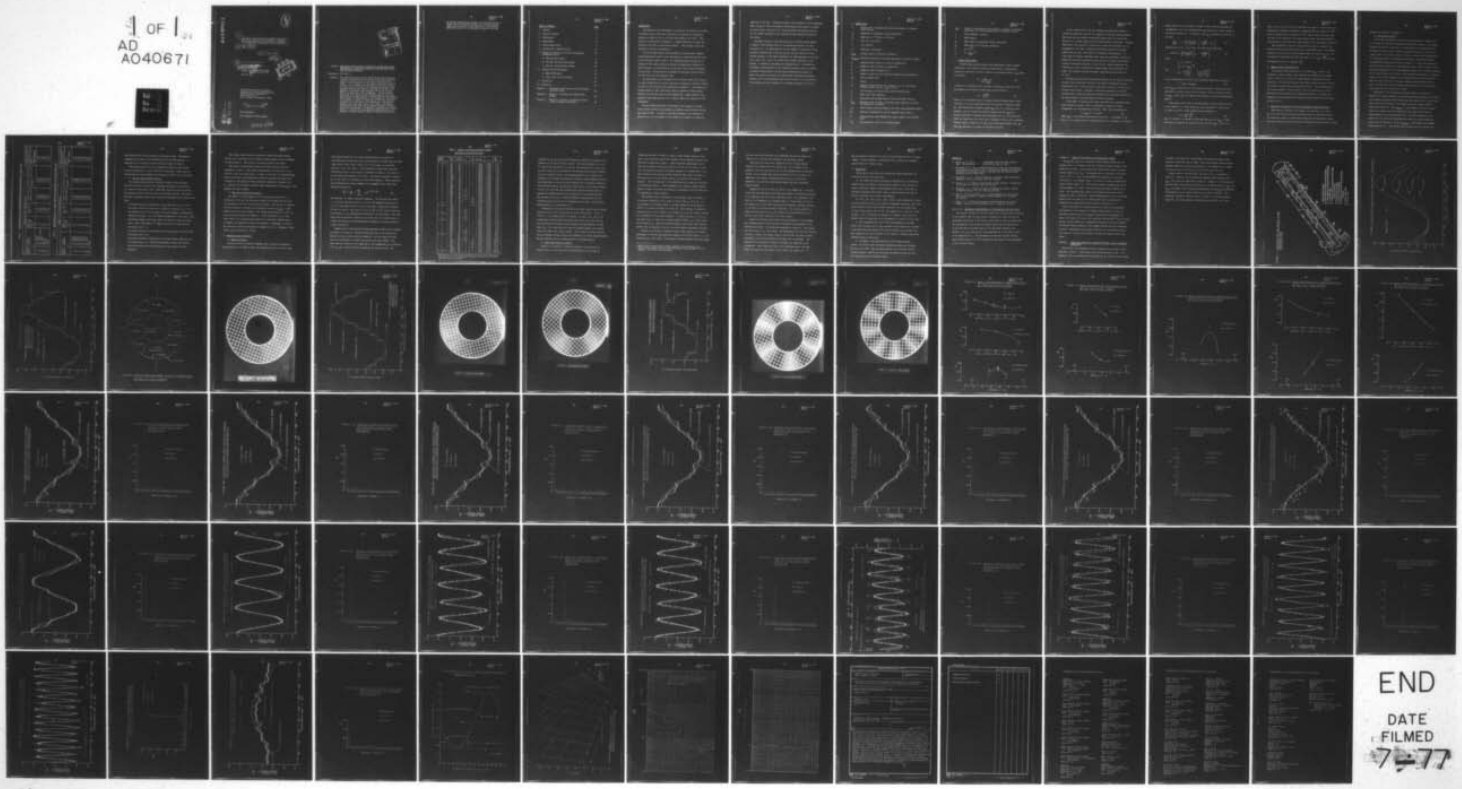

END
DATE FILMED
7-77

(9) Technical Memorandum

THE DESIGN AND EVALUATION OF SCREENS TO PROVIDE MULTI-CYCLE 20% AMPLITUDE SINUSOIDAL VARIATIONS IN THE AFRF ROTOR INLET AXIAL VELOCITY COMPONENT.

(10) Edgar P. Bruce

(11) 8 Jan 74

(12) 78 p.

(14) File No. TM-74-16

January 8, 1974

Contract No. N00017-73-C-1418

(15)

Copy No. 47

The Pennsylvania State University
Institute for Science and Engineering
APPLIED RESEARCH LABORATORY
Post Office Box 30
State College, Pennsylvania 16801

NAVY DEPARTMENT

NAVAL ORDNANCE SYSTEMS COMMAND

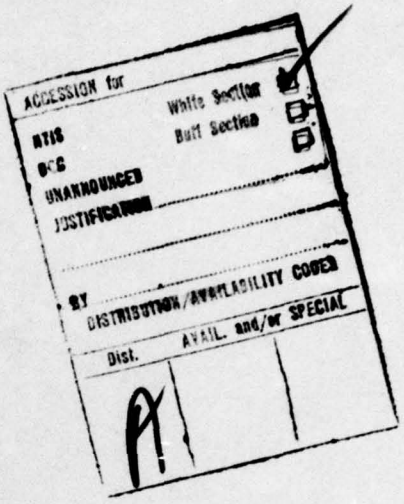

Subject: The Design and Evaluation of Screens to Provide Multi-Cycle 20% Amplitude Sinusoidal Variations in the AFRF Rotor Inlet Axial Velocity Component

References: See Page 21

Abstract: This memorandum describes the results of an effort initiated in April 1973 whose objective was to provide new disturbance producing screens for use in the Axial Flow Research Fan (AFRF). The performance of the screens originally developed for use in this facility was characterized by the generation of axial velocity profiles whose maximum and minimum values differed from the mean value by approximately 6% and by the presence of harmonics whose amplitude was on the order of 20% of the amplitude of the fundamental. The new screens were designed to produce axial velocity profiles with variations about the mean value of $\pm$ 20% and care was exercised in the selection of materials and in the assembly of the screens in an attempt to reduce the amplitude of the other harmonics relative to the amplitude of the fundamental. Results are presented for one-, two-, four-, six-, nine-, and fifteen-cycle screens which show that the design objectives were met to within a few percent. In addition, appendices are included which: 1) describe the performance characteristics of the original one-cycle screen, 2) define a modified approach and

the design characteristics adopted to permit fabrication of twelve- and fifteen-cycle screens, and 3) contain design charts that are useful in the selection of the screening materials required in a development program of this type.

TABLE OF CONTENTS

INTRODUCTION

The purpose of this memorandum is to describe the results of an effort initiated in April 1973 whose objective was to provide new disturbance producing screens for use in the Axial Flow Research Fan (AFRF). This facility is described in Reference 1. A sketch depicting the major components of the AFRF is presented as Figure 1. The original screens are described in detail in Reference 2.

All of the AFRF screens were fabricated by placing screen segments having preselected levels of flow resistance in a prescribed pattern over a low resistance support screen. The circumferentially varying loss in pressure at the screen produces a smoothed circumferential variation in total pressure, or axial velocity, at the rotor inlet station downstream of the screen. The screens can be mounted at any axial position between the test rotor and the bellmouth inlet.

The performance characteristics of the original screens were similar, in terms of magnitude of velocity variation and quality of harmonic content, to those of the one-cycle screen described in Appendix 1. The maximum and minimum values of rotor inlet axial velocity produced by these screens differed from the mean value by approximately 6%. Higher harmonics were generated whose amplitude was on the order of 20% of the amplitude of the fundamental.

The new screens described in this report were designed to produce axial velocity profiles whose maximum and minimum values differed from the mean value by 20%. In addition, care was exercised in the selection of materials and in the assembly of the screens in an attempt to reduce the

amplitude of the other harmonics relative to the amplitude of the fundamental. These changes in screen performance characteristics were desired to enhance the level and the spectrum of the force and moment fluctuations produced on rotor blades operating in the spatially varying flowfield produced by the screens.

This memo contains a brief description of the screen design method, a summary of the characteristics of the screening available for use or purchased for use in fabrication of the new screens, a description of the resistance patterns used in the new screens, and the results of a test program conducted in the AFRF to determine the characteristics of the one-, two-, four-, six-, nine-, and fifteen-cycle screens developed in this program. In addition, appendices are presented which: 1) describe the performance characteristics of the originial one-cycle screen; 2) define a modified design approach and the design characteristics adopted to permit fabrication of twelve- and fifteen-cycle disturbance generating screens, and 3) contain design charts that are useful in the selection of the screening materials required in a development program of this type.

4. NOMENCLATURE

A	Design ratio of maximum axial velocity increment to reference axial velocity
A_f	Magnitude of fundamental Fourier coefficient
A_n	Magnitude of n^{th} Fourier coefficient
c	Grid loss coefficient
d	Wire diameter
K	Resistance coefficient
K_{MIN}	Minimum value of resistance coefficient
$K_{OVERLAY}$	Resistance coefficient increment associated with overlay segment
m	Spacing between centers of wires in a square grid
M	Number of wires per inch in a square grid
n	Summation index in Equation (8)
N	Number of cycles of axial velocity variation per circumference
Δp	Static pressure loss
r	Radius
Re	Reynolds number based on wire diameter d and the intersitial velocity through the grid, $V_{REF.}\ d/(1-s)\nu$
s	Grid solidity, the ratio of open area to blocked area
V	Rotor inlet axial velocity
$\bar{V}$	Circumferential average value of rotor inlet axial velocity
V_{REF}	Reference axial velocity, the uniform axial velocity at a point far upstream of the screen.
x_G	Axial distance from the screen to the rotor inlet measuring station
γ_o	Function in Equations (4) and (5) dependent upon A and X_o
θ	Circumferential angle measured in a plane normal to the facility axis
$\Delta\theta$	Circumferential extent of an overlay segment

θ_{MAX}	Value of θ associated with one-cycle of variation in resistance coefficient for screens having values of N greater than one
ν	Fluid kinematic viscosity
ρ	Fluid density
ϕ_f	Phase angle of fundemental Fourier coefficient
ϕ_n	Phase angle of n^{th} Fourier coefficient
X	$(1 + K)^{1/2}$
X_o	$(1 + K_{MIN})^{1/2}$

5. SCREEN DESIGN METHOD

A fluid stream passing through a grid experiences a loss in static pressure Δp. This pressure drop may be described by a dimensionless resistance coefficient K which is based on the upstream velocity V_{REF} normal to the grid,

$$K = \frac{\Delta p}{(1/2)\rho V_{REF}^2} \qquad (1)$$

A number of investigators (e.g. Weighardt, Reference 3) have found that grid geometry and resistance coefficient may be related by

$$K = \frac{c\,s}{(1-s)^2} \qquad (2)$$

where s is the solidity ratio of the grid (ratio of blocked area to open area) and c is a loss coefficient which is a function of Reynolds number Re. The characteristic Reynolds number $V_{REF}\, d/(1-s)\nu$ is based on wire diameter d and the intersitial velocity through the grid $V_{REF}/(1-s)$. Cornell (Reference 4) analyzed grid performance data for Re $\lesssim$ 20,000 and found for square mesh wire grids that c initially decreased with increasing Reynolds number, leveled off at about 0.80 in the range $600 < Re < 4000$, and then rose gradually to a value of 1.00 at Re $\approx$ 15,000.

In the construction of the one- through nine-cycle AFRF screens an overlay technique was used; that is, segments of wire grid having different mesh sizes and wire diameters were placed side-by-side in a prescribed pattern over a single support screen of low resistance coefficient. McCarthy (Reference 5) has reported the results of a series of experiments for an arrangement of this type. McCarthy's experiments covered the Reynolds number range $600 < Re < 5000$ based on the overlay screen geometry. He found that the combined resistance coefficient was accurately predicted by adding the individual resistance coefficients of the support and overlay screens as predicted using Eqn. (2) with c=0.78. These experiments were conducted in a water tunnel using a support screen with a solidity s of 0.267. The measured combined resistance coefficients varied from 0.80 to 17.00.

McCarthy also developed an analytical solution for the steady, moderately sheared, three-dimensional flow past a wire grid of arbitrary resistance distribution which is placed normal to the axis of a duct of arbitrary but constant cross section. McCarthy's formulation represents an extension of those given by Owen and Zienkiewicz (Reference 6) and Elder (Reference 7) for weakly sheared, two-dimensional flow past wire grids.

In the AFRF, the desired rotor inlet flow field has a spatially fixed axial velocity component V that is independent of radius and varies sinusoidally with circumferential position. Thus V may be expressed as

$$V = V_{REF} (1 + A \sin N\theta) \qquad (3)$$

where V_{REF} is the uniform axial velocity in the duct far upstream of the grid, A is the design ratio of maximum axial velocity increment to reference

axial velocity, N is the number of cycles of axial velocity variation per circumference, and θ is circumferential angle measured in a plane normal to the facility centerline. In terms of V and V_{REF}, McCarthy's solution is of the form

$$\frac{V}{V_{REF}} = 1 - \frac{1.02\,(1 + X)}{(1 - X^3)^{2/3}} \left[\frac{1 + 6X^3}{6X^2} - \gamma_o \right] \qquad (4)$$

Substitution of Eqn. (3) into Eqn. (4) leads to the expression

$$A \sin N\theta = \frac{1.02\,(1 + X)}{(1 + X^3)^{2/3}} \left[\gamma_o - \frac{1 + 6X^3}{6X^2} \right] \qquad (5)$$

where

$$X = (1 + K)^{1/2}$$

$$X_o = (1 + K_{MIN})^{1/2}$$

and

$$\gamma_o = \frac{1 + 6X_o^3}{6\,X_o^2} + \frac{A\,(1 + X_o^3)^{2/3}}{1.02\,(1 + X_o)}$$

At any circumferential position, the resistance coefficient is given by

$$K = K_{MIN} + K_{OVERLAY} \qquad (6)$$

where K_{MIN} is associated with the large wire diameter, large spacing grid selected as a support screen for the assembly. Thus for selected values of K_{MIN}, A and N, Eqn. (5) defines the variation of K with circumferential angle θ.

The support screen used in the AFRF screens is made of brass and has a wire diameter d of 0.135 inches and a wire spacing m of 1.015 inches. In terms of d and m, screen solidity may be expressed as

$$s = 2\left[\frac{d}{m}\right] - \left[\frac{d}{m}\right]^2 \qquad (7)$$

Thus s = 0.248 for the support screen, and from Eqn. (2), $K_{MIN} = 0.343$. The results yielded by the solution of Eqn. (5) with $K_{MIN} = 0.343$, N = 1

and A = 0.05, 0.10, 0.15 and 0.20 are shown in Figure 2. In all cases, the variation of resistance coefficient is characterized by a peak at $\theta = 270^{o}$ that is sharper than the valley at $\theta = 90^{o}$. This is due to the fact that the flow in the vicinity of the screen tends to curve away from regions of high resistance coefficient and toward regions of low resistance coefficient.

The information presented in Figure 2 is all that is required from McCarthy's solution for the construction of the AFRF screens. The required variation of K with θ for screens having values of N other than N = 1 can be obtained by replotting the data from Figure 1 with $\theta_{MAX} = \frac{360^{o}}{N}$ and with intermediate values of θ replaced by $\frac{\theta}{N}$.

6. OVERLAY SCREEN CHARACTERISTICS

To construct AFRF screens with A = 0.20 and $K_{MIN} = 0.343$, it was necessary to select overlay screen segments which subdivided the region from K = 0.343 to K = 1.591 in a finite number of approximately equal increments. The characteristics of the screens available for use as overlay screens in April 1973 are presented in Table 1. The characteristics of screens purchased in May and June of 1973 are summarized in Table 2. The AFRF screens described in the following sections of this memo were constructed using combinations of overlay screens taken from the listings in Table 1 and 2.

7. DESIGN AND FABRICATION OF THE NEW DISTURBANCE GENERATING SCREENS

The procedure followed in the design of the new one-, two-, four-, six-, and nine-cycle disturbance generating screens is described herein. Two additional screens, a twelve-cycle screen and a fifteen-cycle screen, have been designed and fabricated using a slightly different approach. These

screens are described in Appendix 2.

a) The One-Cycle Screen

This screen was designed using the results presented in Figure 2 for A = 0.20 and the overlay screen materials described in Table 1. The design problem is reduced at this point to a determination of the angular extent of segments having levels of combined resistance coefficient, Table 1, of 0.343, 0.484, 0.713, 1.201, 1.329, or 1.746 to provide a good representation of the design variation of resistance coefficient. The selected overlay circumferential dimensions are shown in Figure 3. A full-scale drawing of the type shown in Figure 4 was then made and copied. Note in Figure 4 that the radial dimensions of the overlay segments differ from the radial dimensions of the support screen by 0.10 inch. This provides for clearance to eliminate damage to the overlay segments due to scraping against the facility walls. Full size paper patterns of the overlay segments were obtained from the print. The required number of overlay segments were then cut from screen stock using the paper patterns as a guide.

Fabrication of the disturbance producing screen was initiated by centering the support grid/hub - and outer-casing ring assembly over the full-size drawing and marking with drafting tape the position of the radial lines which define the boundaries of the segment having the highest combined resistance coefficient. The $K_{OVERLAY} = 1.403$ segment was then positioned within this annular sector and fastened to the support screen using a minimum amount of thin tinned copper wire. The grid assembly was then placed over the full-size drawing and the radial lines which define the outer radial boundaries of the two $K_{OVERLAY} = 0.986$ segments were marked using drafting tape. This process was continued until all segments had

TABLE 1. CHARACTERISTICS OF SCREEN COMBINATIONS AVAILABLE FOR USE IN APRIL 1973

OVERLAY SCREEN CHARACTERISTICS						Combined Resistance Coefficient of Support and Overlay Screens $K=K_{MIN}+K_{OVERLAY}$
Screen Number	Screen Material	Number of Wires per inch (M) in^{-1}	Wire Diameter (d) in.	Solidity (s) $s=2(Md)-(Md)^2$	Resistance Coefficient $K_{OVERLAY}=0.78s/(1-s)^2$	
1	St. Steel	2	0.035	0.135	0.141	0.484
6	St. Steel	4	0.035	0.260	0.370	0.713
9	St. Steel & Brass	8	0.028	0.398	0.858	1.201
10	St. Steel	12	0.020	0.422	0.986	1.329
13	Bronze	10	0.028	0.482	1.403	1.746
14	Bronze	6	0.047	0.484	1.419	1.762
15	Brass	12	0.028	0.559	2.248	2.591

TABLE 2. CHARACTERISTICS OF SCREEN COMBINATIONS PURCHASED IN MAY AND JUNE 1973

OVERLAY SCREEN CHARACTERISTICS						Combined Resistance Coefficient of Support and Overlay Screens $K=K_{MIN}+K_{OVERLAY}$
Screen Number	Screen Material	Number of Wires per inch (M) in^{-1}	Wire Diameter (d) in.	Solidity (s) $s=2(Md)-(Md)^2$	Resistance Coefficient $K_{OVERLAY}=0.78s/(1-s)^2$	
2	Al. Alloy	10	0.008	0.154	0.168	0.511
3	St. Steel	10	0.010	0.190	0.226	0.569
4	St. Steel	4	0.028	0.211	0.264	0.607
5	St. Steel	6	0.023	0.257	0.363	0.706
7	St. Steel	8	0.023	0.334	0.587	0.930
8	St. Steel	10	0.020	0.360	0.685	1.028
9	St. Steel	8	0.028	0.398	0.858	1.201
10	St. Steel	12	0.020	0.422	0.986	1.329
11	St. Steel	16	0.016	0.446	1.133	1.476
12	Brass	20	0.0135	0.467	1.283	1.626

been positioned and firmly secured to the support screen. This general procedure was followed in the fabrication of all the AFRF screens. A photograph of the resulting one-cycle screen is shown in Figure 5.

The overlay segments for this disturbance producing screen contain wires with diameters of 0.020, 0.028, and 0.035-inches. These wires are strong enough to resist damage during handling if normal care is exercised.

b) The Two- and Four-Cycle Screens

The overlay screen materials described in Table 2 were purchased after the one-cycle screen had been designed, fabricated, and subjected to a series of preliminary tests. These tests showed that the new screen was producing results that were close to the design objective. The charts presented in Appendix 3 were used in selecting additional overlay screens that would:

1) provide resistance coefficients in the range from 0.100 to 0.300 with large values of M (mesh size or number of wires per inch). This was necessary since as N increases, the overlay segment circumferential dimension decreases. When this dimension approaches m (Note that $m = \frac{1}{M}$) the overlay segment falls apart while it is being cut from the screen stock. Thus Screen Number 1 of Table 1 was not well suited for use in screens with $N > 1$.

2) provide resistance coefficients in the range between 0.370 and 0.858 with large values of M.

3) provide resistance coefficients in the range between 0.986 and 1.403 with large values of M. These screens permit a closer match between the grid resistance and the design value in the region of maximum resistance.

The overlay screen materials described in Table 2 are all suitable for use in the fabrication of the grids of concern herein with the exception of Screen Number 2. This screen is too weak to hold its own shape.

The overlay characteristics selected for the two-cycle screen are presented in Figure 6. This overlay screen pattern was also used in fabrication of the four-cycle screen. However, in this case the circumferential extent of the individual segments was reduced to one-half the value shown in Figure 6. Photographs of these screens are presented in Figures 7 and 8. Care must be exercised in handling these screens since the $K_{OVERLAY} = 0.226$ segments are easily damaged.

c) The Six-aand Nine-Cycle Screens

The number of overlay segments and the resistance pattern used in fabrication of the six- and nine-cycle screens were changed from that used in fabrication of the two- and four-cycle screens. This was done to simplify the grid fabrication problem and to eliminate the use of $K_{OVERLAY} = 0.226$ segments which are easily damaged. The overlay characteristics for the six-cycle screen are presented in Figure 9. In the fabrication of the nine-cycle screen, the circumferential extent of the individual segments shown in Figure 9 was reduced by a factor of two-thirds. Photographs of the six- and nine-cycle screens are presented in Figures 10 and 11. Handling of these screens has not presented a problem.

8. MEASURED SCREEN PERFORMANCE

a) Basic Performance

During the period from May to December 1973, a series of experiments were conducted in the AFRF to define the characteristics of the rotor inlet

flow fields produced by the screens described above as a function of circumferential average rotor inlet axial velocity $\bar{V}$, distance from the rotor inlet station (Probe Insert Station 1-D) to the screen x_G, and radial position at the rotor inlet r. The conditions at which these tests were conducted and some of the results are presented in Table 3. The value of r at the annulus mid-radius is 7.75 inches. The results presented in Table 3 are in the form of a coefficient A_f and a phase angle θ_f. These quantities were determined from Fourier analysis of the measured rotor inlet axial velocity expressed as

$$\frac{V}{\bar{V}} = \frac{A_o}{2} + \sum_{n=1}^{\infty} A_n e^{i(N\theta + \phi_n)} \qquad (8)$$

The subscript f in Table 3 denotes fundamental. For the one-cycle screen f = 1, for the two-cycle screen f = 2, etc. The summation was carried to n = 25 in most cases and to n = 30 in a few cases. Results were compared for one run (Run No. 109) with n = 9, 12, 15, 18, 21, 24, and 25—there was no difference in the corresponding coefficients and phase angles. The phase angle data as presented in Table 3 is of little use in this memo except as a means of checking for consistancy among runs made with a given screen at a given time period.

Summary plots which describe the data presented in Table 3 are presented as Figures 12 through 16. Identical scales are used on the ordinate and abscissa on these curves except for Figure 16. In this figure the scale used for the ordinate is one-half that used in the other figures. The plots show the variation of the magnitude of the fundamental A_f as a function of $\bar{V}$, x_G, and r within the limits imposed by the available data. The

TABLE 3. SUMMARY OF TEST PROGRAM CONDUCTED TO DEFINE FLOW FIELDS PRODUCED BY AFRF SCREENS

Type of Screen	Date of Test	Run Number*	r in.	x_G in.	$\bar{V}$ ft/sec.	A_f	ϕ_f Deg.
1 - cycle	9/7	104	7.75	55.6	43.55	0.1814	-2.00
	9/7	105			43.65	0.1816	-1.54
	5/1	55			43.74	0.1808	0.51
	9/7	106			57.16	0.1789	-1.71
	5/1	56			57.35	0.1778	1.34
	9/7	107			65.68	0.1770	-1.89
	5/2	60			66.46	0.1759	0.49
	5/1	57			66.56	0.1741	1.39
	7/13	79			69.81	0.1738	1.71
	7/13	77			78.25	0.1720	2.13
	9/7	108			78.76	0.1751	-1.42
	5/2	58			79.21	0.1746	1.24
	9/4	98			79.25	0.1762	0.07
	5/3	61			79.40	0.1743	1.20
	7/13	80			87.11	0.1721	2.18
	8/30	96			95.79	0.1746	-0.85
	9/4	97			96.16	0.1738	0.12
	5/3	64	6.75		78.57	0.1667	0.63
	8/30	94			78.86	0.1725	-3.35
	5/3	65			79.20	0.1708	0.44
	5/3	63	8.75		78.96	0.1641	1.41
	5/3	62			79.76	0.1686	-0.49
	5/4	68	7.75	30.5	79.37	0.1868	0.45
	5/4	69			80.28	0.1853	0.02
	5/3	66		12.5	78.18	0.1884	-4.56
	5/3	67			78.44	0.1878	-4.65
2 - cycle	7/10	70		55.6	64.98	0.2093	-4.27
	7/12	73			77.70	0.1986	-3.93
	7/12	74			78.36	0.1980	-3.84
	8/29	93	6.75		78.68	0.2058	-3.30
	8/29	92	8.75		78.22	0.1971	-3.79
4 - cycle	7/12	76	7.75		78.23	0.2221	-2.41
	7/12	75			78.32	0.2100	-3.49
	8/29	90	6.75		78.71	0.2031	-5.82
	8/29	91	8.75		77.44	0.1942	-2.74
6 - cycle	8/24	81	7.75		42.81	0.1847	-1.52
	8/24	82			56.59	0.1774	-2.31
	8/24	83			64.89	0.1753	-1.40
	8/24	85			77.61	0.1685	-4.26
	8/24	84			78.36	0.1724	-2.01
	8/27	86			89.21	0.1685	-0.81
	8/27	87			90.51	0.1714	-1.29
	8/29	89	6.75		78.44	0.1566	-6.07
	8/28	88	8.75		76.96	0.1859	-3.19
9 - cycle	9/6	100	7.75		79.47	0.1195	86.41
	9/6	101			79.81	0.1191	86.87
	9/7	103	6.75		78.52	0.1004	79.53
	9/6	102	8.75		77.87	0.1449	87.73
	11/12	114	7.75	30.0	77.18	0.1611	165.39
	11/9	113			77.68	0.1619	165.36
	11/7	111		21.9	77.41	0.1779	160.70
	11/9	112			77.48	0.1773	160.23
	10/25	110		12.4	77.52	0.1964	171.85
	10/25	109			77.63	0.1967	171.71
15 - cycle	12/12	116			79.94	0.1702	285.33
	12/11	115			80.08	0.1725	288.25

*The assistance of Albert Hinger in conducting Run Numbers 55 through 58, and 61 through 69, and of Fred Eisenhuth in conducting Run Numbers 109 through 114 is gratefully acknowledged.

variation of A_1, A_2, and A_6 with $\bar{V}$ exhibits a trend that is similar to the variation of K with Re found by Cornell. Thus the dependence of A_f upon $\bar{V}$ is due to the dependence of K upon Re. The variation of A_1 and A_9 with x_G, which shows that A_f decreases as the distance from the grid increases, is due to turbulent mixing. The characteristics of the turbulence are different in the regions downstream of different overlay segments--thus the flow downstream of the grid is quite complex from a turbulence standpoint. The more rapid decay of A_9 relative to the decay of A_1 with axial distance is due to the fact that the circumferential distance between regions of maximum and minimum velocity is much smaller for the nine-cycle screen. The variation of A_f with r exhibits different characteristics for the different screens and can not be explained at this point. In the screen design method, A_f is independent of r.

Examination of Figures 12 through 16 and Table 3 shows that the design objective of $A_f = 0.20$ has been met to within a few percent. For $A_f = 0.20$ at r = 7.75 inches with $\bar{V}$ = 80 ft/sec., the one-, six-, nine-, and fifteen-cycle screens should be placed close to the rotor inlet and the two- and four-cycle screens should be placed just downstream of the AFRF inlet (x_G = 55.6 inches when the screen is inserted against the upstream side of the AFRF inlet support struts). The different locations required for the different screens reflects the differences in design characteristics and the different levels of succeptibility to turbulent mixing.

b) Rotor Inlet Velocity Profiles

Results are presented in Figures 17 through 31 which define the characteristics of the rotor inlet velocity profile for the range of

conditions described in Table 3.* Each of these figures consists of two parts. The first part depicts the variation of the measured velocity ratio $V/\overline{V}$ with circumferential angle θ. Curves have been superimposed on the data which compare the design variation of $V/\overline{V}$ with θ, for which A = 0.20, with the variation obtained from Fourier analysis of the data with $A = A_f$. Each of these curves has been plotted using the phase angle from Table 3. The second part of these figures contains the results of the Fourier analysis. Here the magnitude of the coefficients A_n is shown as a function of the harmonic number n. This information is of value in determining the degree to which the screens are effective as generators of a flow field that is dominated by a single harmonic.

The velocity profile generated by the one-cycle screen is similar in all respects regardless of the values of $\overline{V}$ and r when x_G = 55.6 in. As x_G decreases, an increasing degree of scatter appears in the variation of $V/\overline{V}$ with θ as shown in Figures 18, 22 and 23. This increase in scatter is accompanied by a slight increase in the magnitude of A_1 and a larger increase in the magnitude of the higher harmonics. In Figure 23 with x_G = 12.5 in., the worst case, the value of the largest higher harmonic, A_5, is only 11.3% of the value of A_1. Thus this screen produces a rotor inlet axial velocity profile that is dominated by A_1 for the entire range of operating conditions.

Results are presented in Figures 24 and 25 which describe the nominal performance of the two- and four-cycle screens with $\overline{V} \approx 78.3$ ft/sec., r = 7.75 inches and x_G = 55.6 inches. The results of Fourier analysis show that strong

---

* Sandy Atkins, Brandt Atkins, Robert Eisenhuth, Fred Eisenhuth, and Robert Davis assisted with the data reduction at various stages in this program. Their help was appreciated.

two- and four-cycle disturbances are generated and that the design condition of $A_f = 0.20$ has been exceeded in the four-cycle screen.

The six-cycle screen data, Figures 26 and 27, contains several harmonics that exceed 10% of the value of A_6. This decrease in the quality of the flow field may be due to the increased effect of turbulent mixing. At the nominal AFRF operating condition of $\bar{V} = 80$ ft/sec, the magnitude of the highest undesirable harmonic, A_2, is 15.6% of the magnitude of A_6 with the screen mounted against the inlet centerbody support struts.

Figures 28, 29 and 30 show the effect on the composition of the rotor inlet flow field generated by the nine-cycle screen of successive reductions in the distance from the screen to the rotor inlet. As x_G decreases, the level of the fundamental A_9 increases toward the design value of 0.20 and the quality of the flow field increases as evidenced by a gradual reduction in the level of the other harmonic amplitudes. The results presented in Figure 30b show that with $x_G = 12.4$ inches, this screen generates one of the best flow fields obtained in this test program.

Twelve- and fifteen-cycle screens were also designed in this program, and a limited number of runs were made to evaluate the performance of the fifteen-cycle screen. The results are presented in Figure 31. This screen was tested only at $x_G = 12.4$ inches. The measurements show that the fifteenth harmonic is close to the design value of 0.20 and that the first, seventh, fourteenth, and sixteenth harmonics are larger than is desirable. The magnitude of the fourteenth harmonic is 19.9% of the magnitude of the fundamental. These results are felt to be encouraging since a new procedure was adopted in the design of this screen (see Appendix 2). It

may be possible to improve this type of screen through the use of a larger number of overlay segments in conjunction with a smaller wire diameter, smaller mesh size support screen.

9. CONCLUSIONS

The results of this disturbance generating screen development and evaluation program have shown that:

1) The analytical method developed by McCarthy can be successfully applied within its region of applicability--namely to treat the case of steady, moderately sheared, three-dimensional flow past a wire grid of arbitrary resistance distribution which is placed normal to the axis of a duct of arbitrary but constant cross-section.

2) One-, two-, four-, six-, nine-, twelve-, and fifteen-cycle screens are now available for use in the AFRF which generate sinusoidal rotor inlet axial velocity profiles whose maximum variation from the average value is close to the design level of 20%. The composition of these flow fields is good -- i.e., in general, the presence of harmonics whose magnitude exceeds 10% of the magnitude of the fundamental is limited to a few cases.

3) The characteristics of the flow field generated at the AFRF rotor inlet by screens of the type described in this report are a function of the AFRF operating condition ($\bar{V}$) and the location of the screen (x_G). This dependence has been attributed to the effects of Reynolds number and turbulent mixing, respectively.

4) By slightly modifying McCarthy's screen design approach, twelve- and fifteen-cycle disturbance generating screens were designed for use in the AFRF. This new design method, which utilizes multiple overlay segments, could be used to extend the present capability above the fifteen-cycles per revolution level.

REFERENCES

1. Bruce, E. P., "The ORL Fluids Engineering Unit Axial Flow Research Fan," ORL Technical Memorandum TM 72-109, June 22, 1972.

2. Henderson, R. E., "The Unsteady Response of an Axial Flow Turbomachine to an Upstream Disturbance," Ph.D. Dissertation, Engineering Department, University of Cambridge, England, 1972 (see also ARL Technical Memorandum TM 72-218, October 1972).

3. Weighardt, K. E. G., "On the Resistance of Screens," The Aeronautical Quarterly, Volume 4, February 1953, pp. 186-192.

4. Cornell, W. G., "Losses in Flow Normal to Plane Screens," Transactions of the ASME, Vol. 80, May 1958, pp. 791-799.

5. McCarthy, J. H., "Steady Flow Past Non-Uniform Wire Grids," Journal of Fluid Mechanics, Vol. 19, 1964, pp. 491-512.

6. Owen, P. R. and Zienkiewicz, H. K., "The Production of Uniform Shear Flow in a Wind Tunnel," Journal of Fluid Mechanics, Vol. 2, 1957, pp. 521-531.

7. Elder, J. W., "Steady Flow Through Non-Uniform Guazes of Arbitrary Shape," Journal of Fluid Mechanics, Vol. 5, 1959, pp. 355-368.

APPENDIX 1. PERFORMANCE CHARACTERISTICS OF THE ORIGINAL ONE-CYCLE SCREEN

The measured variation of the rotor inlet axial velocity profile produced by the original AFRF one-cycle screen is presented in Figure 32a and the associated distribution of the Fourier coefficients is shown in Figure 32b. The performance of this screen was disappointing since the magnitude of A_1 was well below the design value of 0.10 and higher harmonics were present, e.g., A_9 in Figure 32b, whose magnitude was on the order to 20% of the magnitude of A_1. The performance of the other original screens--those having values of N of two through six--was similar to the performance of the one-cycle screen.

APPENDIX 2. DESIGN OF THE TWELVE- AND FIFTEEN-CYCLE SCREENS

The approach taken in the design of these screens differs from the approach used in the design of the one- through nine-cycle screens in one significant respect. In the twelve- and fifteen-cycle screens, multiple overlay segments were used. The maximum level of resistance coefficient for A = 0.20, K = 1.591, was approximated by combining the resistance coefficients of the support screen, K = 0.343; of a large circumferential extent overlay segment, K = 0.587; and of a small circumferential extent overlay segment, K = 0.685. The sum of these resistance coefficients is 1.651. The circumferential extent of the twelve-cycle screen overlay segments is shown in Figure 33. The circumferential extent of the overlay segments that were used in the fifteen-cycle screen were obtained by multiplying the twelve-cycle screen values by a factor of 0.8.

Use of this method of screen fabrication is based on the assumption that McCarthy's test results for a single overlay screen, in which the resistance coefficient for the support screen/overlay combination was shown to be equal to the sum of the resistance coefficients of the individual screens, can be extended to a combination containing two overlay segments. The limited results obtained in this program indicate that this assumption is valid. Consequently this approach could be used to construct screens with values of N greater than fifteen if a need for screens of this type arises.

APPENDIX 3. CHARTS FOR SELECTION OF SCREENS TO PROVIDE A GIVEN RESISTANCE COEFFICIENT

Three charts were prepared as an aid in selecting the overlay screens described in Table 2. These charts proved to be extremely useful. Consequently, they are presented here as Figures 34, 35, and 36 so that persons

involved in the selection of square mesh wire screening having a given resistance coefficient may use them. These charts relate screen solidity, Reynolds number and resistance coefficient to wire diameter d and number of wires per inch M for 0.01 in. $\leq$ d $\leq$ 0.09 in. and 2 $\leq$ M $\leq$ 20.

Screen solidity, defined by Eqn. (7) with $M = \frac{1}{m}$, is presented in Figure 34. Values of the characteristic Reynolds number computed with V_{REF} = 100 ft/sec are presented in Figure 35. Values of the characteristic Reynolds number associated with operation at a different value of V_{REF}, say V_{REF} = 80 ft/sec, can be obtained by multiplying the $(Re)_{100}$ value obtained from Figure 35 by the velocity ratio--in this case by (80/100). The resistance coefficient defined by Eqn. (2) with c = 0.78 is presented in Figure 36. The data presented in Figure 36 apply for 600 < Re < 5000.

FIGURE 1. SCHEMATIC OF ARL AXIAL-FLOW RESEARCH FAN

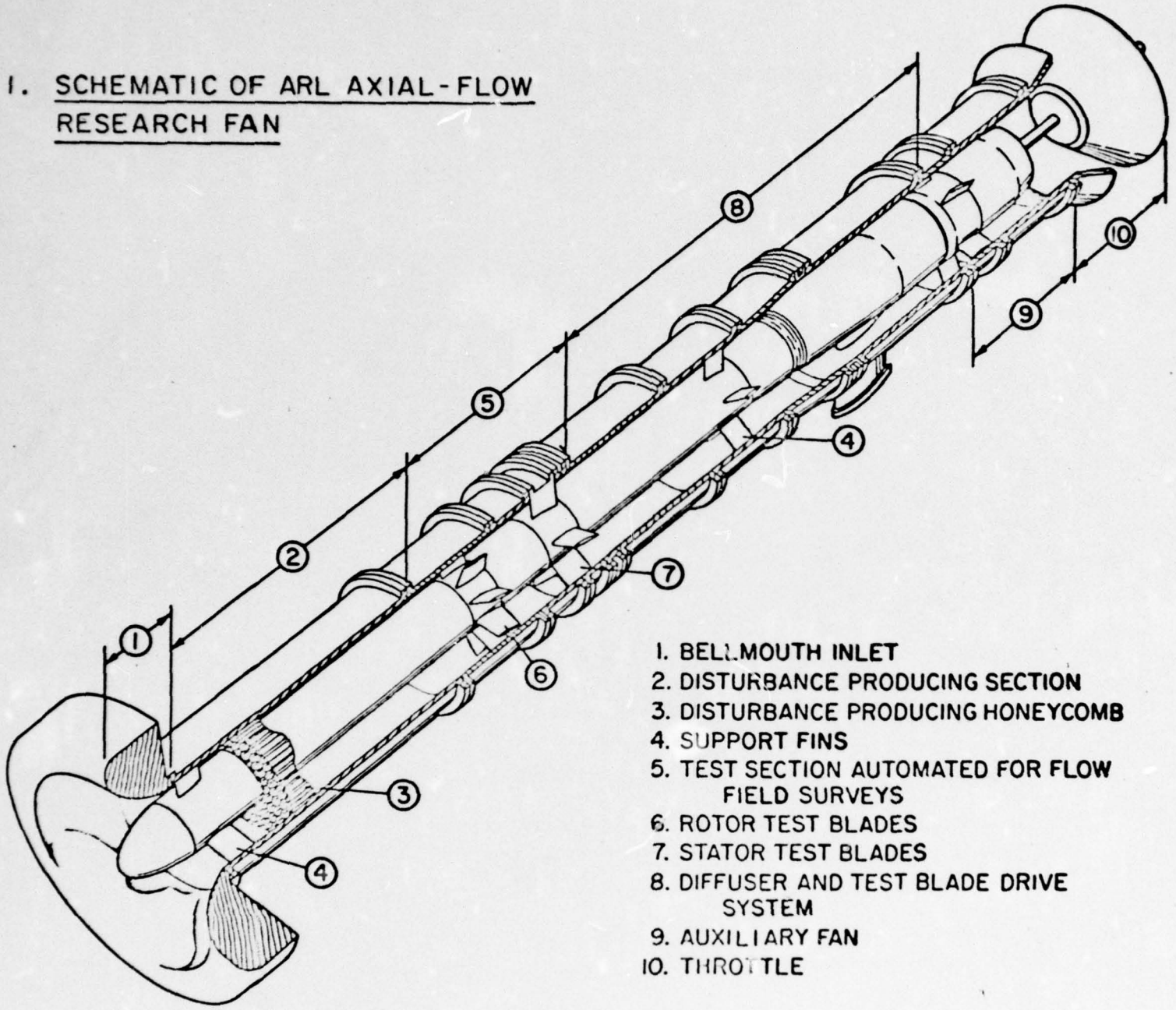

1. BELLMOUTH INLET
2. DISTURBANCE PRODUCING SECTION
3. DISTURBANCE PRODUCING HONEYCOMB
4. SUPPORT FINS
5. TEST SECTION AUTOMATED FOR FLOW FIELD SURVEYS
6. ROTOR TEST BLADES
7. STATOR TEST BLADES
8. DIFFUSER AND TEST BLADE DRIVE SYSTEM
9. AUXILIARY FAN
10. THROTTLE

January 8, 1974
EPB:vcb

FIGURE 2. PREDICTED VARIATION OF RESISTANCE COEFFICIENT

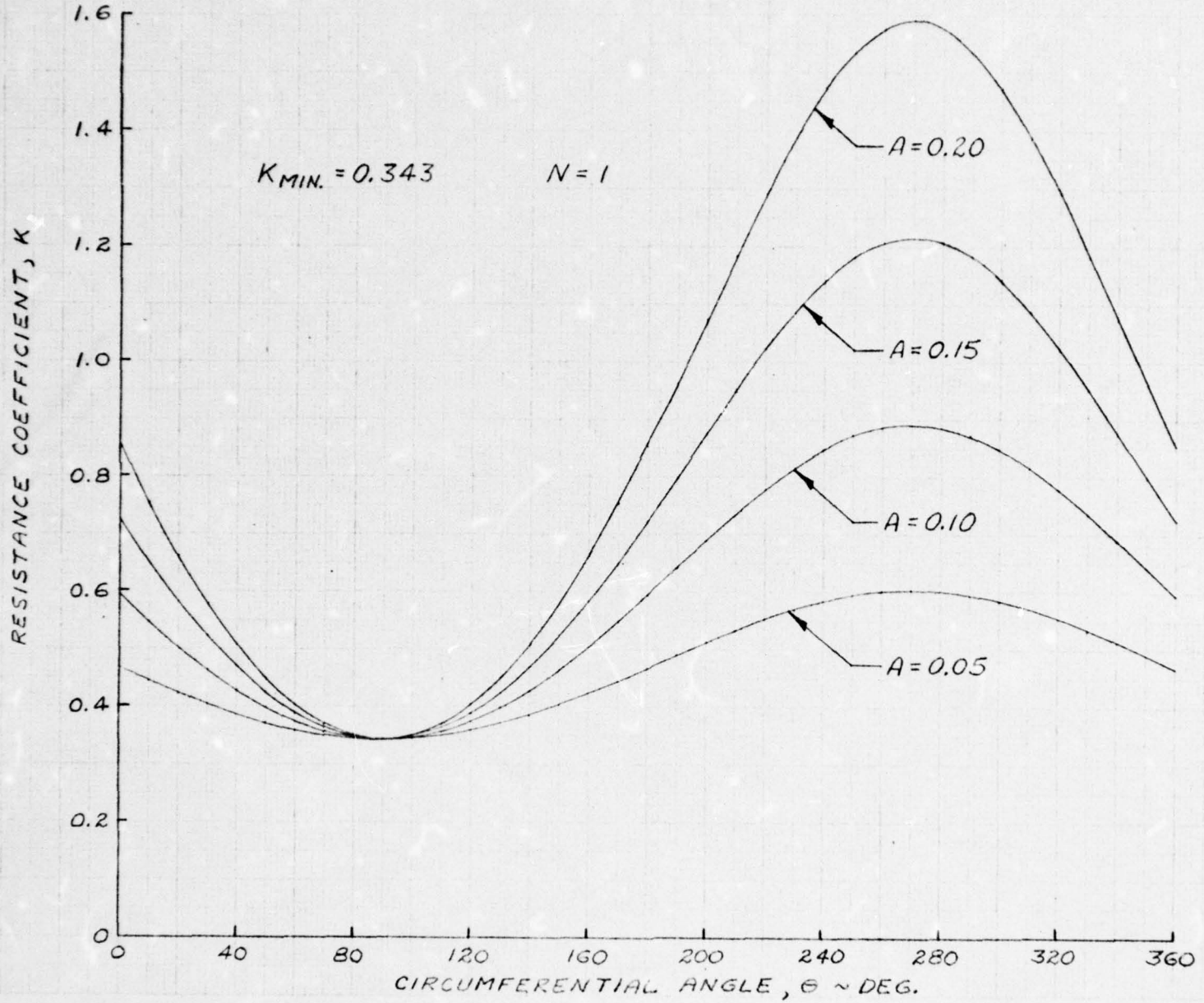

January 8, 1974
EPB:vcb

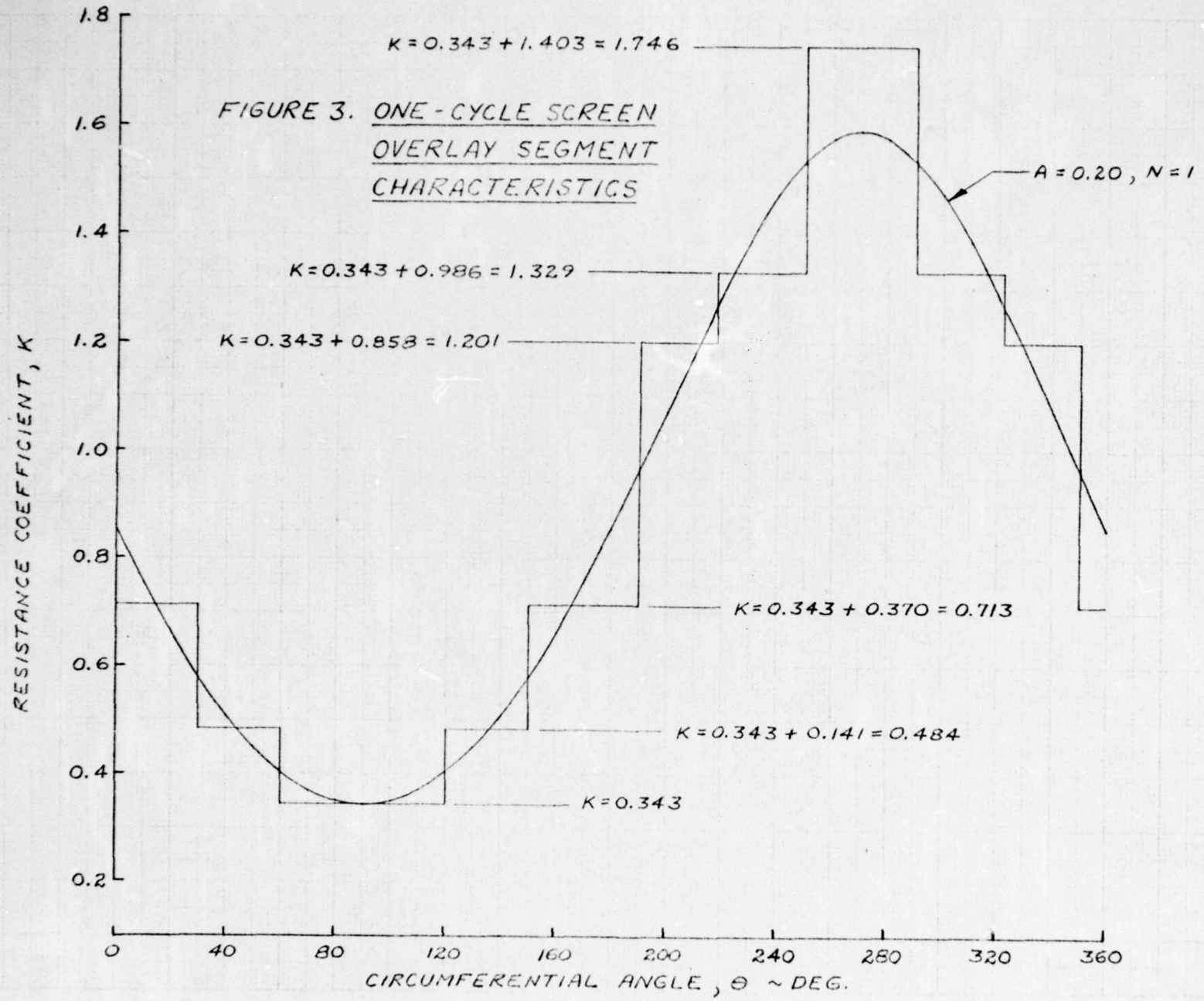

FIGURE 3. ONE-CYCLE SCREEN OVERLAY SEGMENT CHARACTERISTICS

January 8, 1974
EPB:vcb

January 8, 1974
EPB:vcb

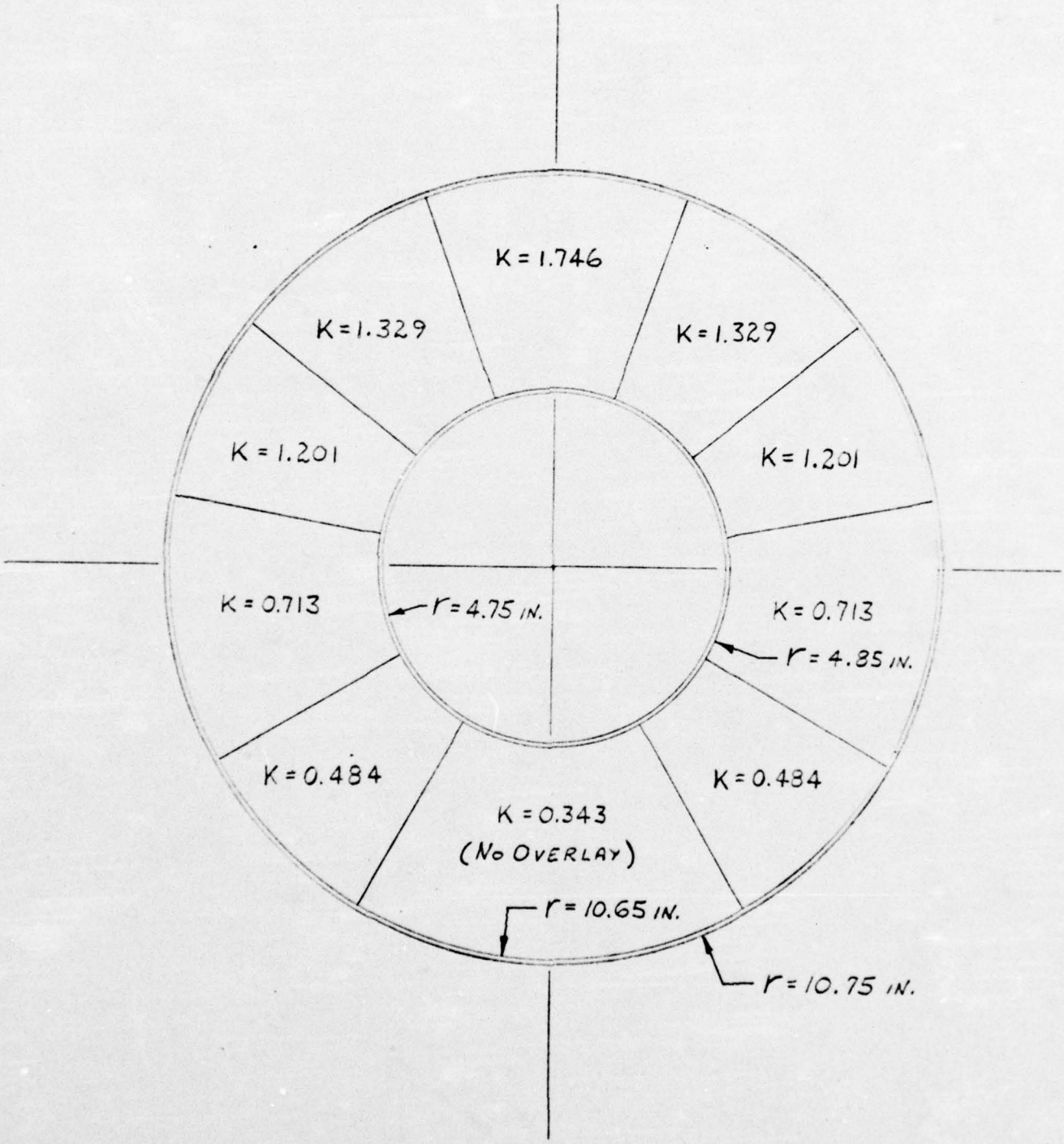

FIGURE 4. TYPE OF DRAWING MADE TO AID IN FABRICATION OF THE ONE-CYCLE SCREEN

January 8, 1974
EPB:veb

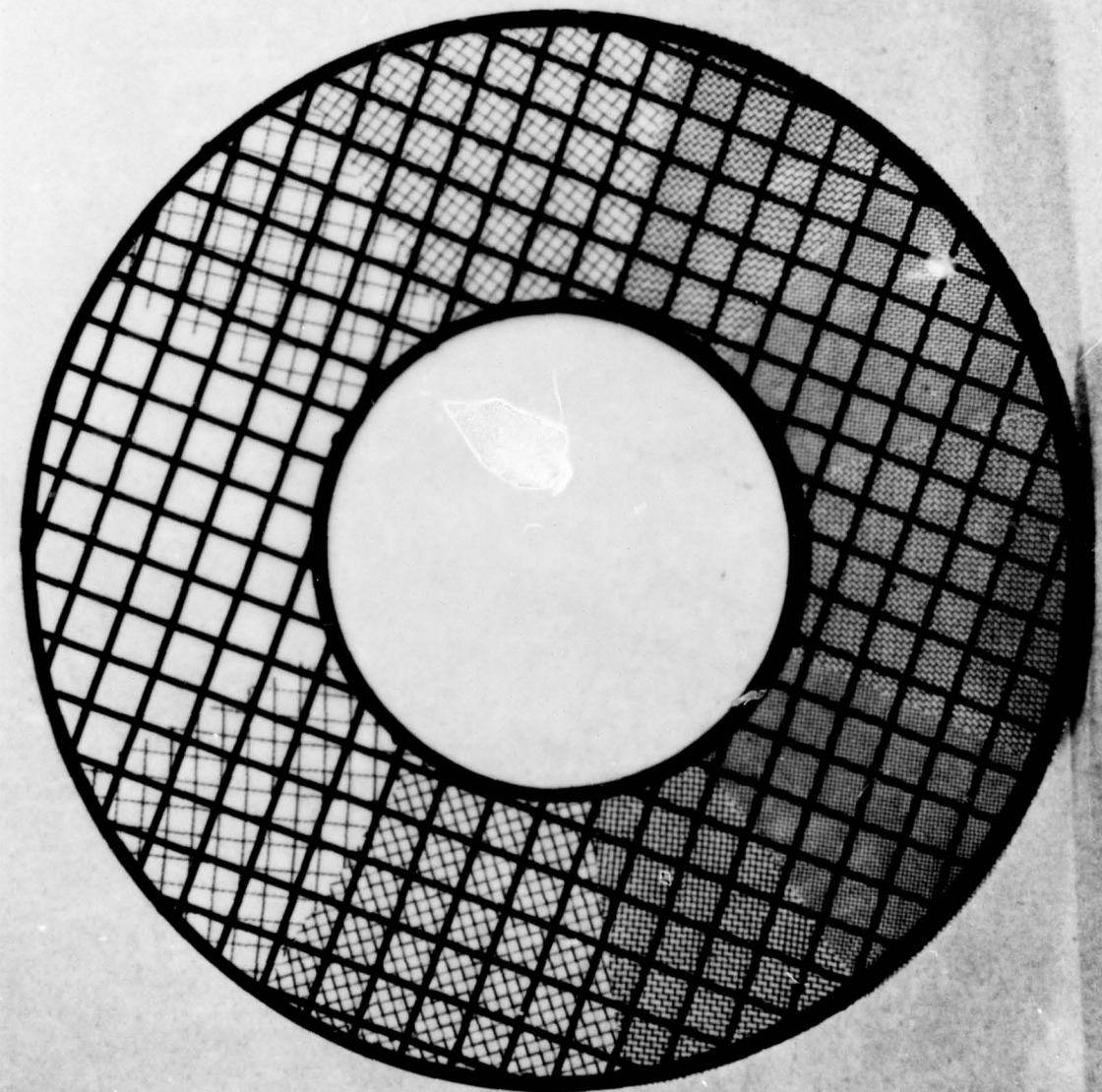

Figure 6. [illegible]

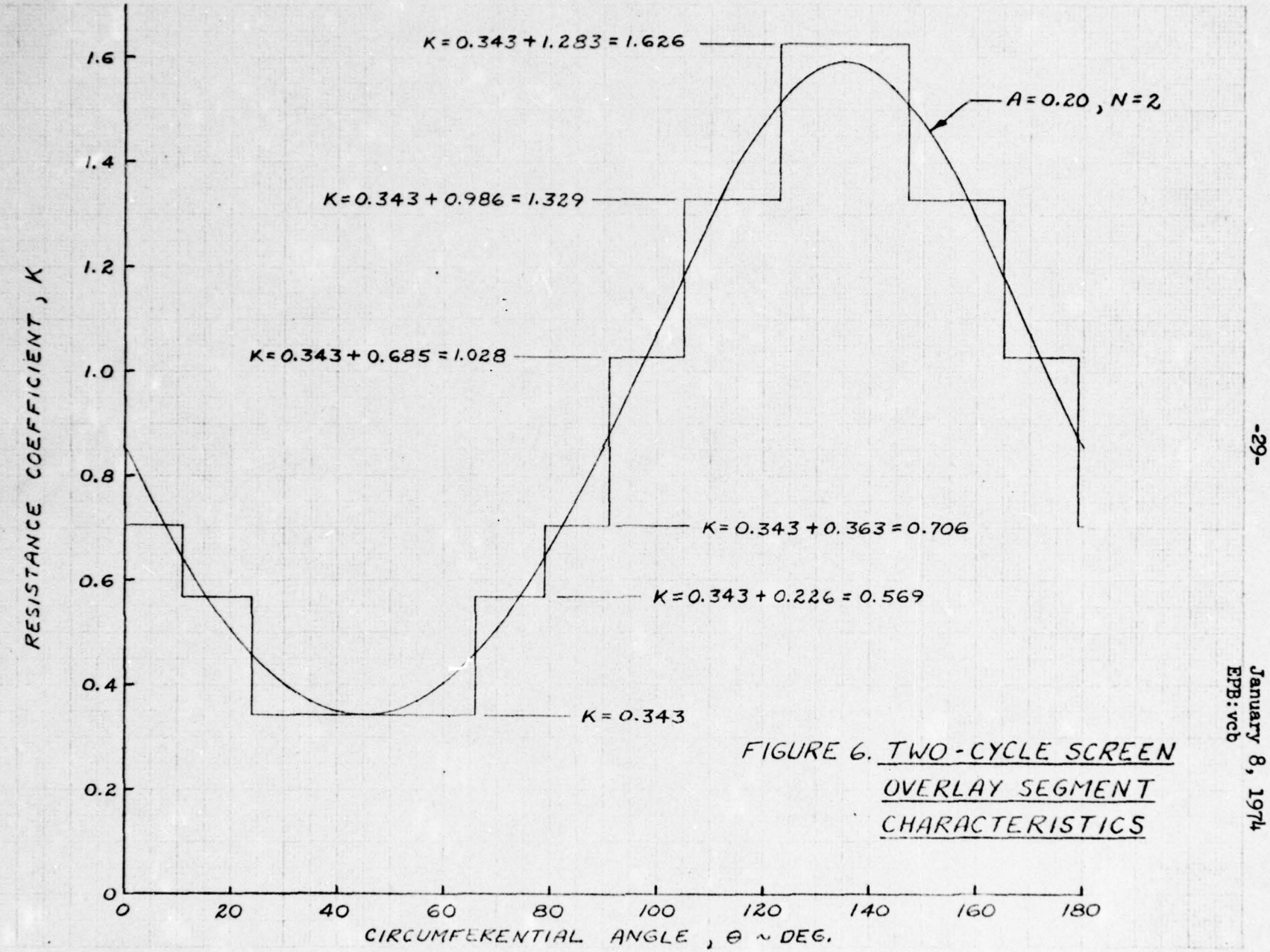

FIGURE 6. TWO-CYCLE SCREEN OVERLAY SEGMENT CHARACTERISTICS

January 8, 1974
EPB:vcb

January 8, 1974
EPB:vcb

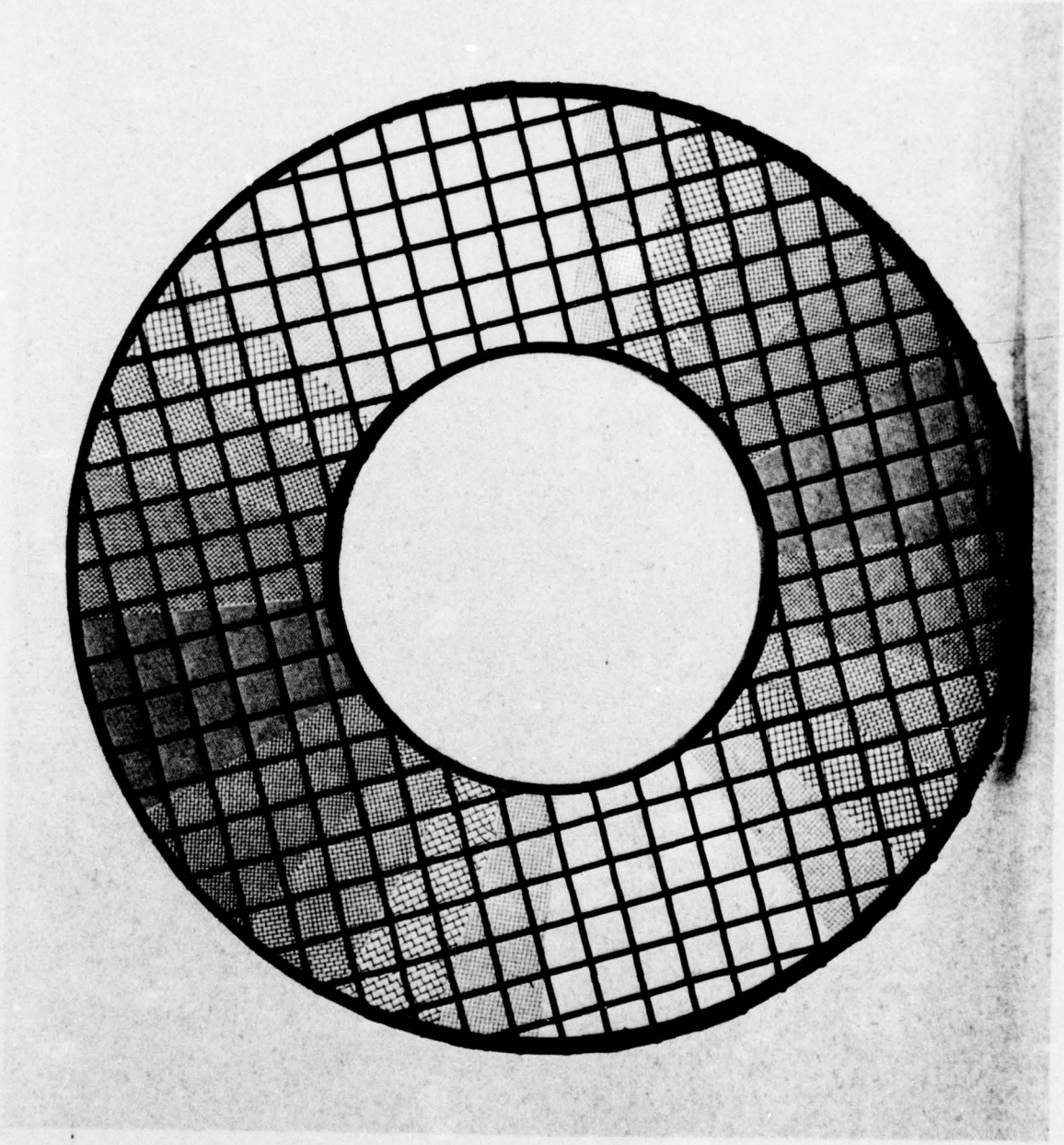

FIGURE 7. THE TWO-CYCLE SCREEN

January 8, 1974
EPB:veb

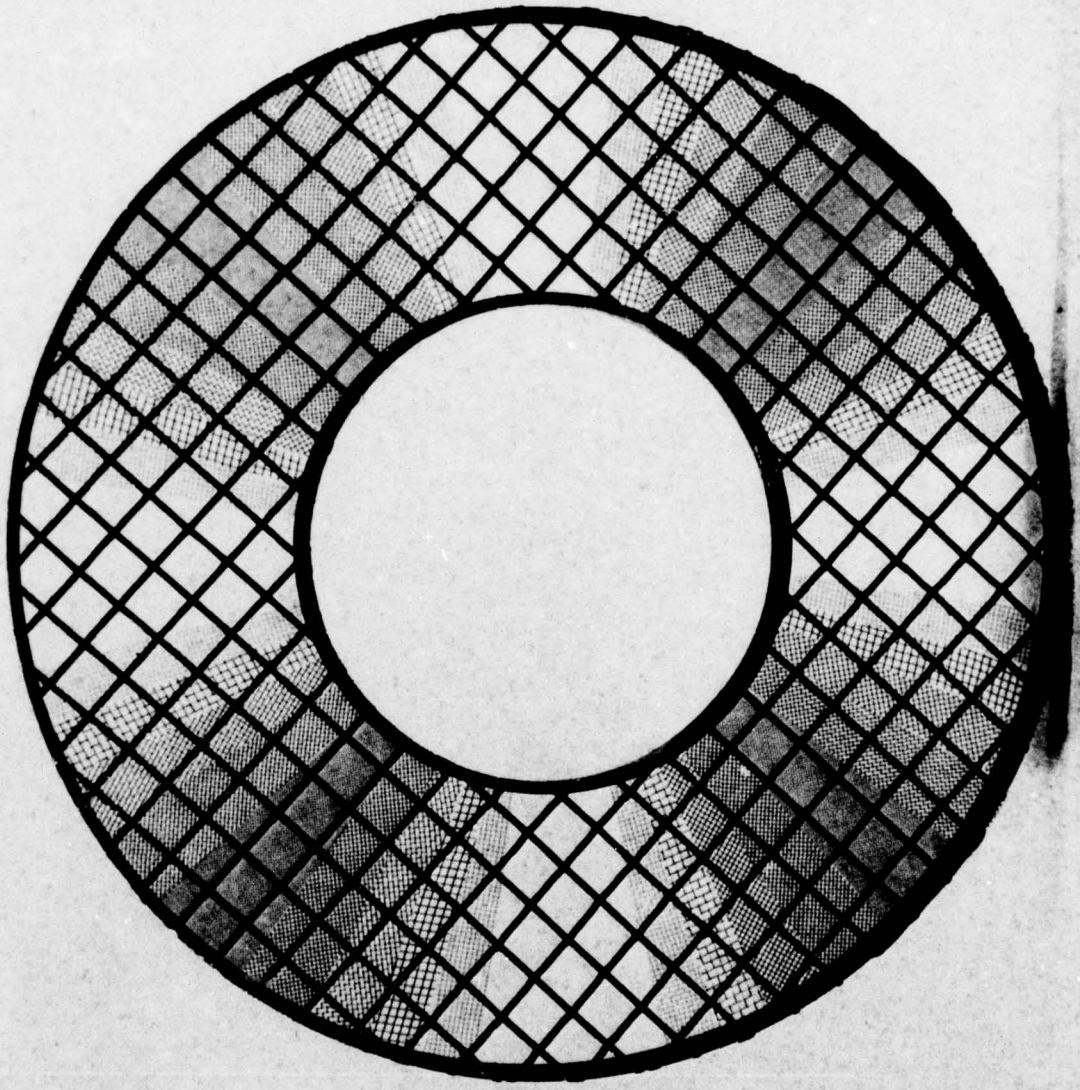

FIGURE 8. THE FOUR-CYCLE SCREEN

FIGURE 9. SIX-CYCLE SCREEN OVERLAY SEGMENT CHARACTERISTICS

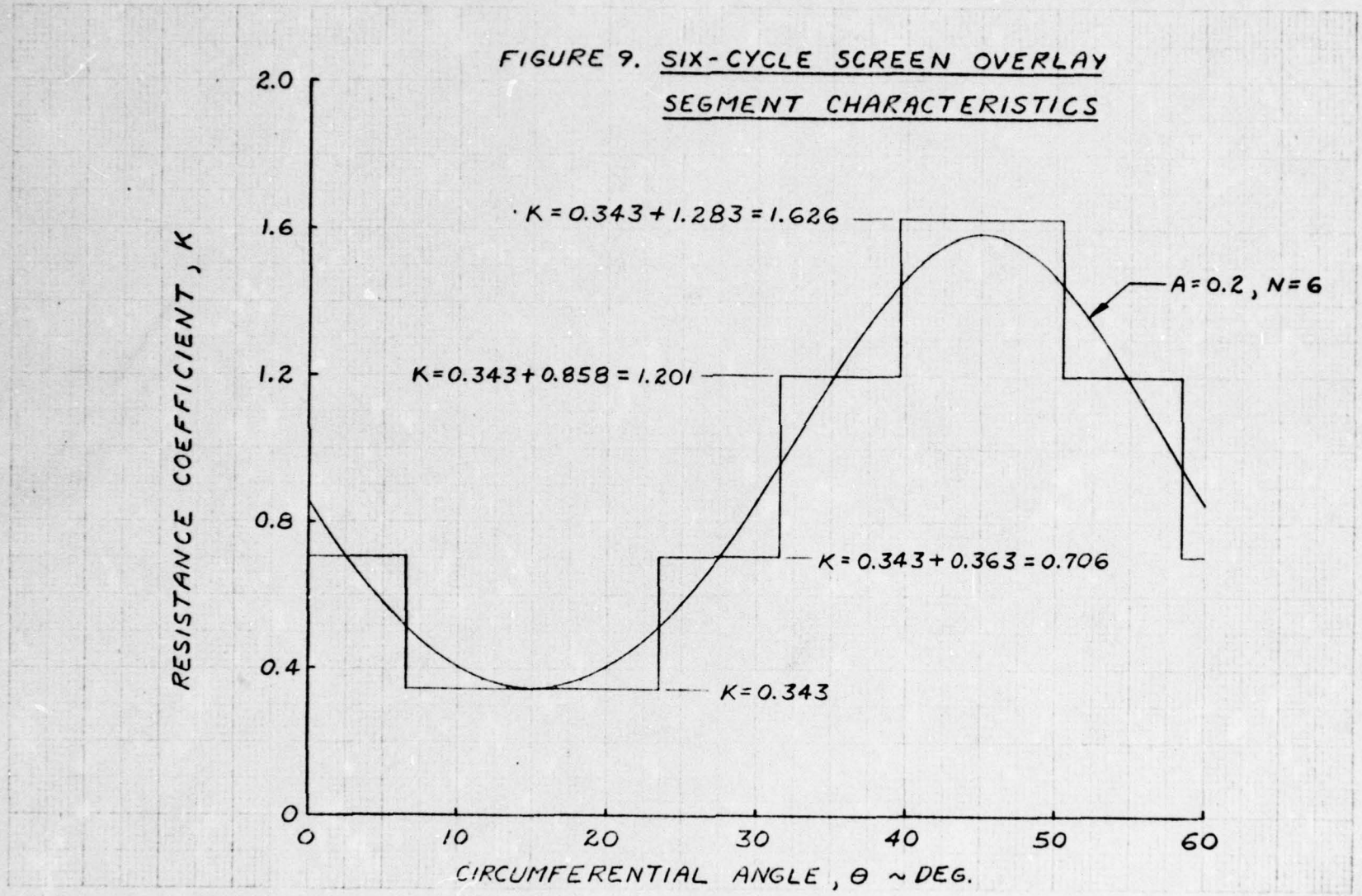

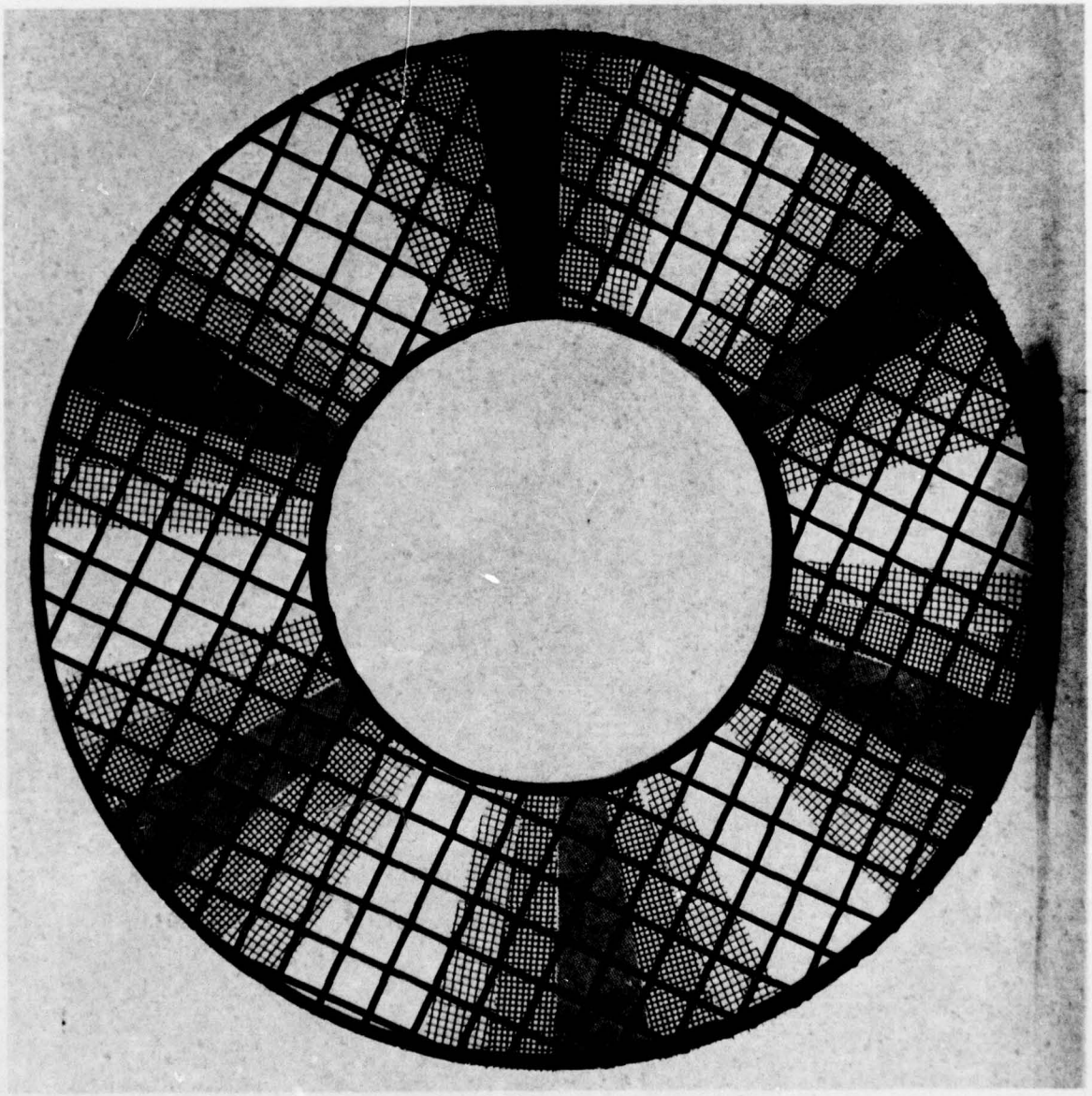

FIGURE 19. THE SIX-CYCLE SCREEN

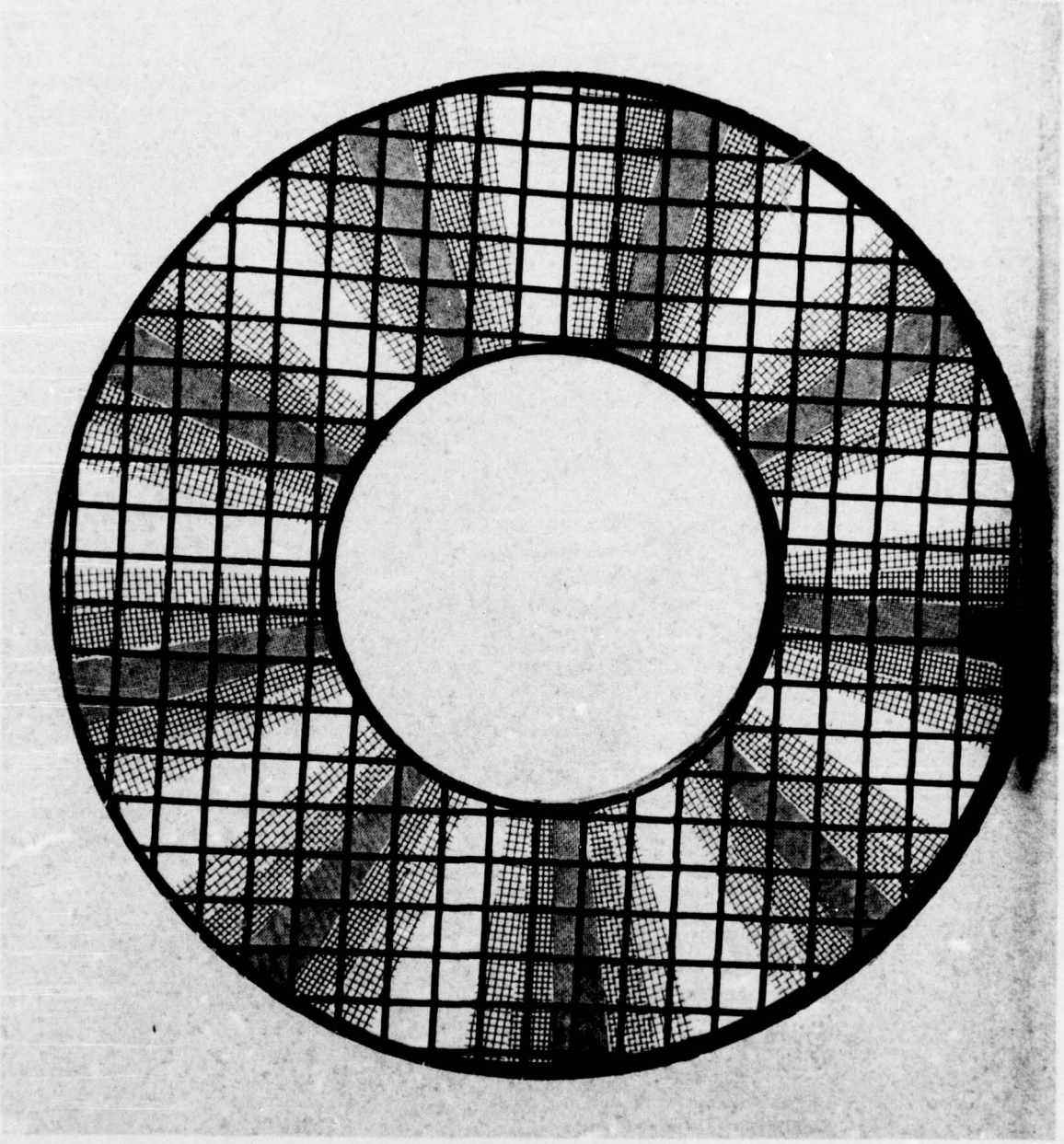

FIGURE 11. THE NINE-CYCLE SCREEN

January 8, 1974
EPB:vcb

FIGURE 12. BASIC PERFORMANCE CHARACTERISTICS OF THE ONE-CYCLE SCREEN

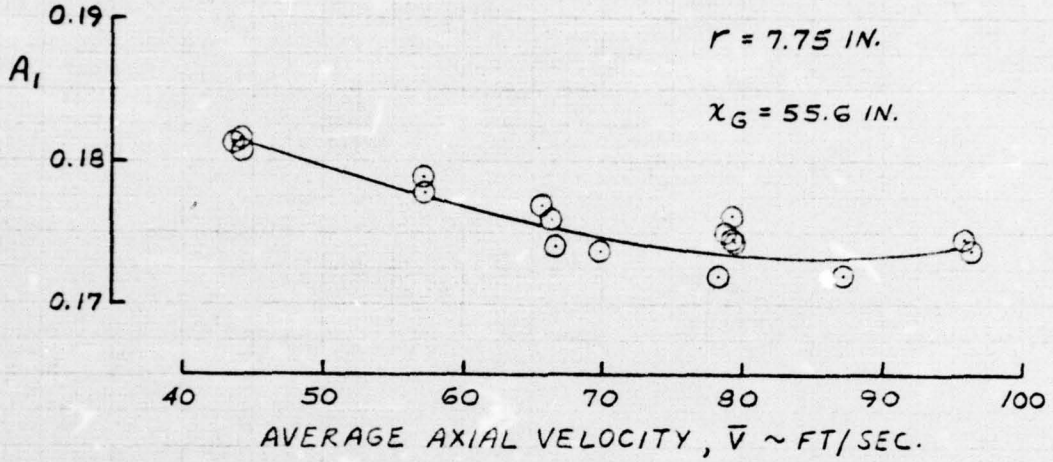

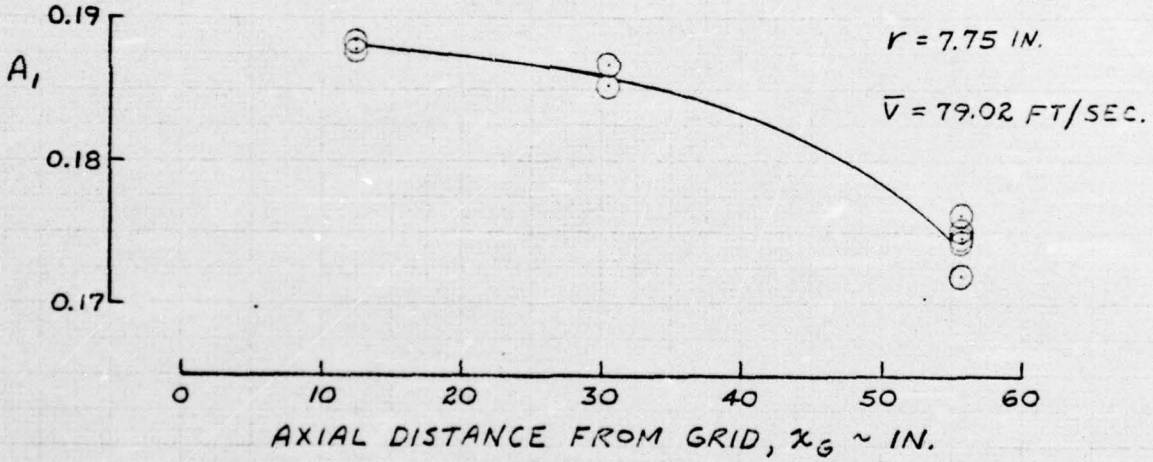

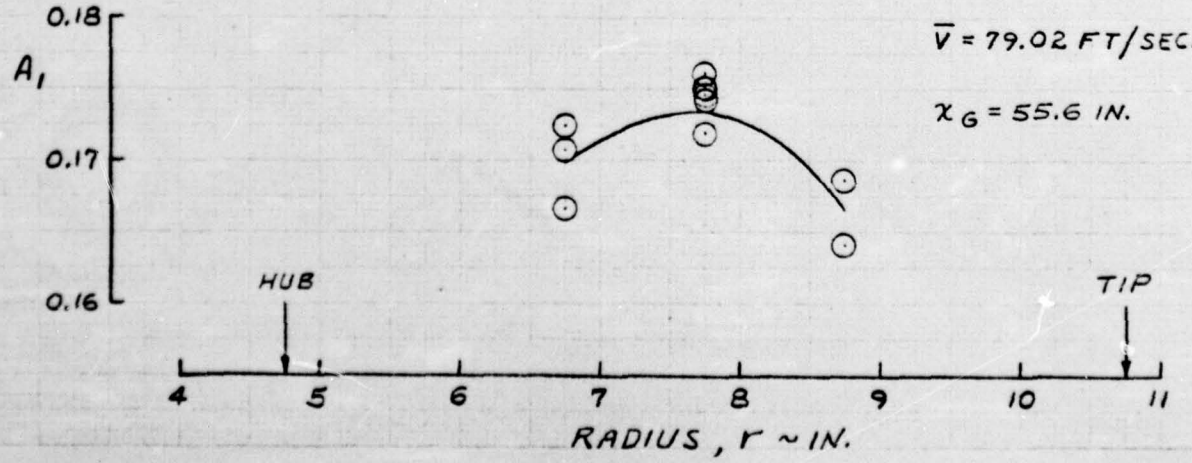

January 8, 1974
EPB:vcb

FIGURE 13. BASIC PERFORMANCE CHARACTERISTICS OF THE TWO-CYCLE SCREEN

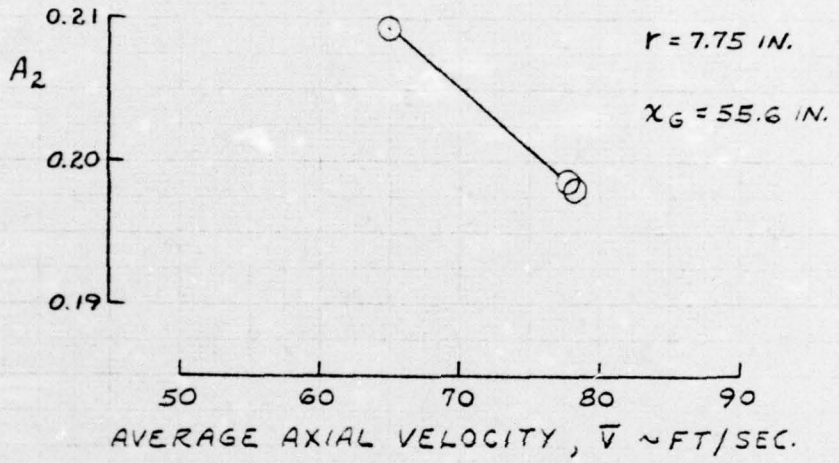

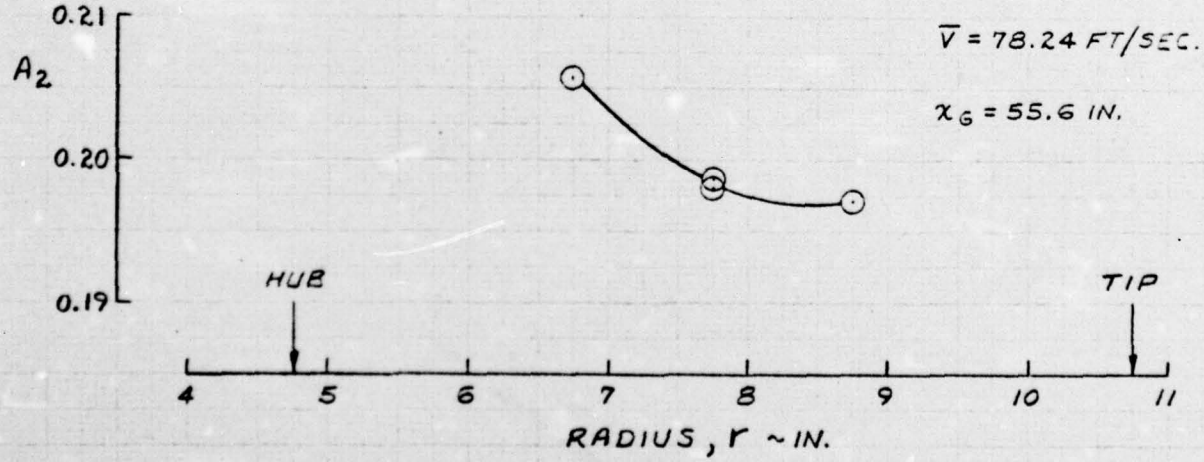

January 8, 1974
EPB:vcb

FIGURE 14. BASIC PERFORMANCE CHARACTERISTICS OF THE FOUR-CYCLE SCREEN

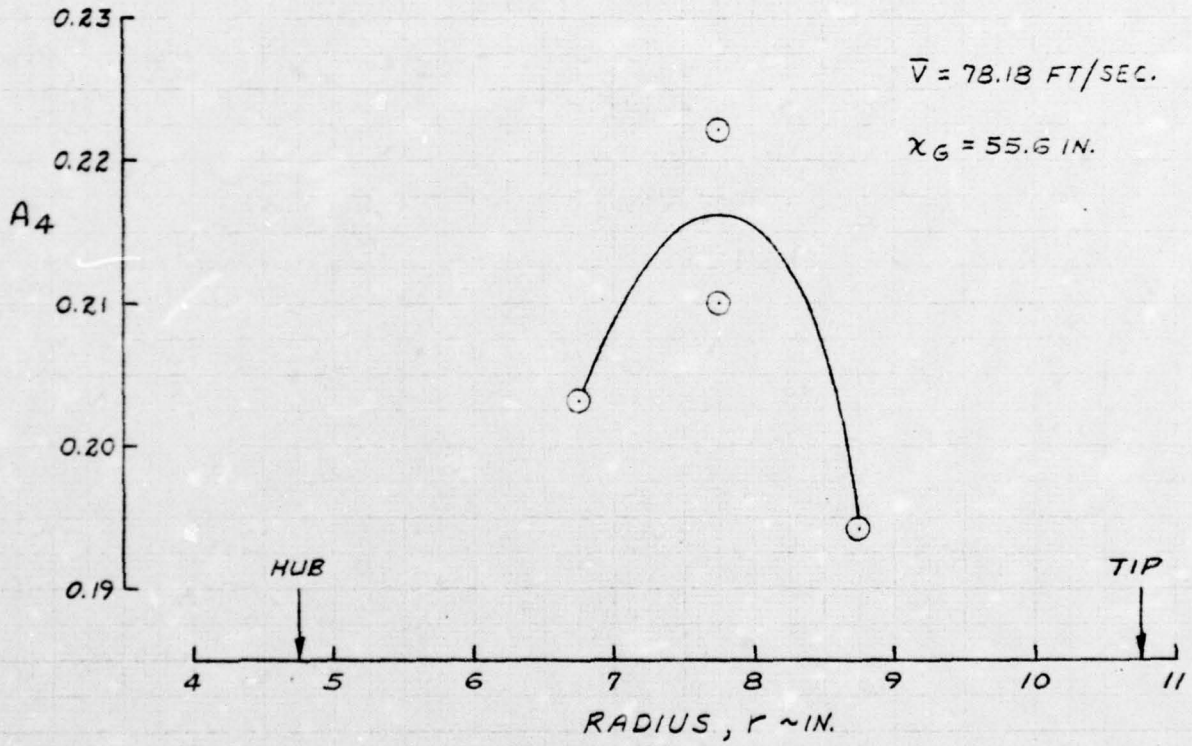

January 8, 1974
EPB:vcb

FIGURE 15. BASIC PERFORMANCE CHARACTERISTICS OF THE SIX-CYCLE SCREEN

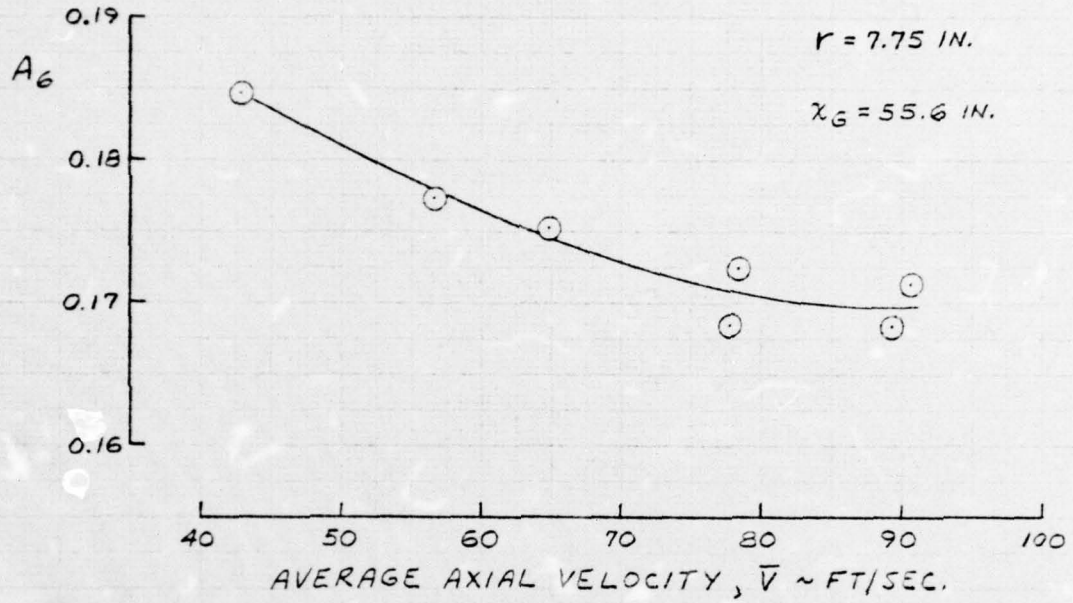

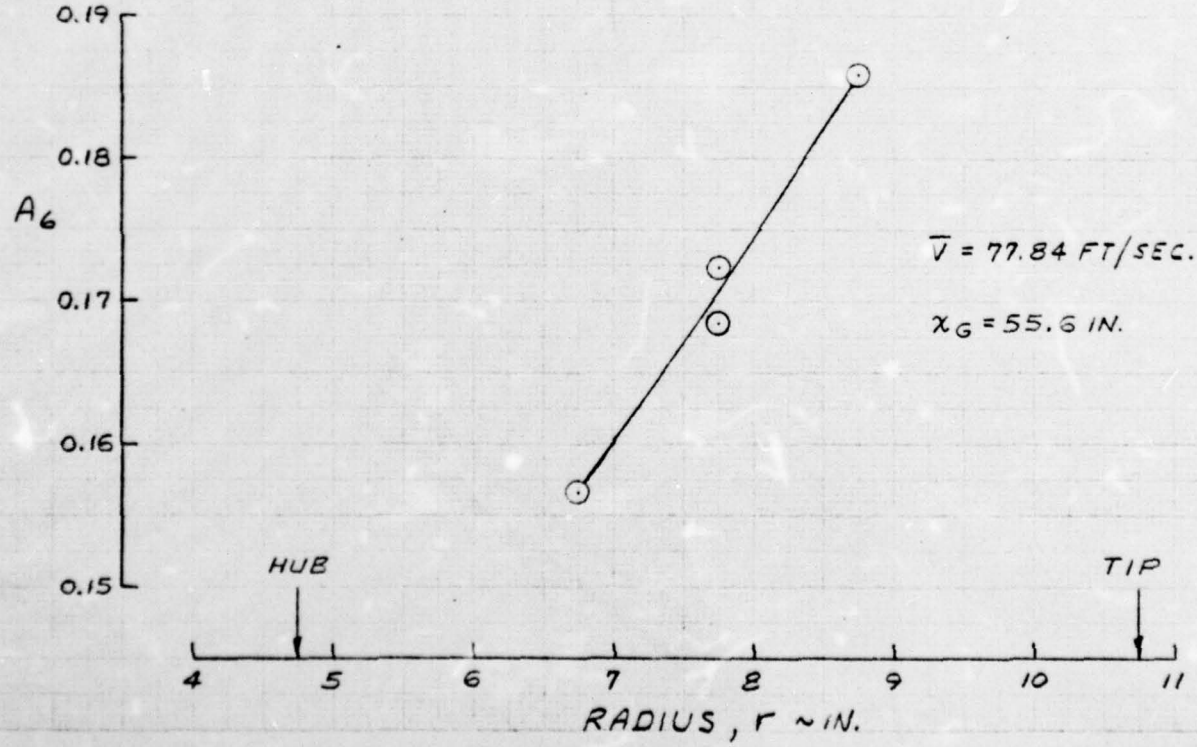

January 8, 1974
EPB:vcb

FIGURE 16. BASIC PERFORMANCE CHARACTERISTICS OF THE NINE-CYCLE SCREEN

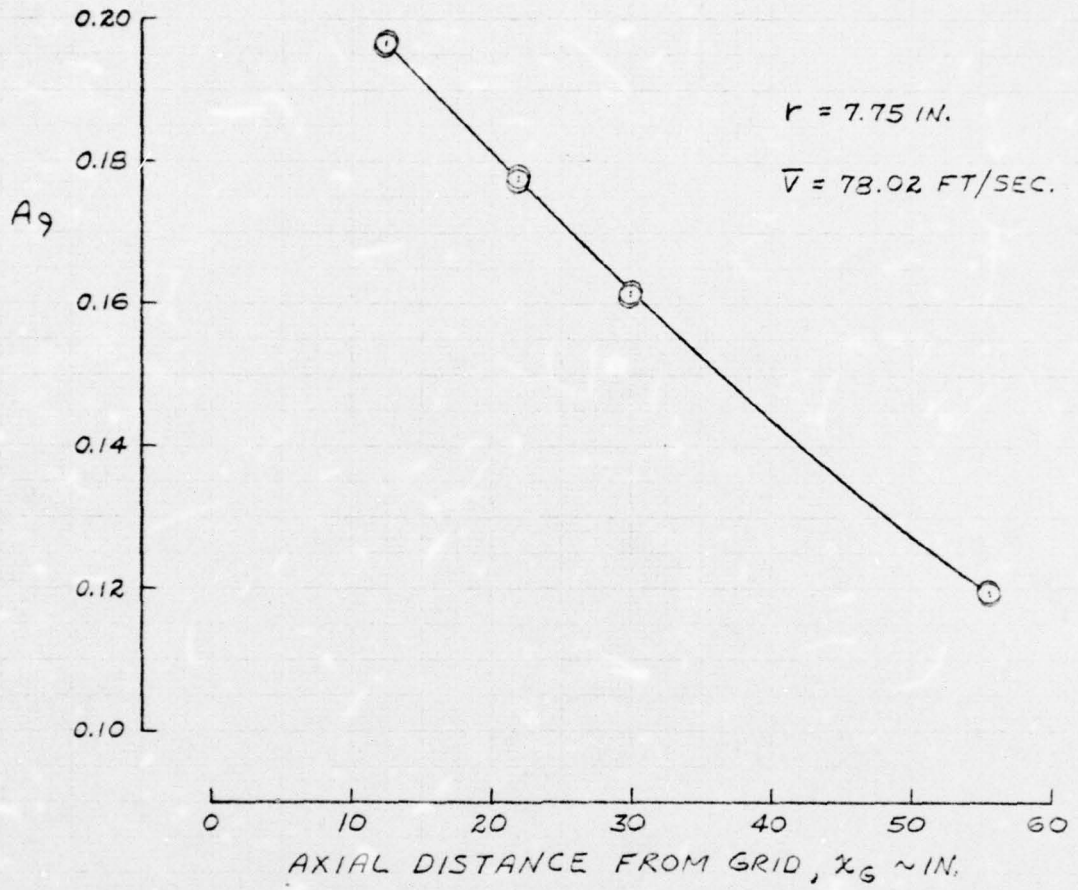

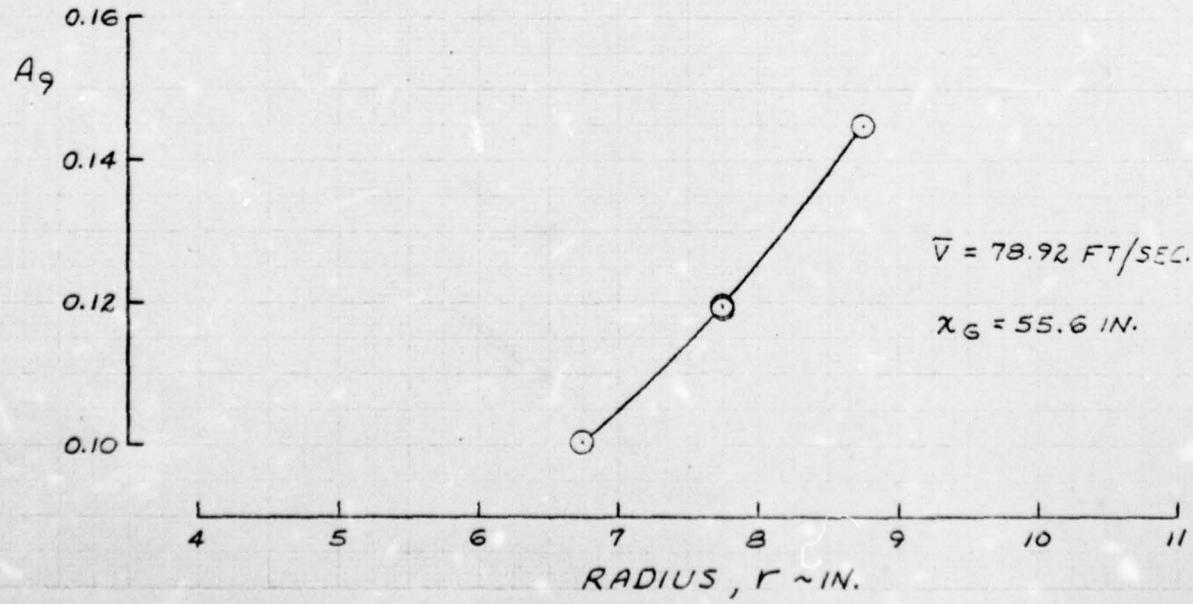

FIGURE 17a. MEASURED ROTOR INLET VELOCITY PROFILE FOR ONE-CYCLE SCREEN RUN NUMBER 104

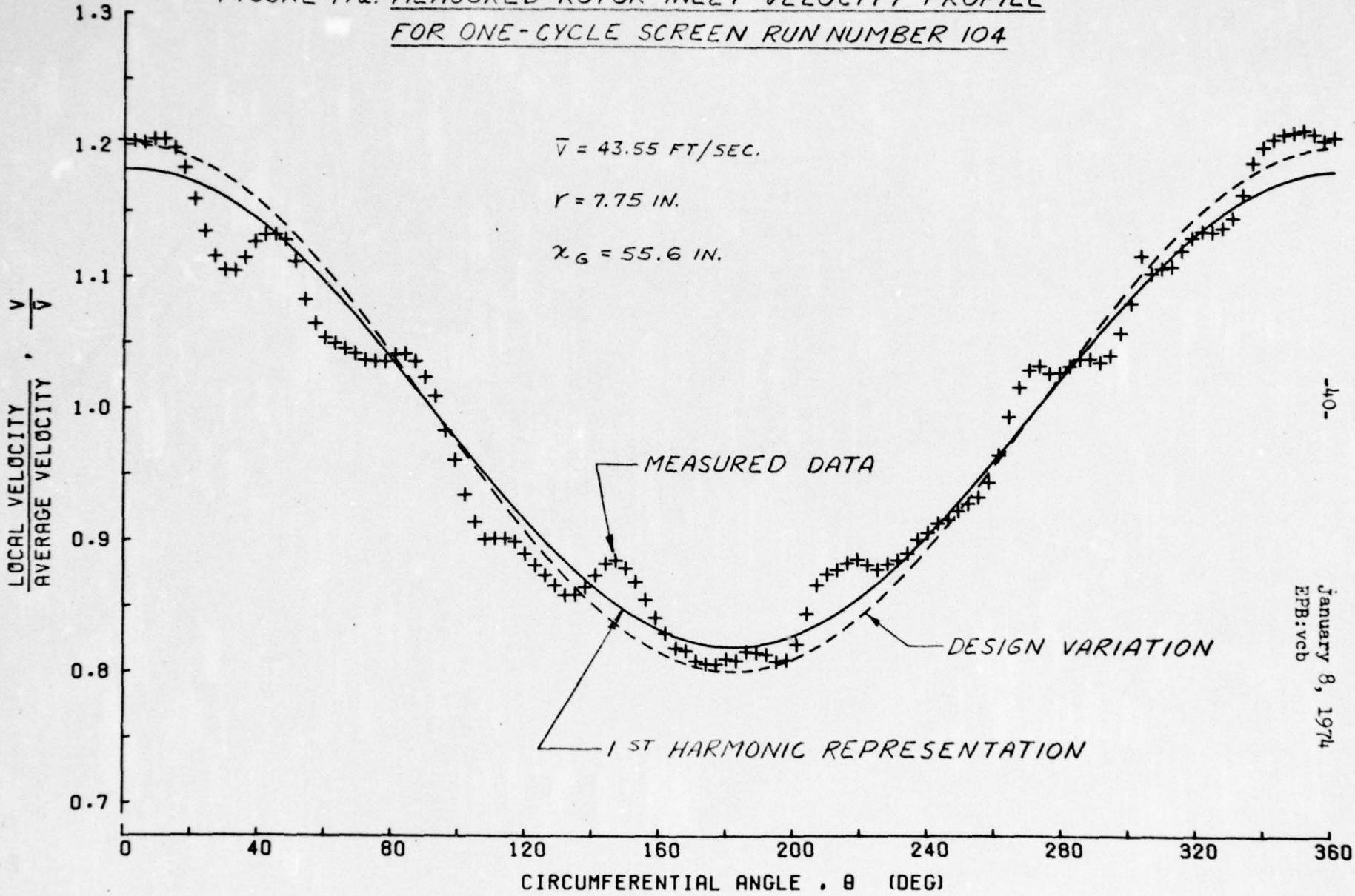

January 8, 1974
EPB:vcb

January 8, 1974
EPB:vcb

FIGURE 17b. FOURIER COEFFICIENT MAGNITUDE FOR ONE-CYCLE SCREEN RUN NUMBER 104

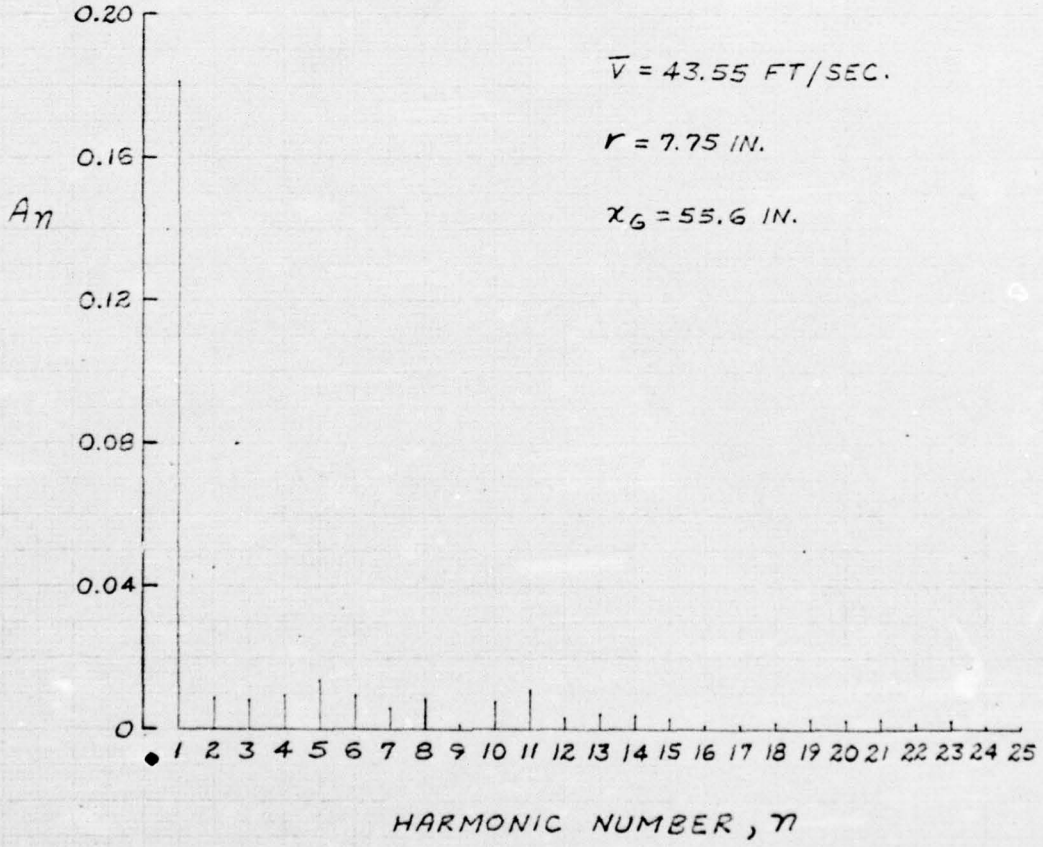

FIGURE 18a. MEASURED ROTOR INLET VELOCITY PROFILE FOR ONE-CYCLE SCREEN RUN NUMBER 61

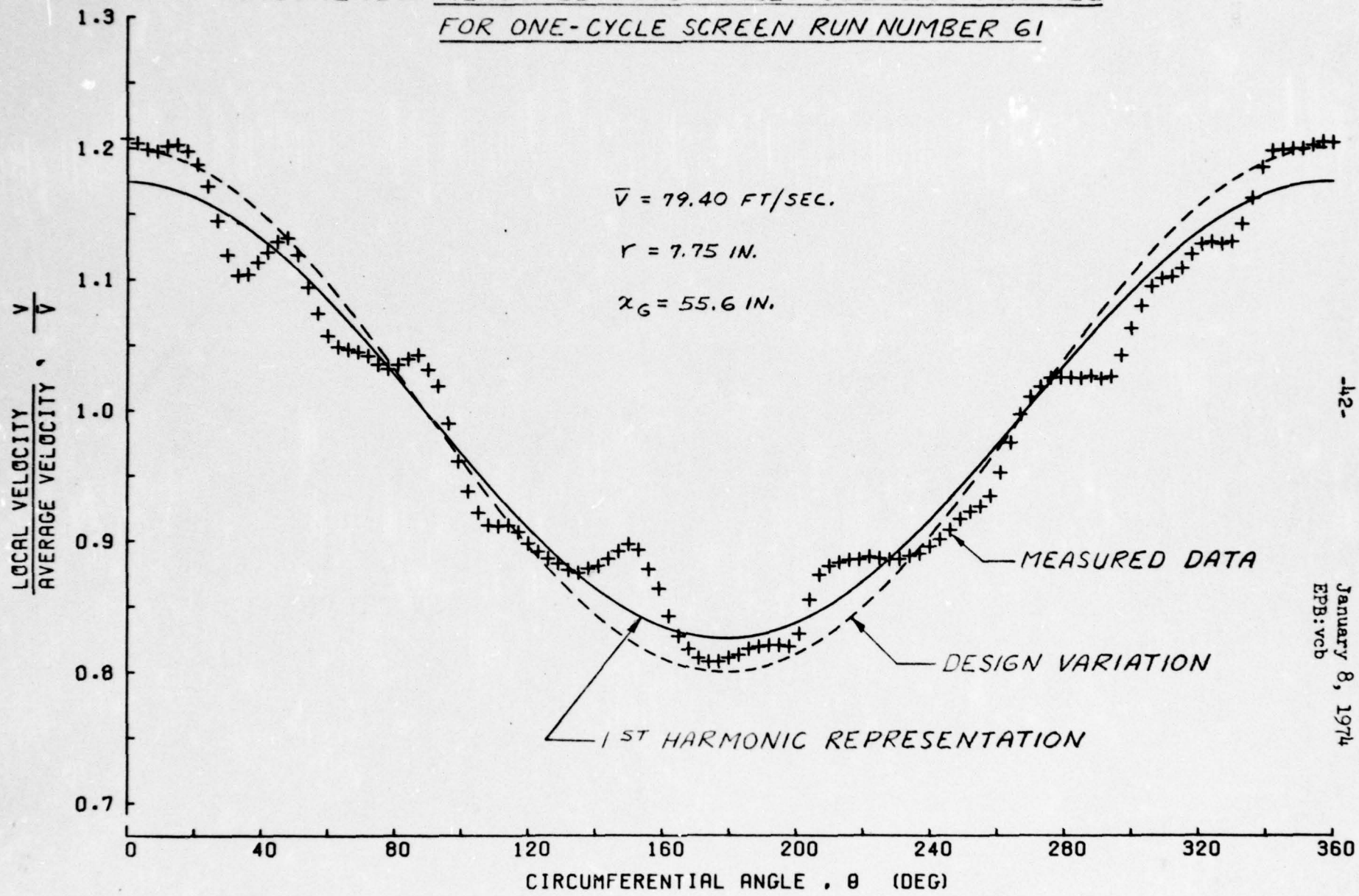

January 8, 1974
EPB:vcb

January 8, 1974
EPB:vcb

FIGURE 18b. FOURIER COEFFICIENT MAGNITUDE FOR ONE-CYCLE SCREEN RUN NUMBER 61

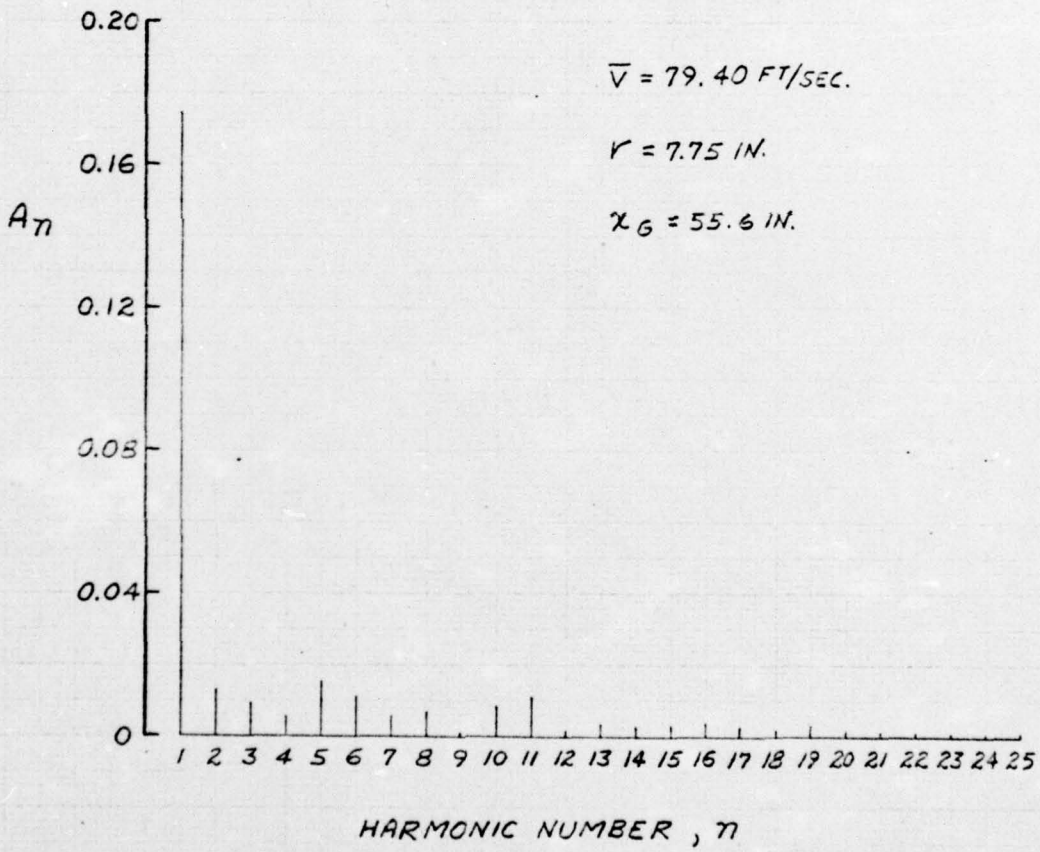

FIGURE 19a. MEASURED ROTOR INLET VELOCITY PROFILE FOR ONE-CYCLE SCREEN RUN NUMBER 97

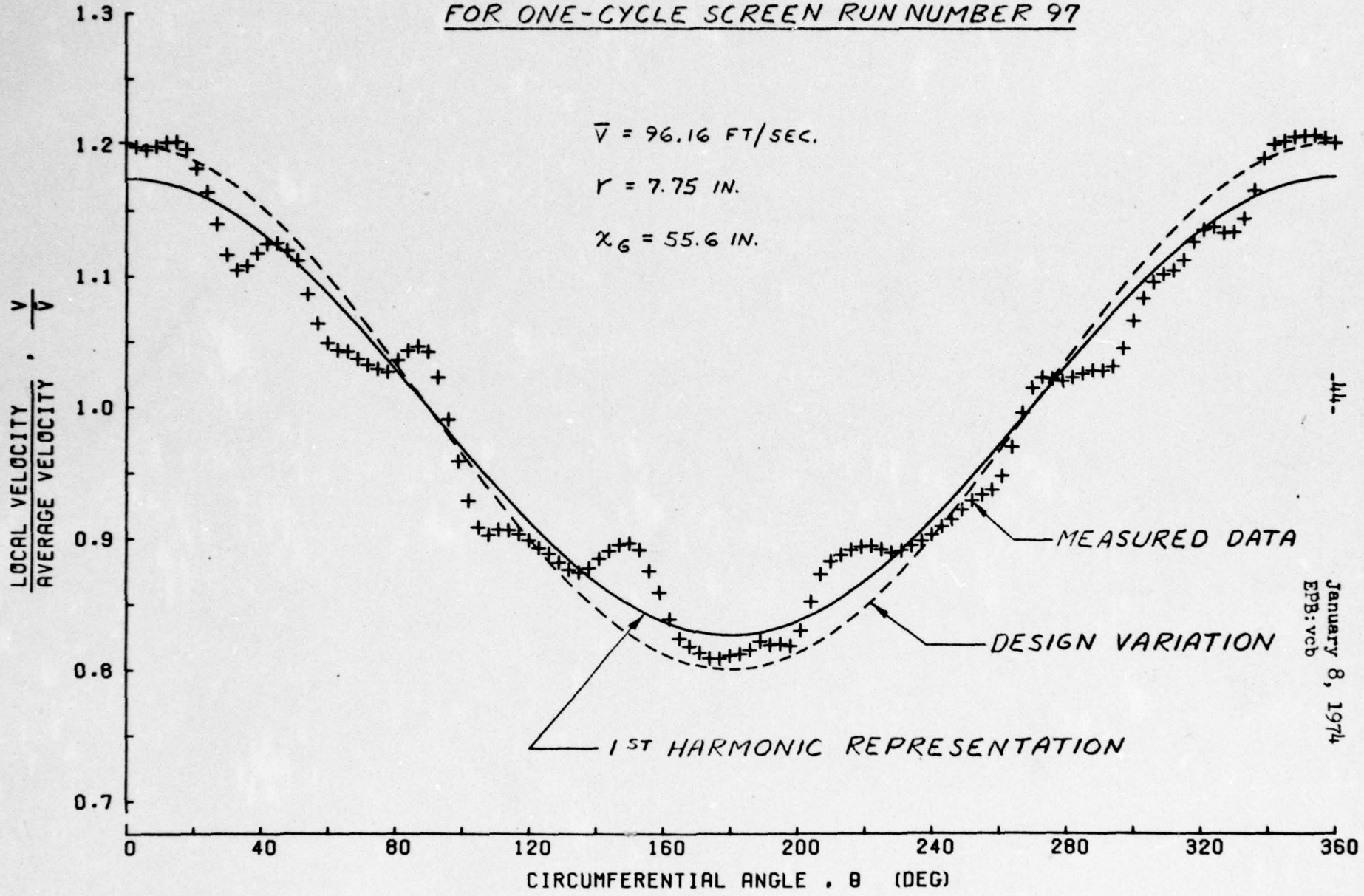

January 8, 1974
EPB:vcb

January 8, 1974
EPB:vcb

FIGURE 19b. FOURIER COEFFICIENT MAGNITUDE FOR ONE-CYCLE SCREEN RUN NUMBER 97

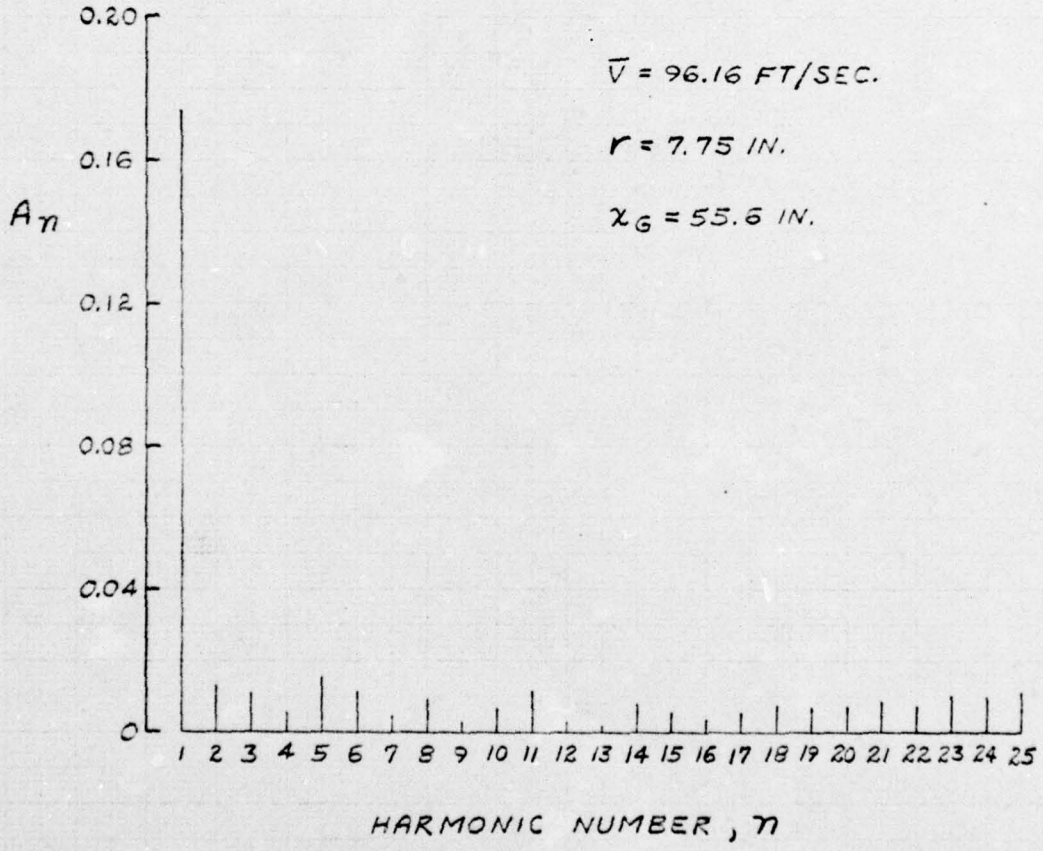

FIGURE 20a. MEASURED ROTOR INLET VELOCITY PROFILE FOR ONE-CYCLE SCREEN RUN NUMBER 65

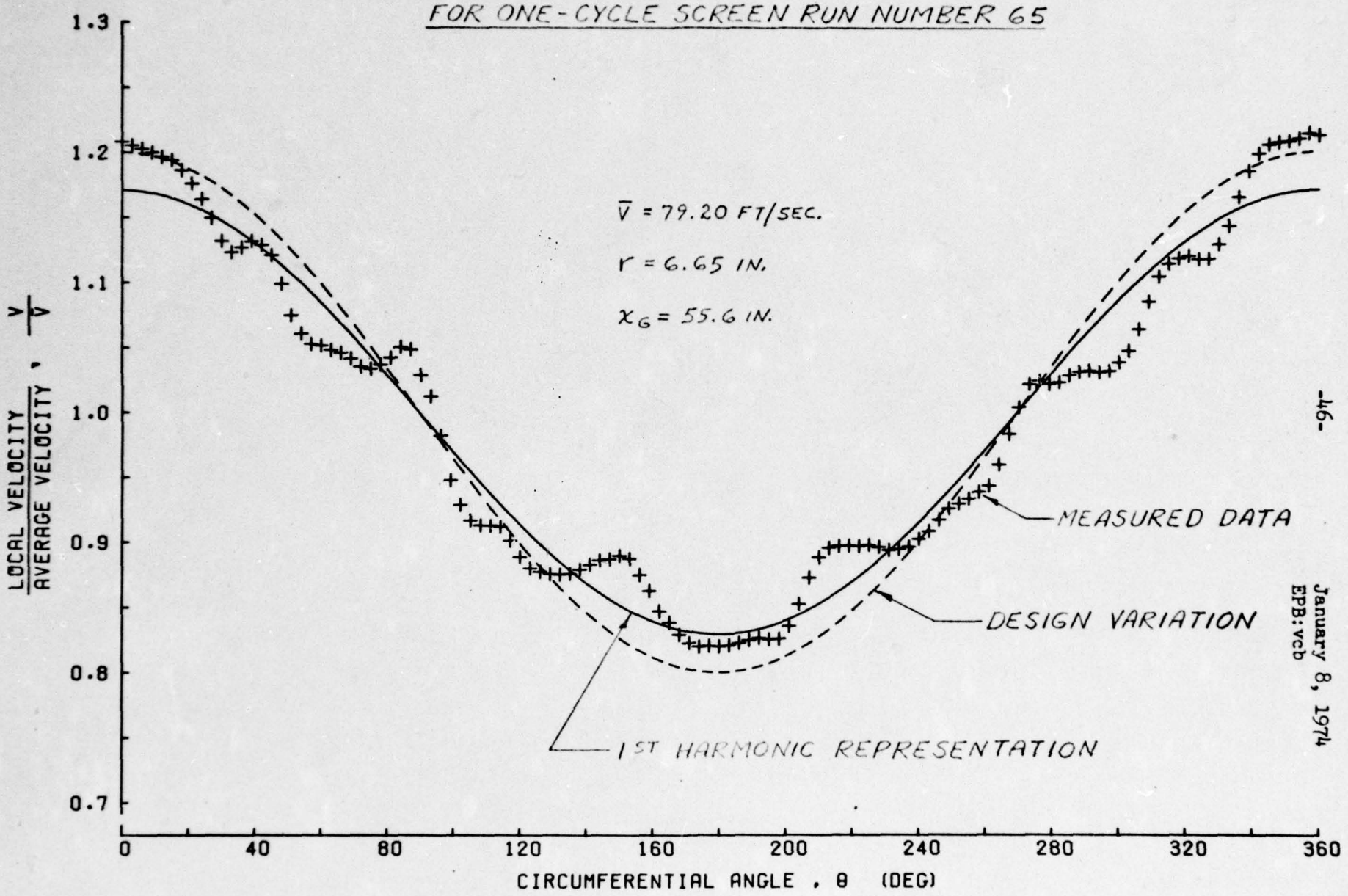

January 8, 1974
EPB:vcb

FIGURE 20b. FOURIER COEFFICIENT MAGNITUDE FOR ONE-CYCLE SCREEN RUN NUMBER 65

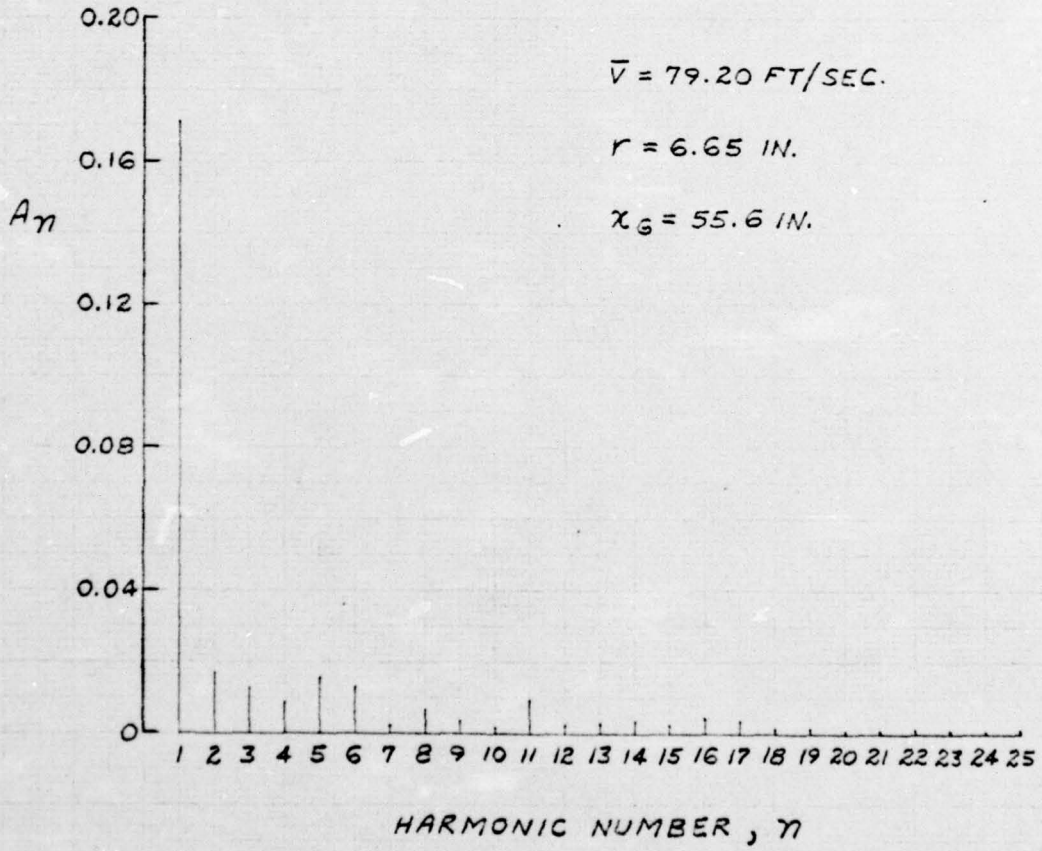

FIGURE 21a. MEASURED ROTOR INLET VELOCITY PROFILE FOR ONE-CYCLE SCREEN RUN NUMBER 63

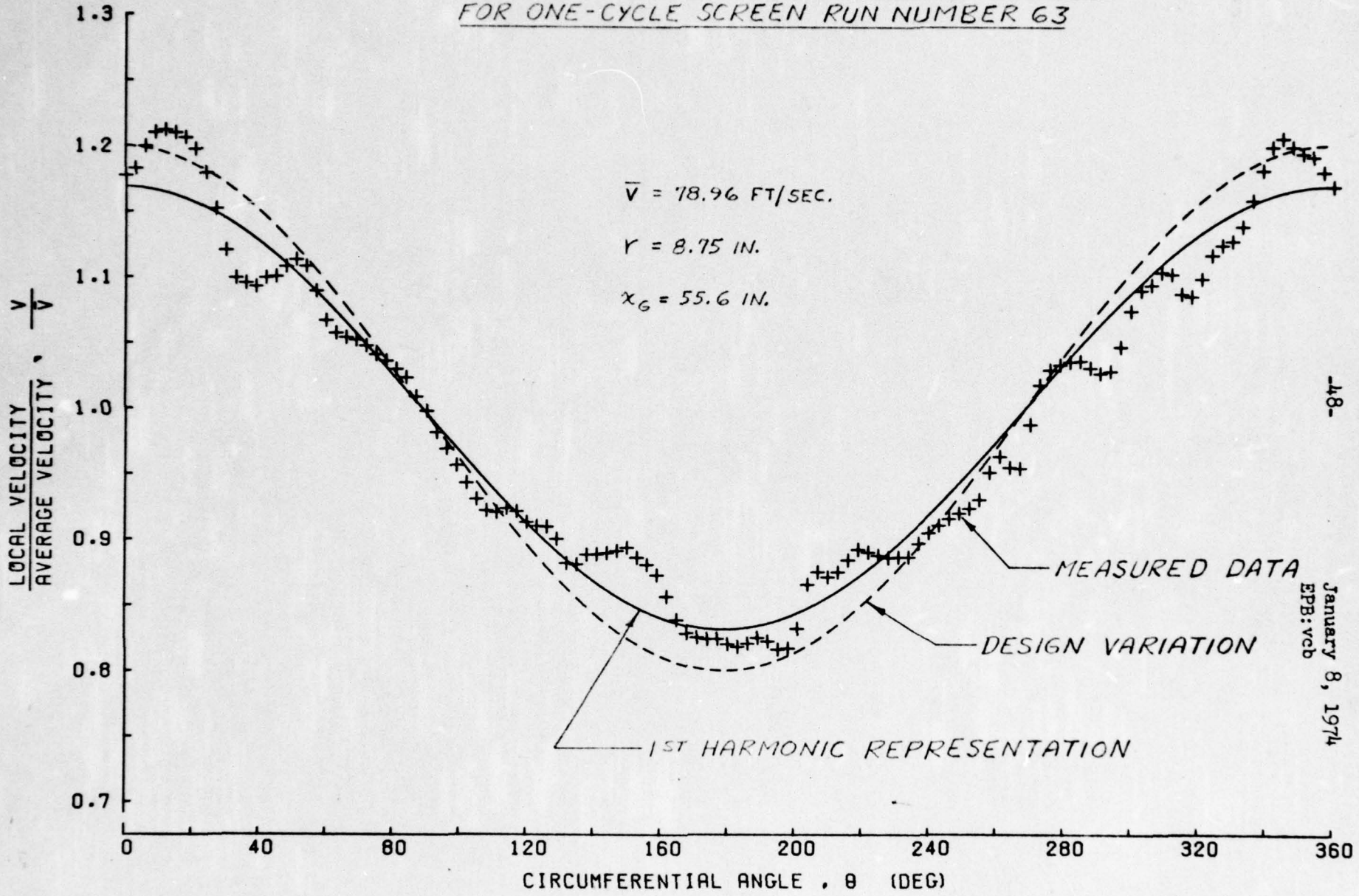

January 8, 1974
EPB:vcb

January 8, 1974
EPB:vcb

FIGURE 21a. FOURIER COEFFICIENT MAGNITUDE FOR ONE-CYCLE SCREEN RUN NUMBER 63

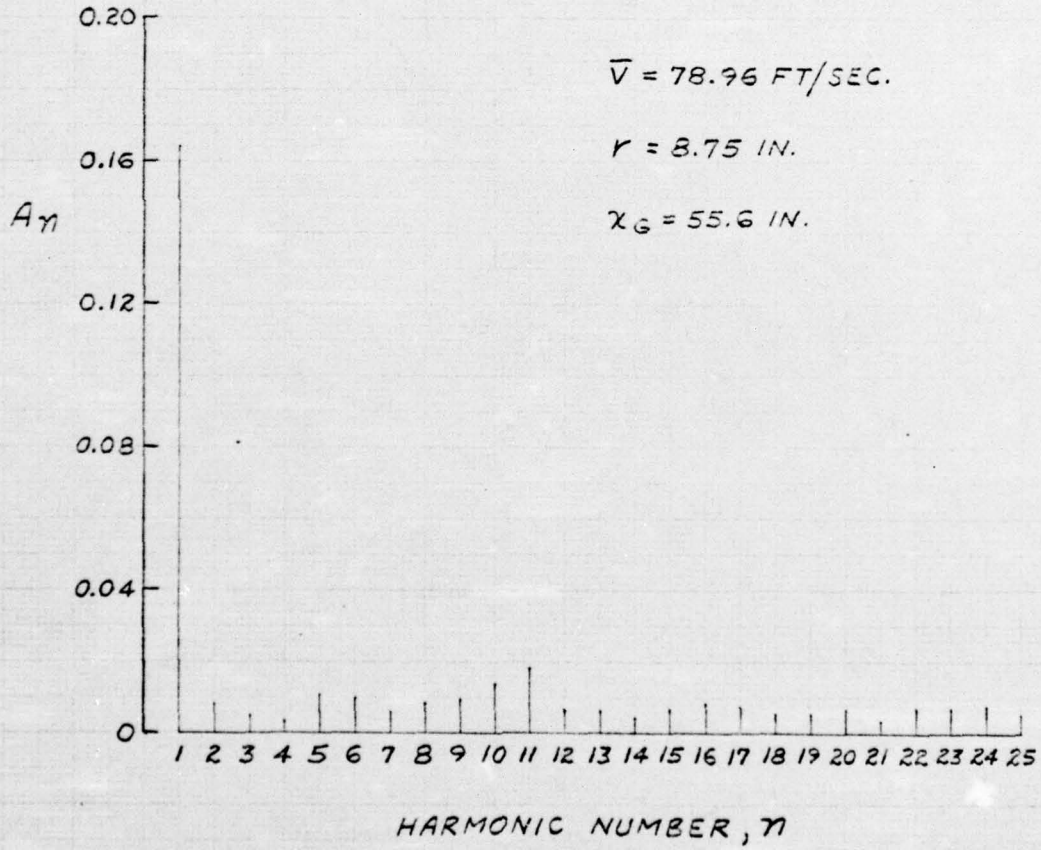

FIGURE 22a. MEASURED ROTOR INLET VELOCITY PROFILE FOR ONE-CYCLE SCREEN RUN NUMBER 68

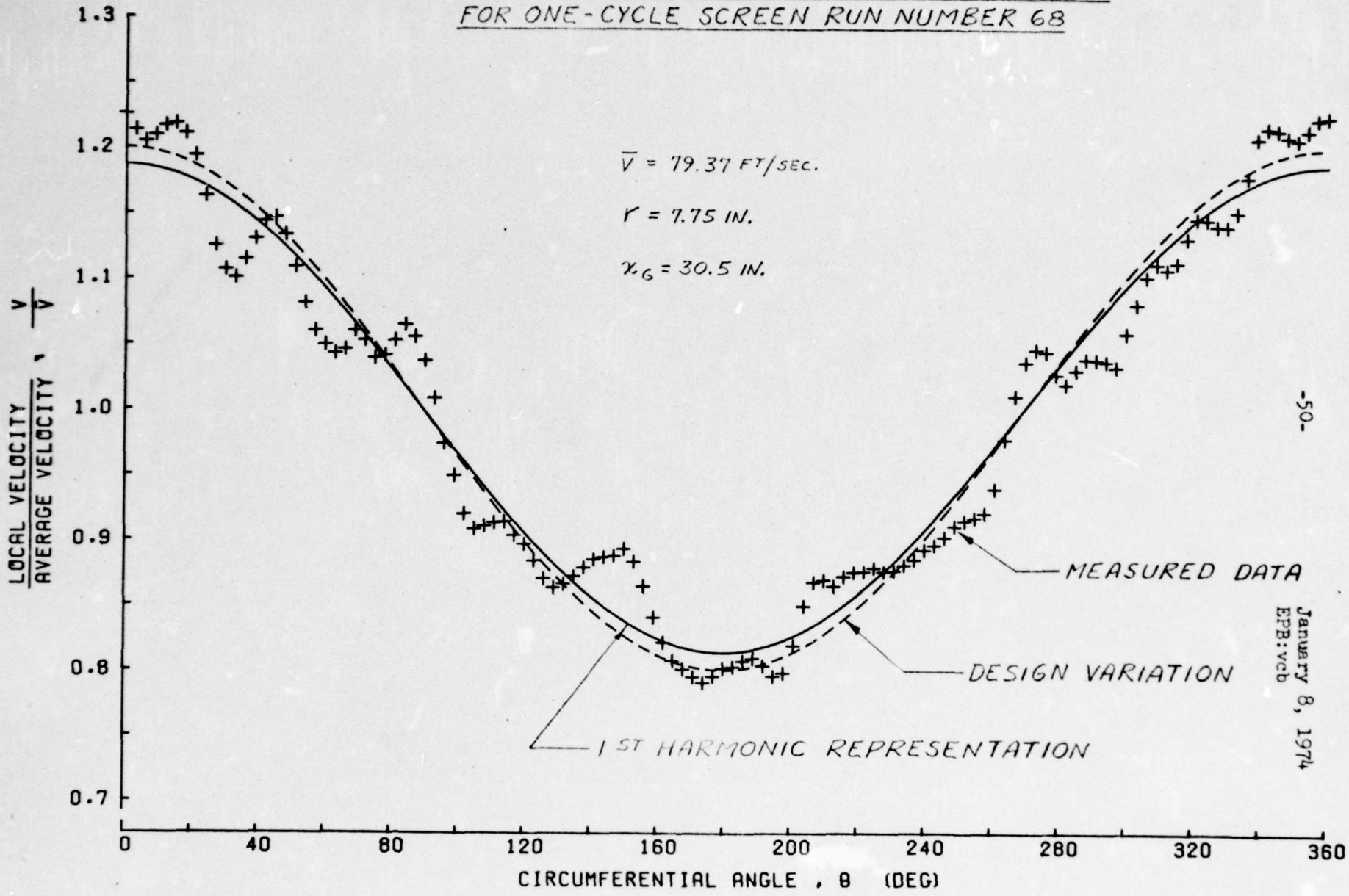

January 8, 1974
EPB:vcb

January 8, 1974
EPB:vcb

FIGURE 22b. FOURIER COEFFICIENT MAGNITUDE FOR ONE-CYCLE SCREEN RUN NUMBER 68

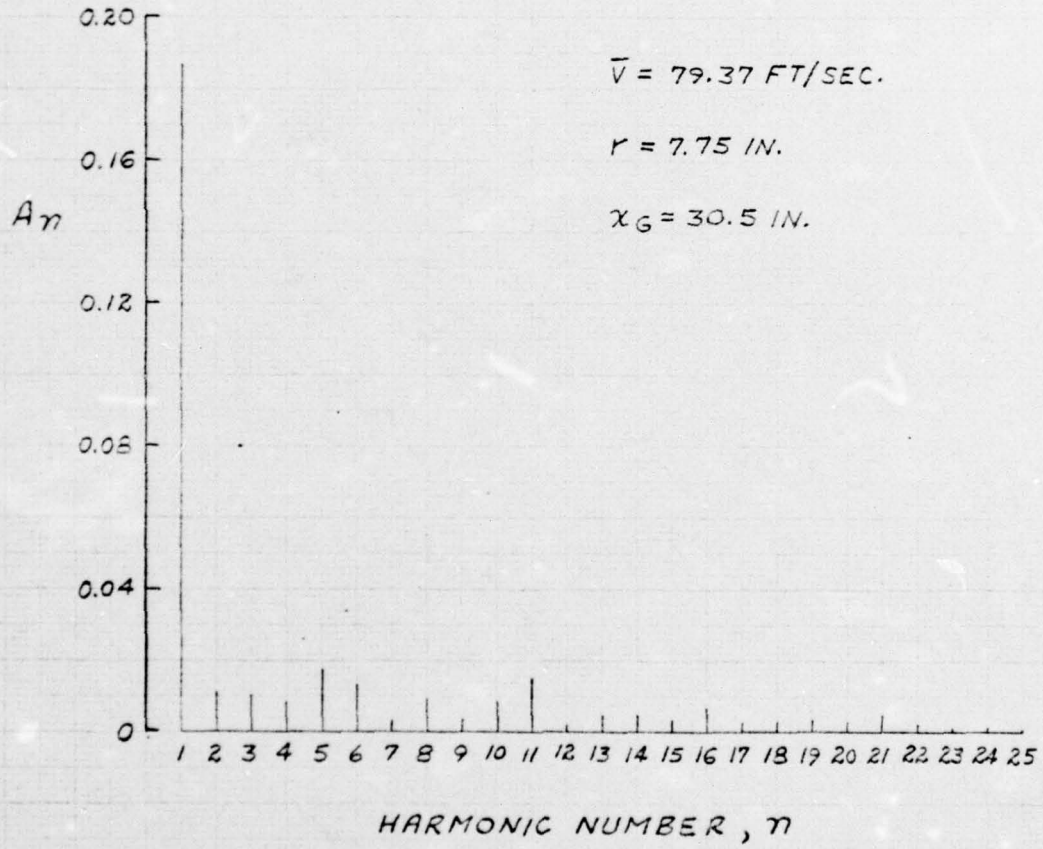

FIGURE 23a. MEASURED ROTOR INLET VELOCITY PROFILE FOR ONE-CYCLE SCREEN RUN NUMBER 67

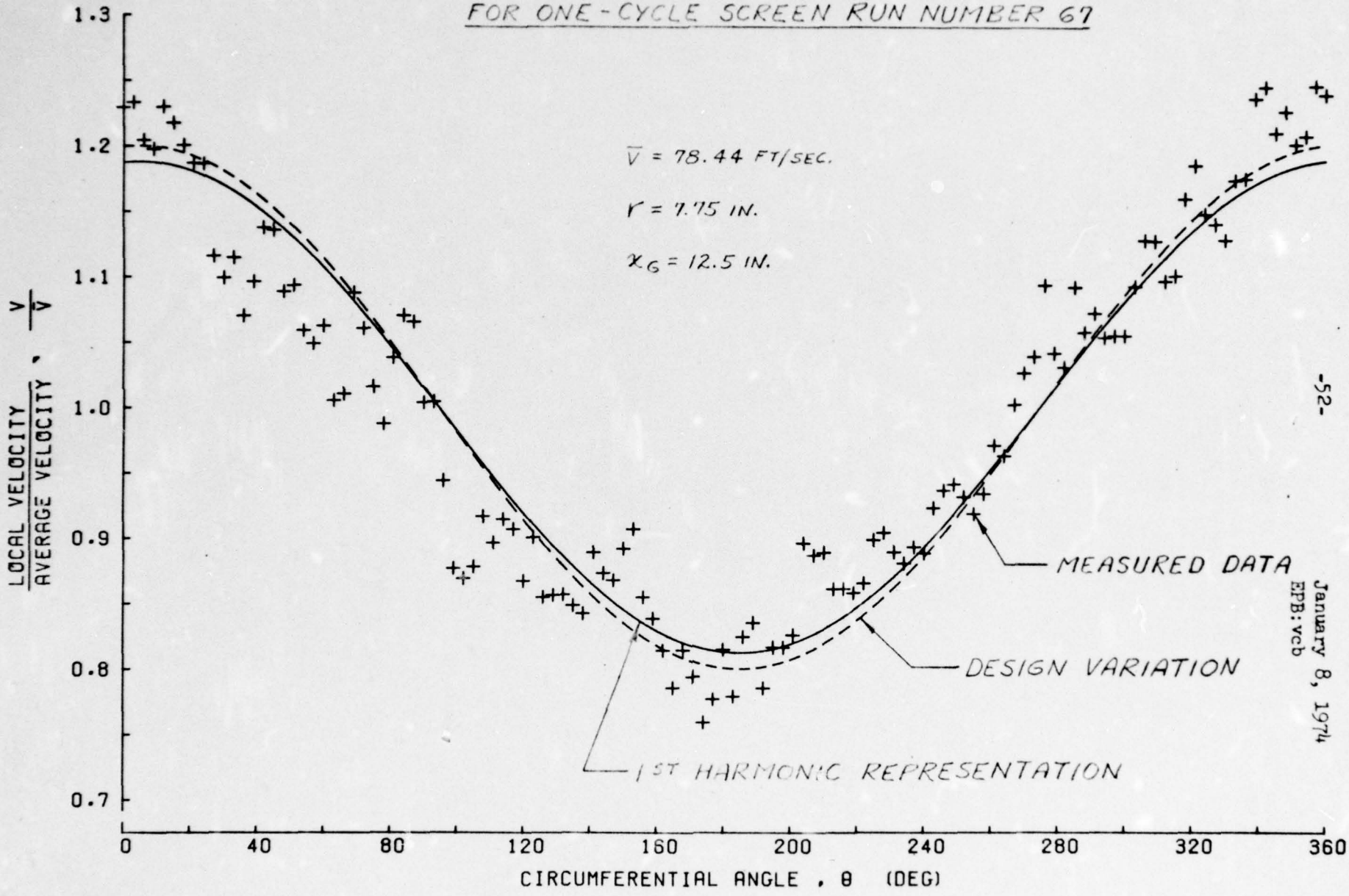

January 8, 1974
EPB:vcb

FIGURE 23b. FOURIER COEFFICIENT MAGNITUDE FOR ONE-CYCLE SCREEN RUN NUMBER 67

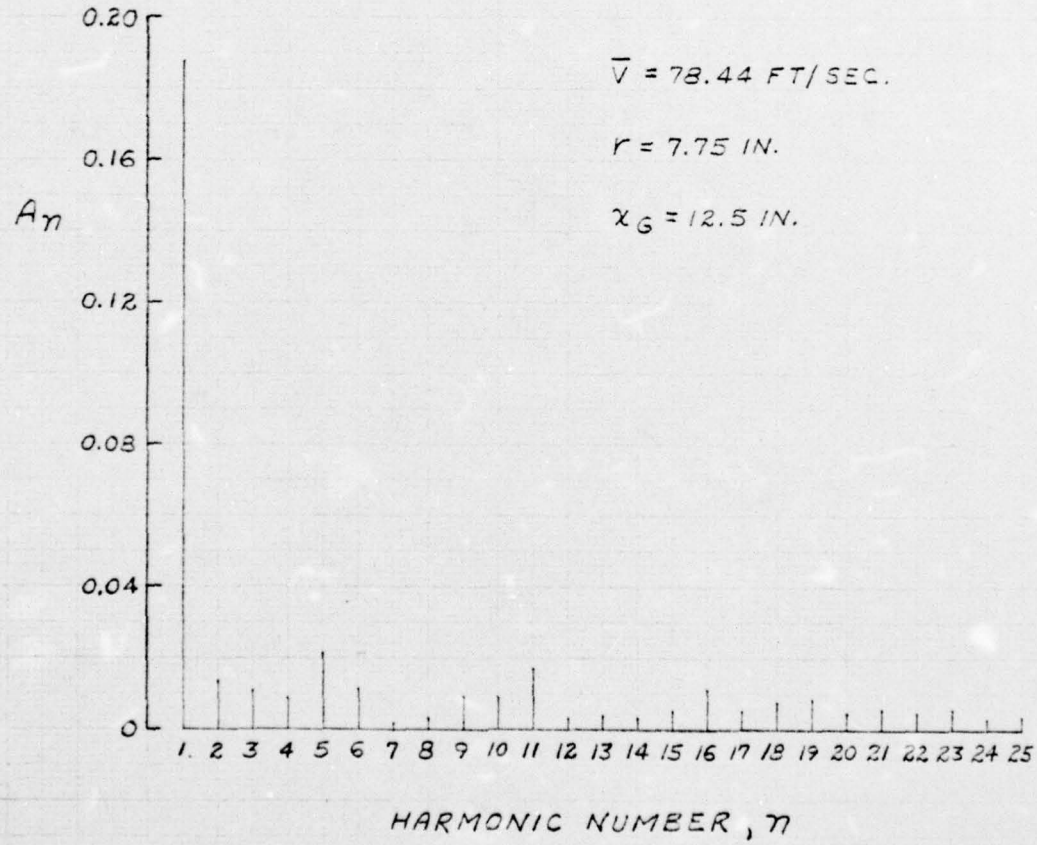

FIGURE 24a. MEASURED ROTOR INLET VELOCITY PROFILE FOR TWO-CYCLE SCREEN RUN NUMBER 74

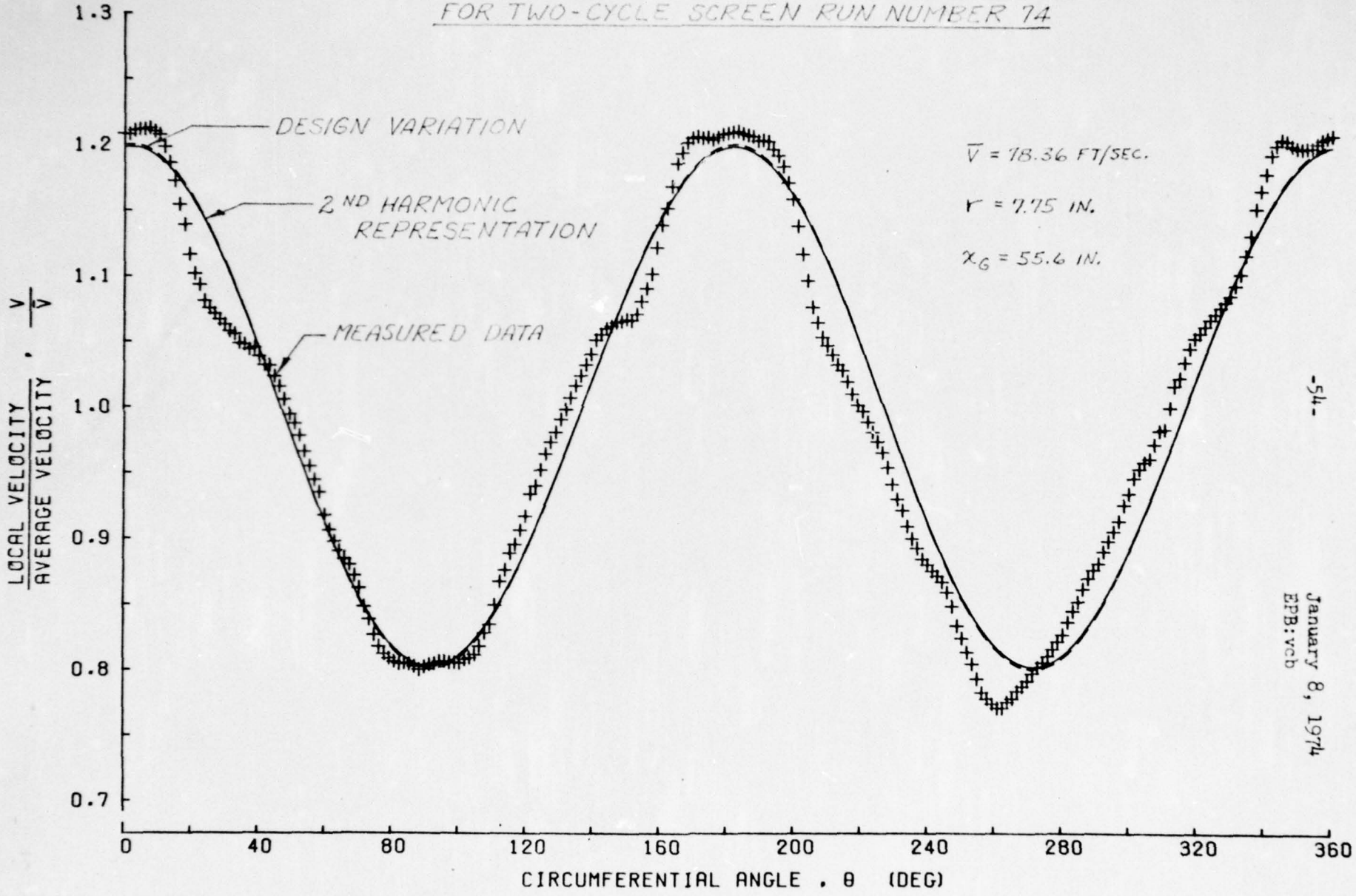

January 8, 1974
EPB:vcb

January 8, 1974
EPB:vcb

FIGURE 24b. FOURIER COEFFICIENT MAGNITUDE FOR TWO-CYCLE SCREEN RUN NUMBER 74

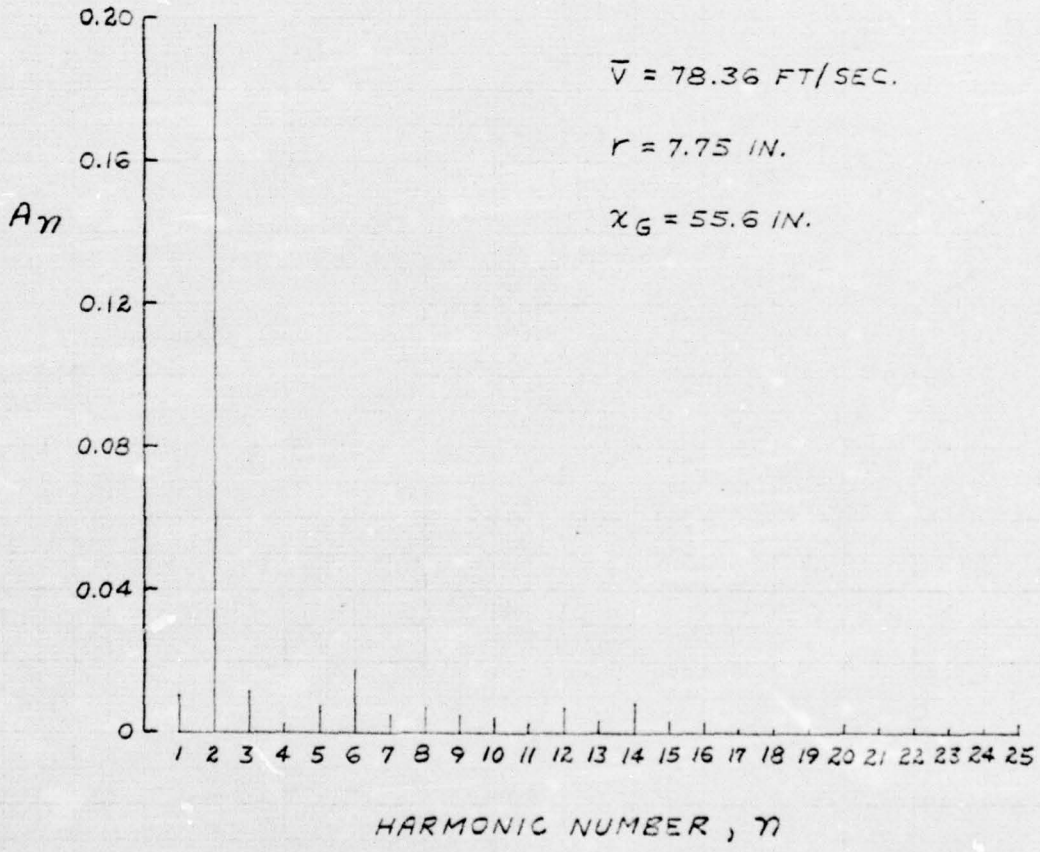

FIGURE 25a. MEASURED ROTOR INLET VELOCITY PROFILE FOR FOUR-CYCLE SCREEN RUN NUMBER 76

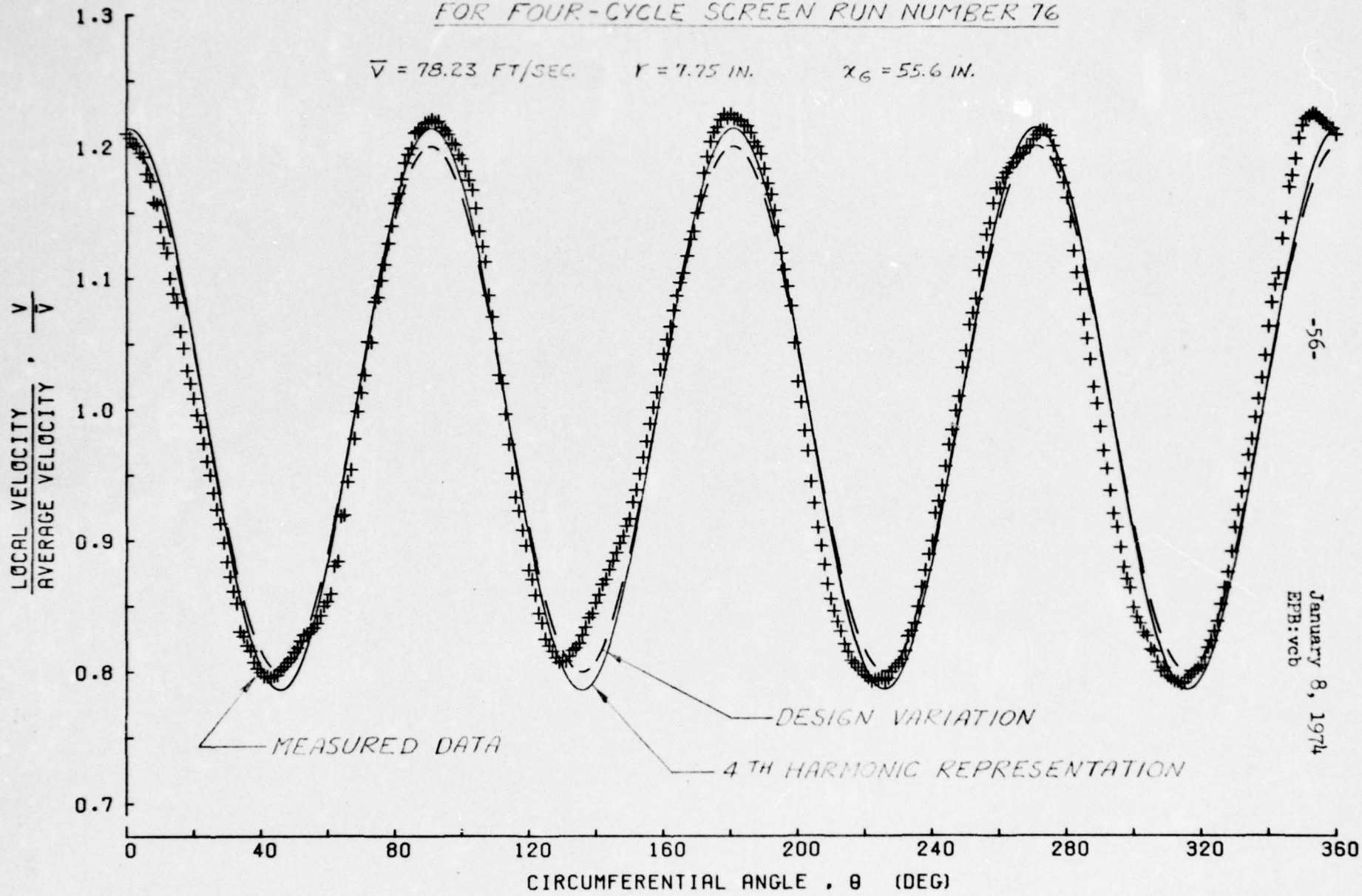

January 8, 1974
EPB:vcb

January 8, 1974
EPB: vcb

FIGURE 25ℓ. FOURIER COEFFICIENT MAGNITUDE FOR FOUR-CYCLE SCREEN RUN NUMBER 76

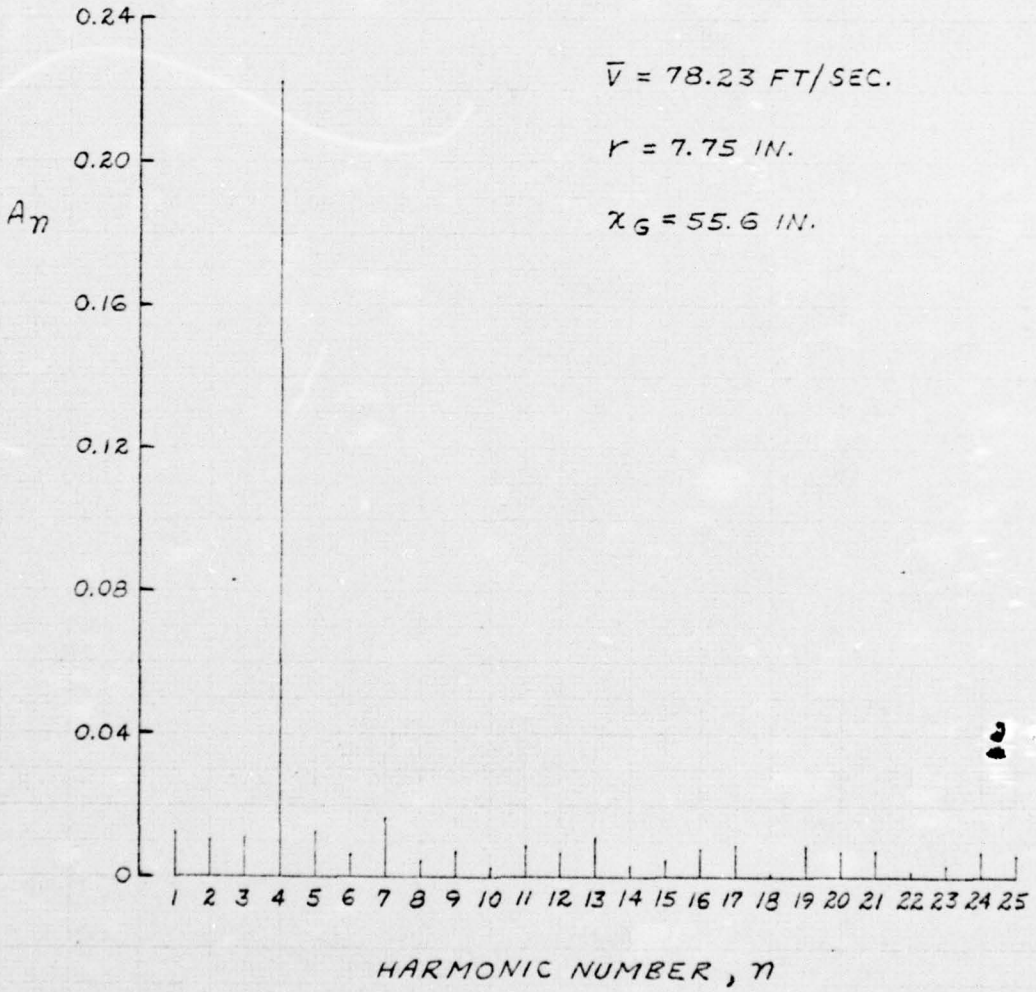

FIGURE 26a. MEASURED ROTOR INLET VELOCITY PROFILE FOR SIX-CYCLE SCREEN RUN NUMBER 81

$\bar{V}$ = 42.81 FT/SEC. r = 7.75 IN. x_G = 55.6 IN.

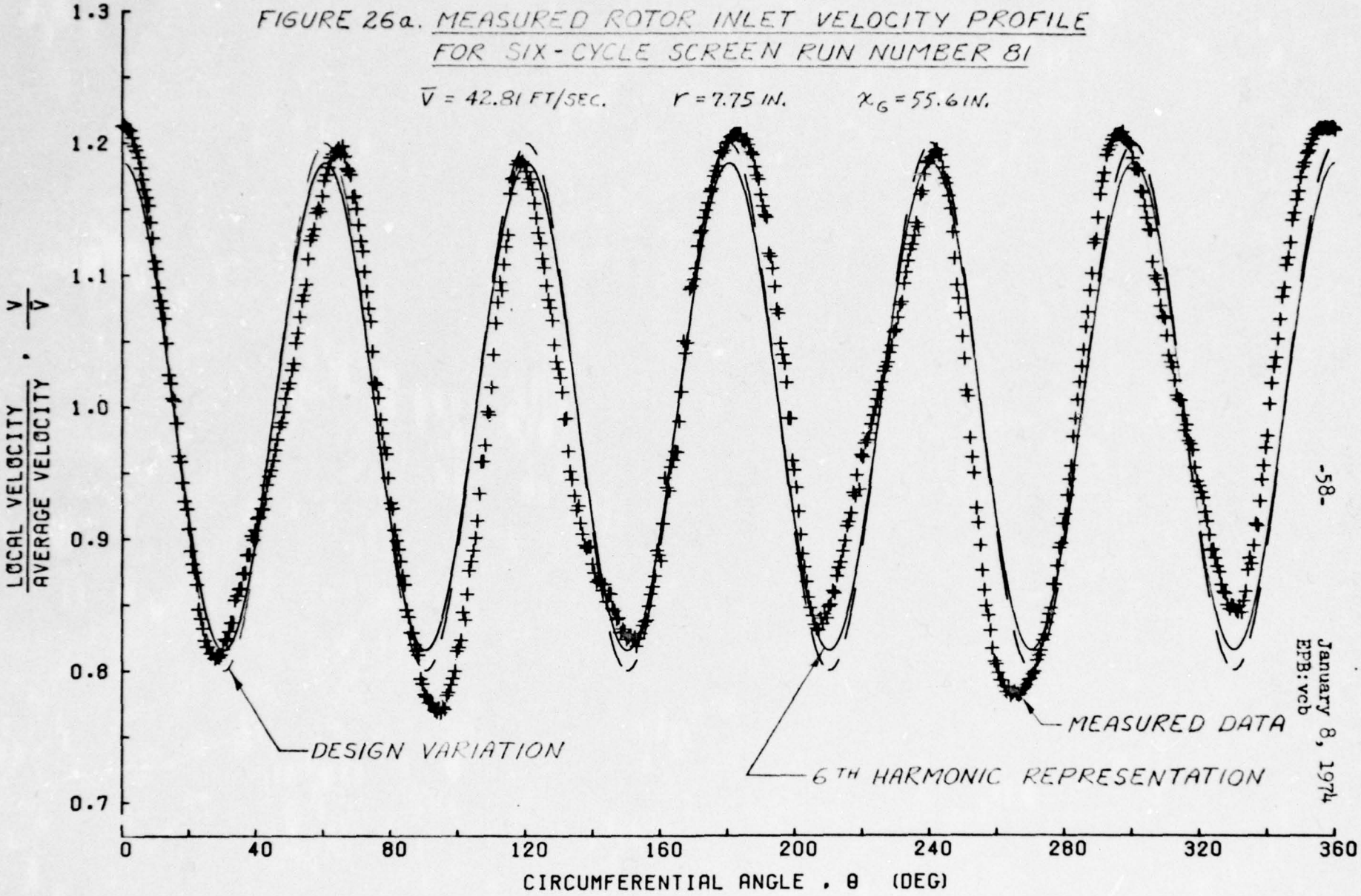

January 8, 1974
EPB:vcb

January 8, 1974
EPB:vcb

FIGURE 26b. FOURIER COEFFICIENT MAGNITUDE FOR SIX-CYCLE SCREEN RUN NUMBER 81

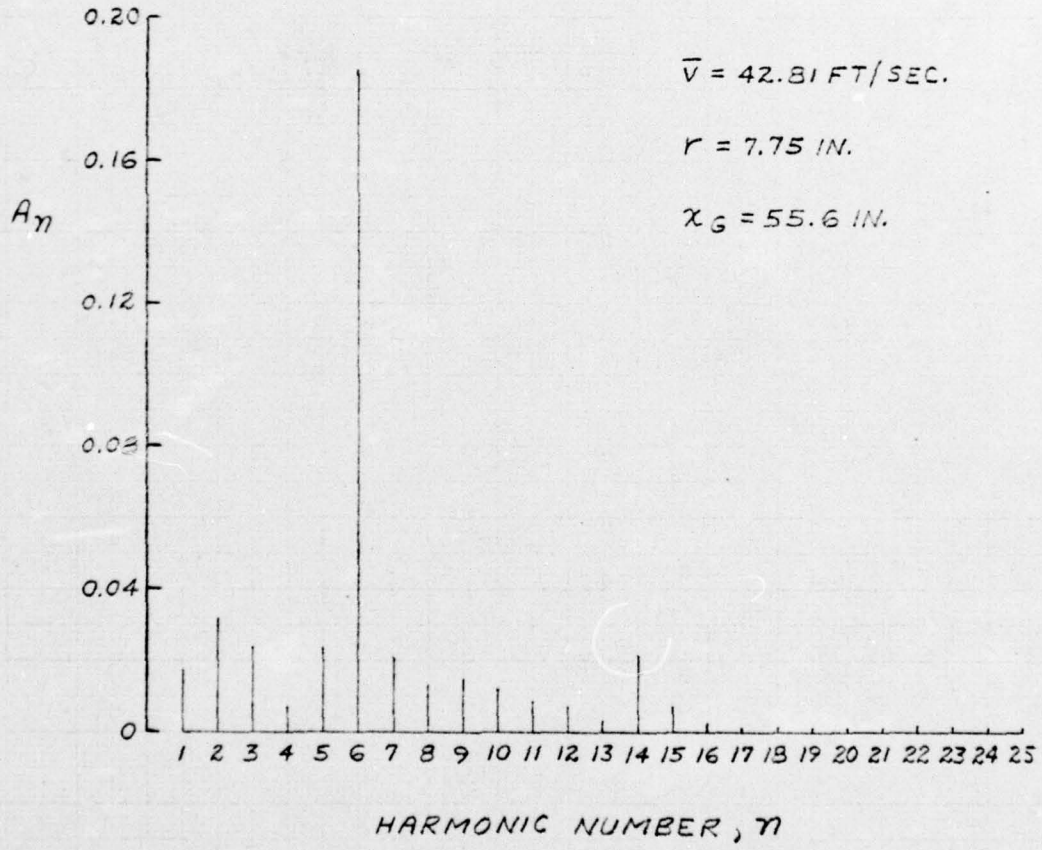

FIGURE 27a. MEASURED ROTOR INLET VELOCITY PROFILE FOR SIX-CYCLE SCREEN RUN NUMBER 84

$\bar{V}$ = 78.36 FT/SEC. r = 7.75 IN. x_G = 55.6 IN.

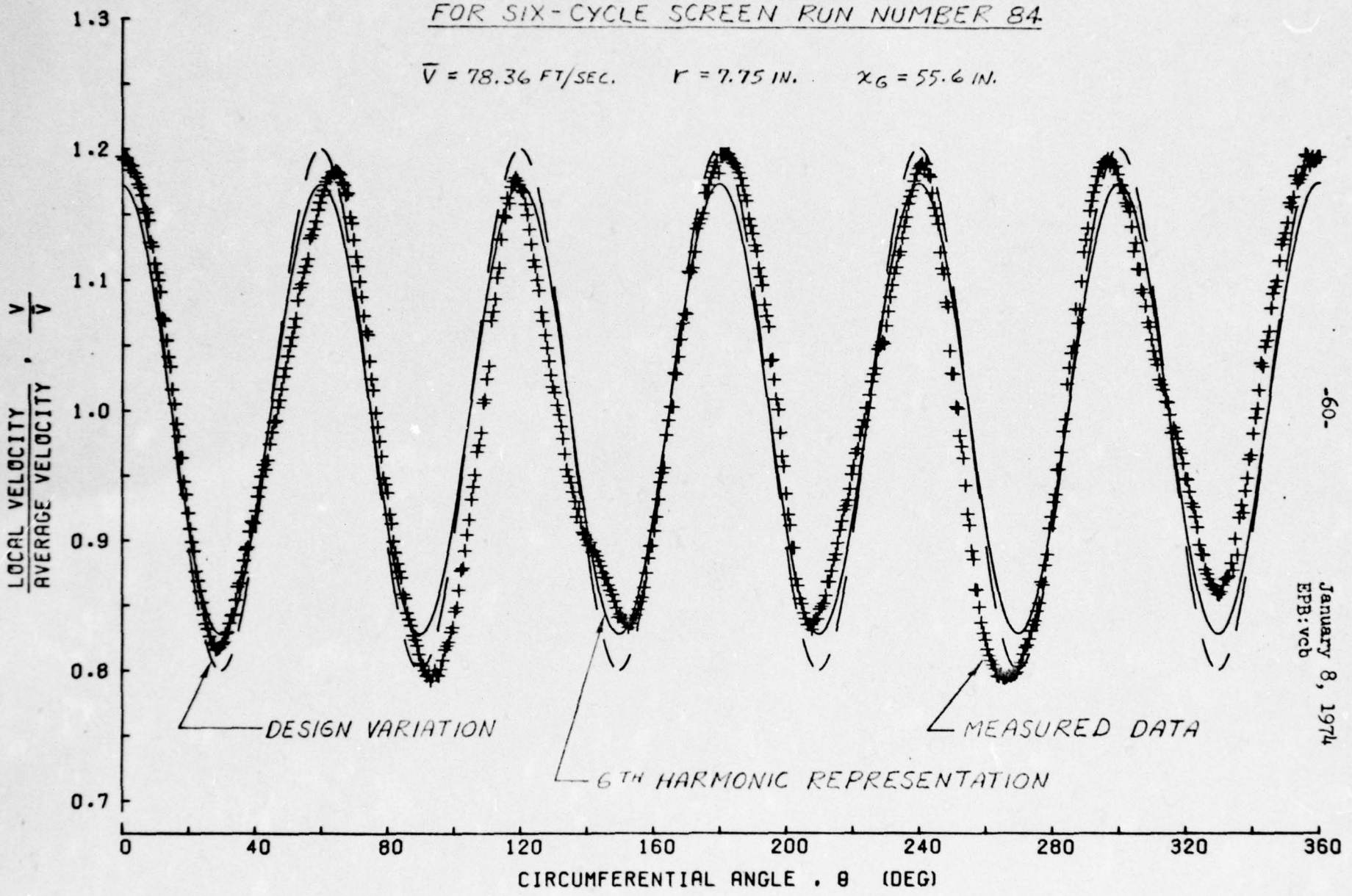

January 8, 1974
EPB:vcb

January 8, 1974
EPB:vcb

FIGURE 27a. FOURIER COEFFICIENT MAGNITUDE FOR SIX-CYCLE SCREEN RUN NUMBER 84

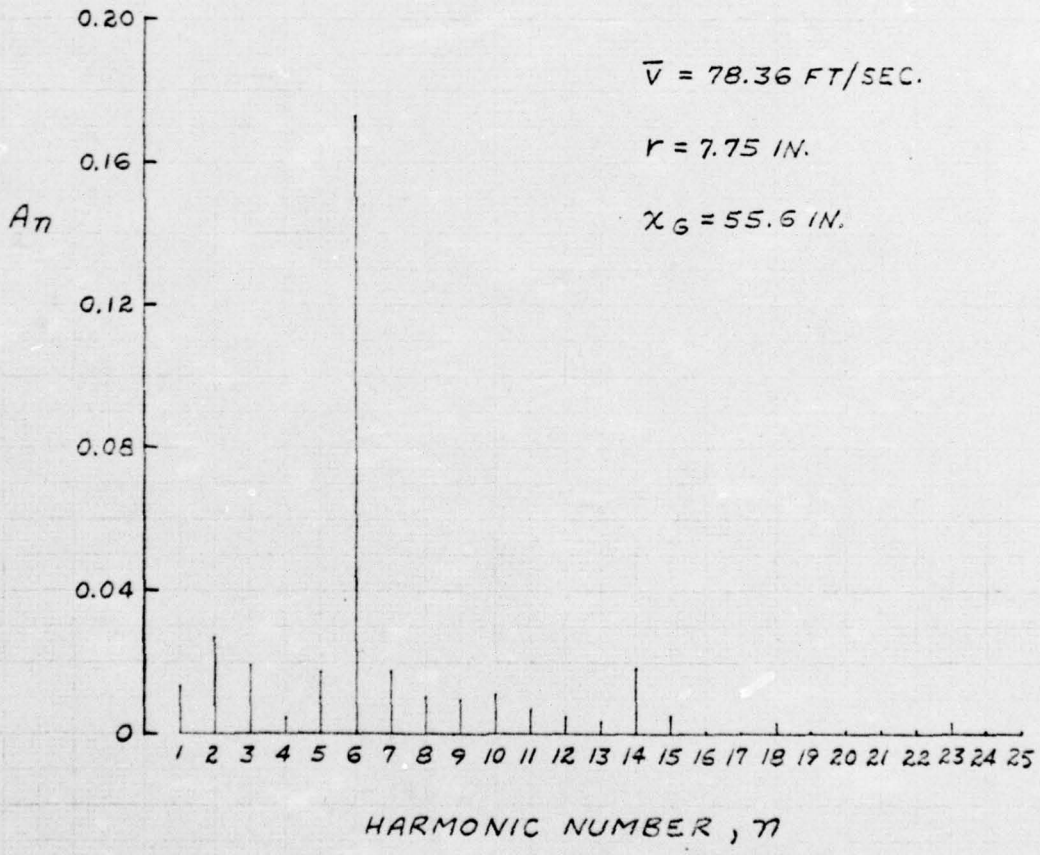

FIGURE 28a. MEASURED ROTOR INLET VELOCITY PROFILE FOR NINE-CYCLE SCREEN RUN NUMBER 100

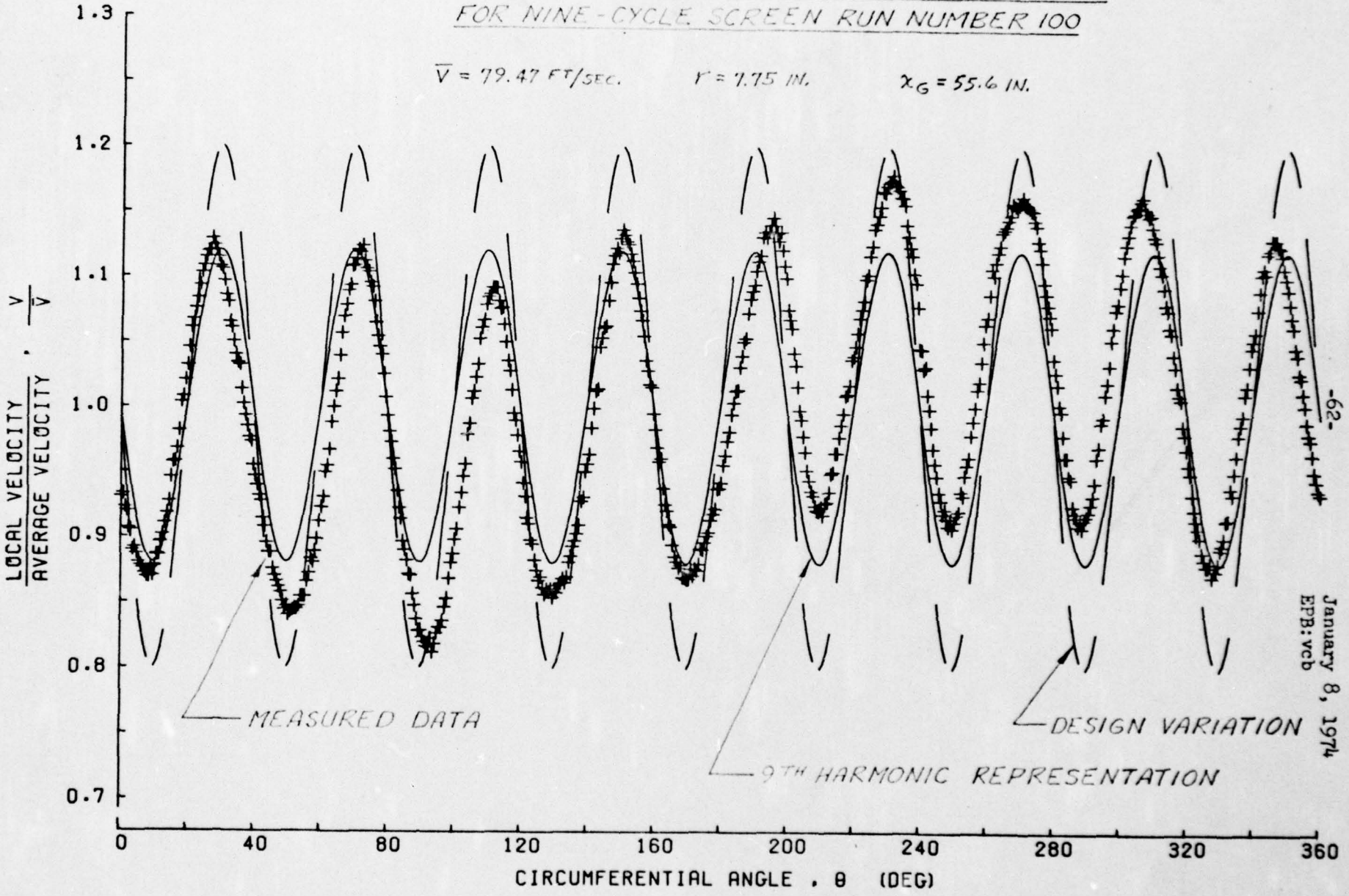

January 8, 1974
EPB:vcb

FIGURE 28b. FOURIER COEFFICIENT MAGNITUDE FOR NINE-CYCLE SCREEN RUN NUMBER 100

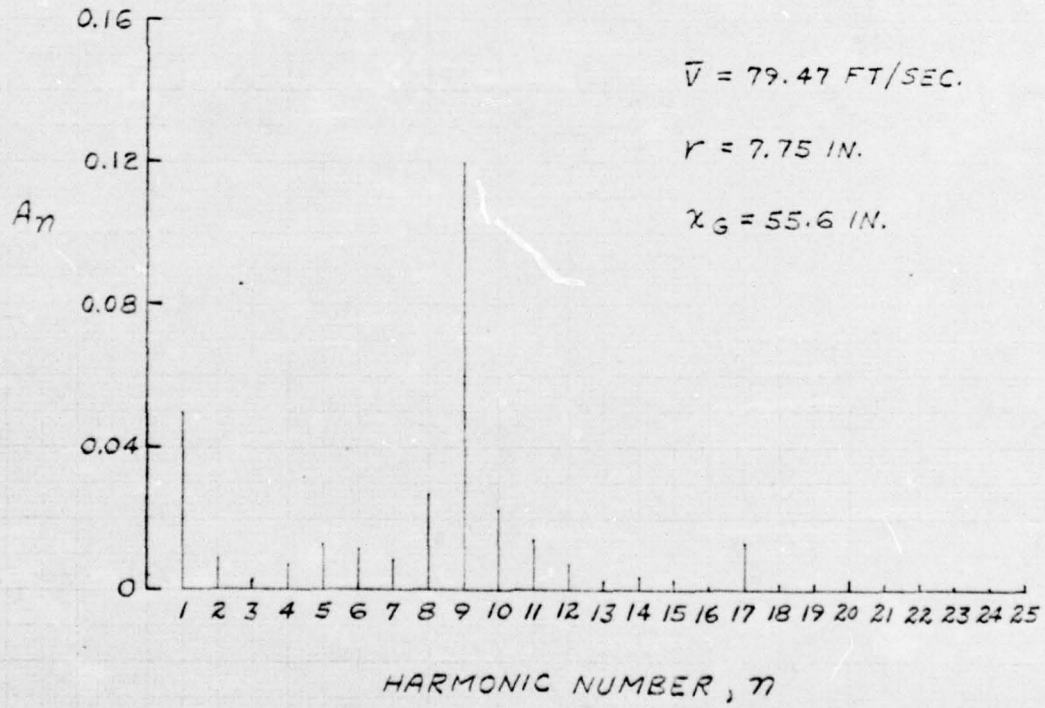

FIGURE 29 a. MEASURED ROTOR INLET VELOCITY PROFILE FOR NINE-CYCLE SCREEN RUN NUMBER 113

$\bar{V}$ = 77.68 FT/SEC. r = 7.75 IN. x_6 = 30.0 IN.

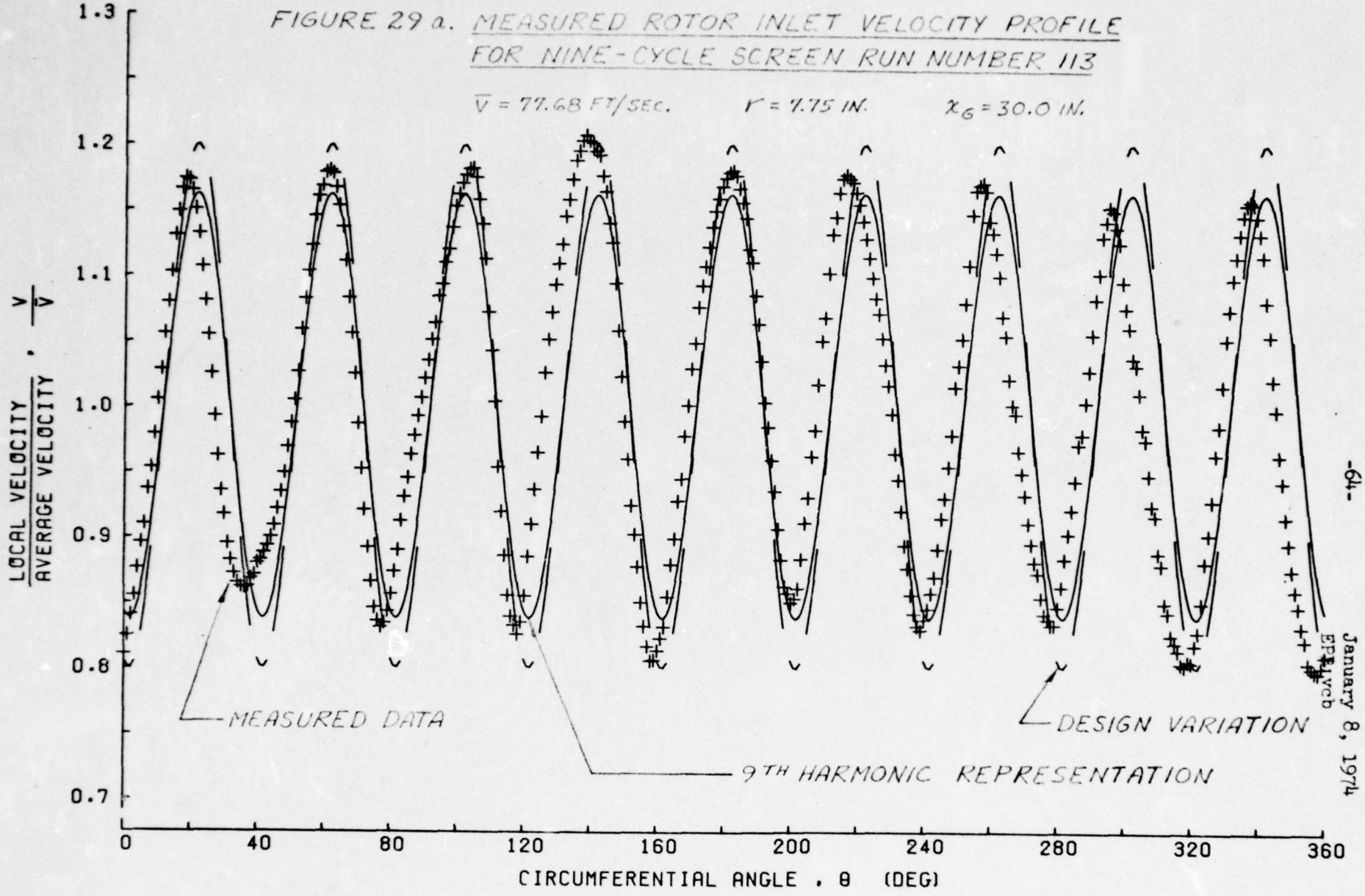

January 8, 1974
EPLycb

January 8, 1974
EPB: vcb

FIGURE 29b. FOURIER COEFFICIENT MAGNITUDE FOR NINE-CYCLE SCREEN RUN NUMBER 113

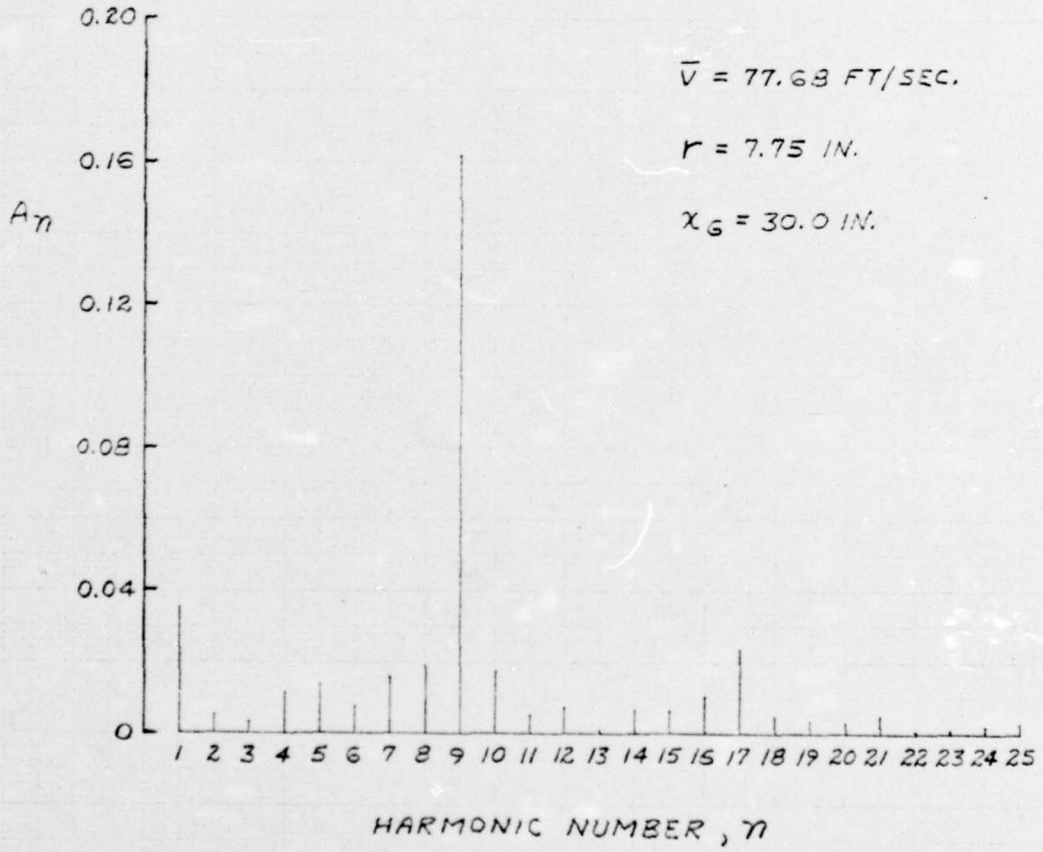

FIGURE 30 a. MEASURED ROTOR INLET VELOCITY PROFILE FOR NINE-CYCLE SCREEN RUN NUMBER 109

$\bar{V}$ = 77.63 FT/SEC. r = 7.75 IN. x_G = 12.4 IN.

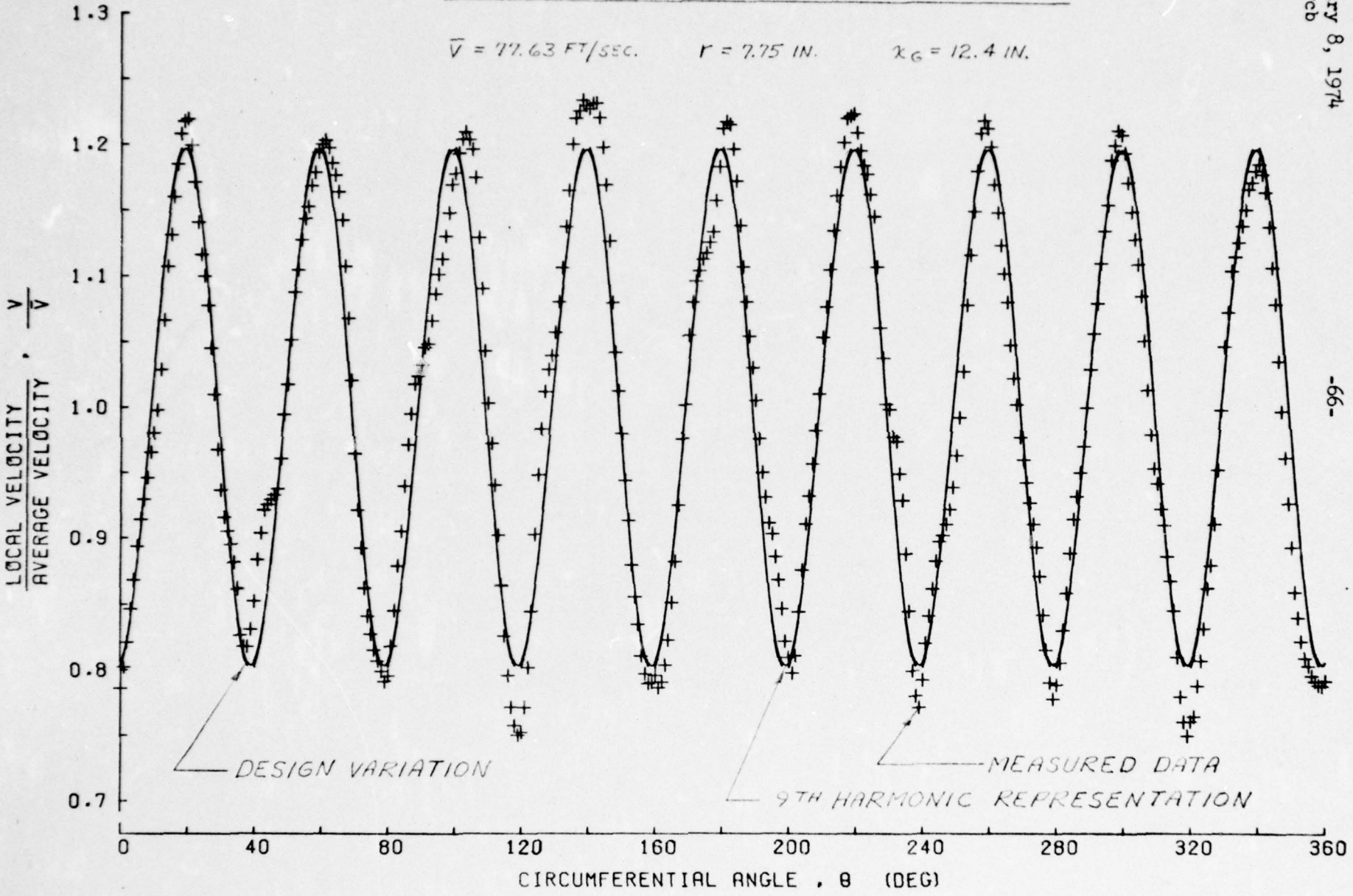

January 8, 1974
EPB:vcb

January 8, 1974
EPB:vcb

FIGURE 30b. FOURIER COEFFICIENT MAGNITUDE FOR NINE-CYCLE SCREEN RUN NUMBER 109

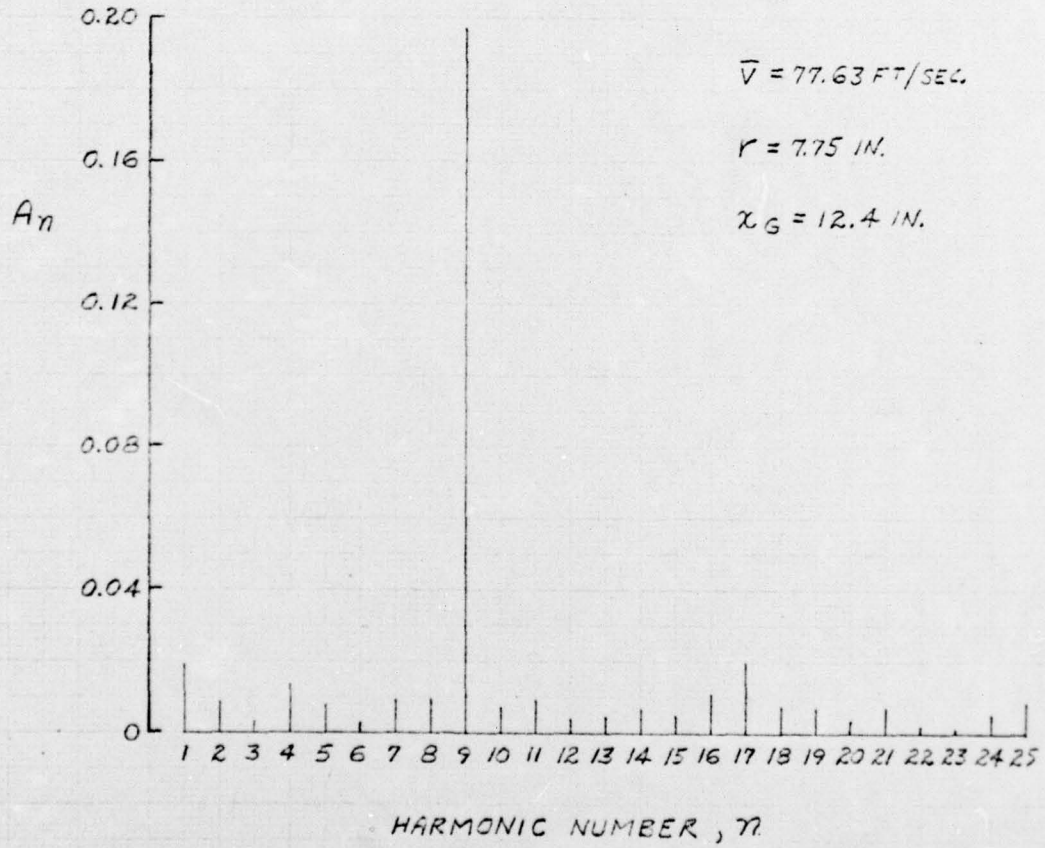

FIGURE 31a. MEASURED ROTOR INLET VELOCITY PROFILE FOR FIFTEEN-CYCLE SCREEN RUN NUMBER 115

$\bar{V}$ = 80.08 FT/SEC. r = 7.75 IN. x_G = 12.4 IN.

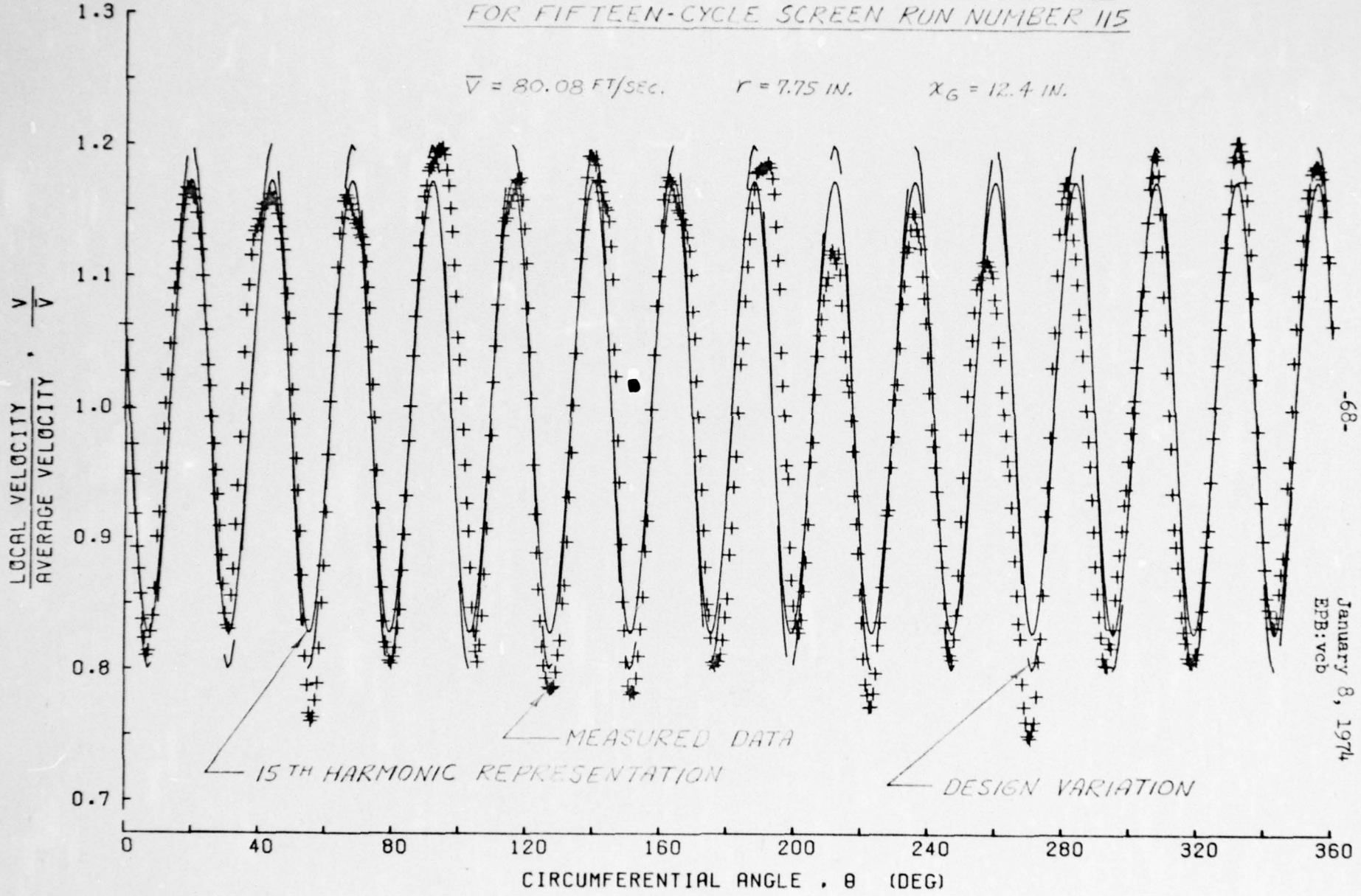

January 8, 1974
EPB:vcb

FIGURE 31 c. FOURIER COEFFICIENT MAGNITUDE FOR FIFTEEN-CYCLE SCREEN RUN NUMBER 115

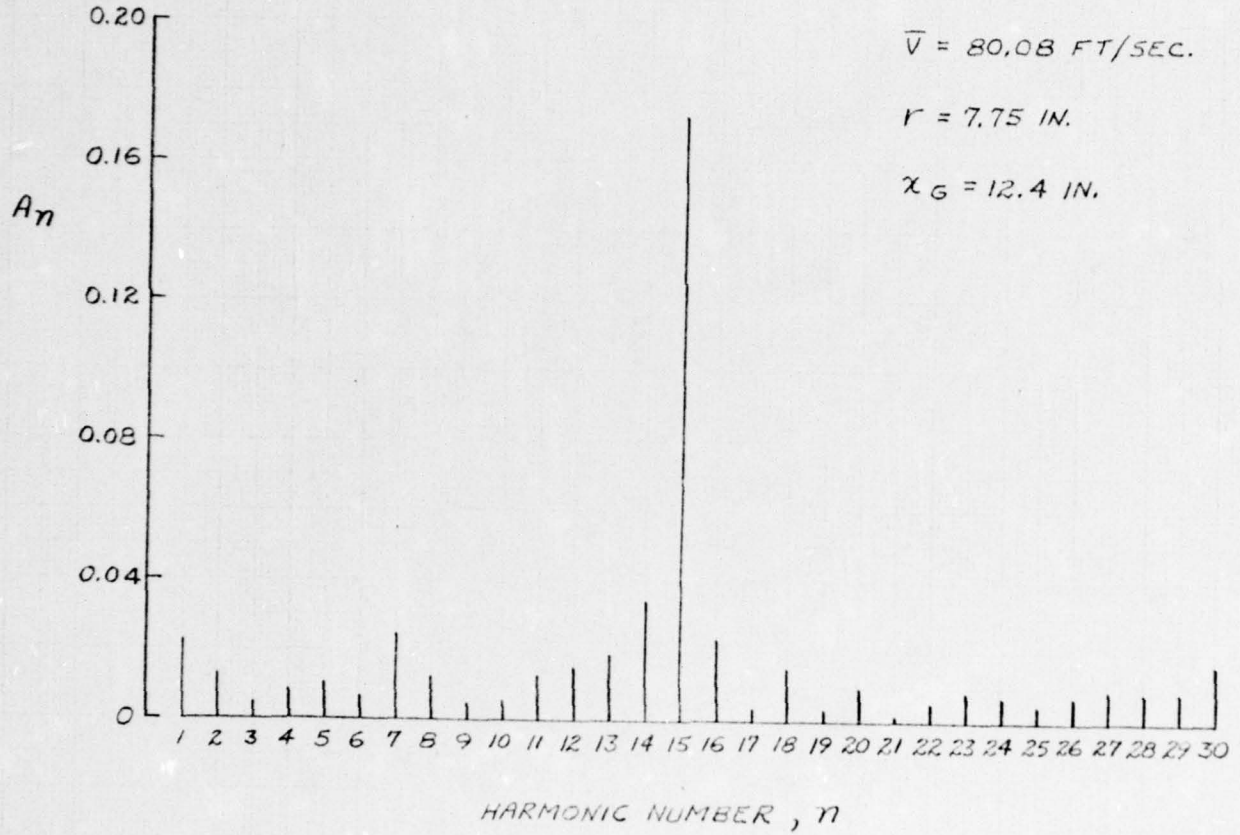

January 8, 1974
EPB:vcb

FIGURE 32a. MEASURED ROTOR INLET VELOCITY PROFILE FOR ORIGINAL ONE-CYCLE SCREEN RUN NUMBER 49

$\bar{V}$ = 63.75 FT/SEC. r = 7.75 IN. x_G = 55.6 IN.

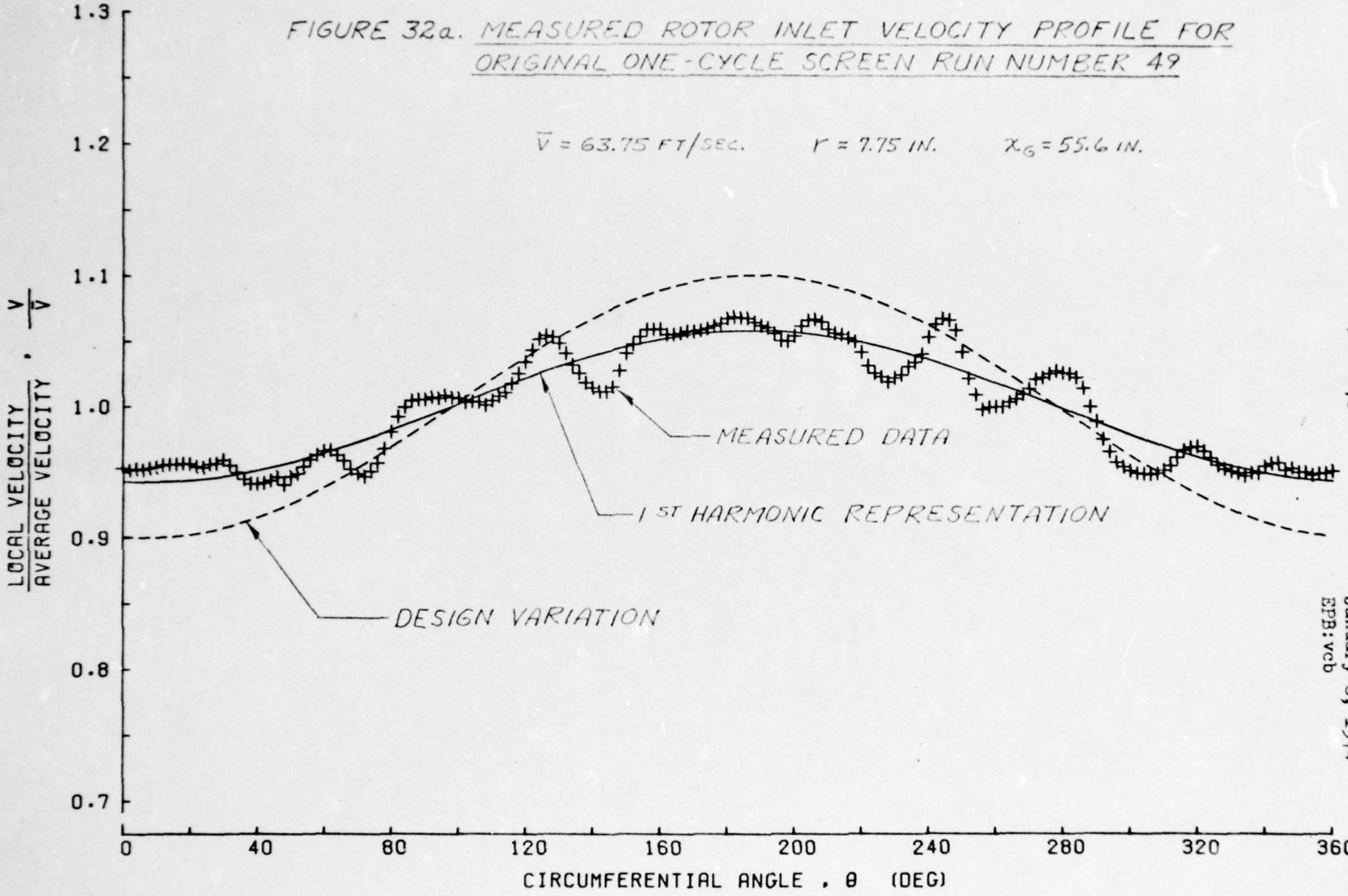

January 8, 1974
EPB:vcb

FIGURE 32b. FOURIER COEFFICIENT MAGNITUDE FOR ORIGINAL ONE-CYCLE SCREEN RUN NUMBER 49

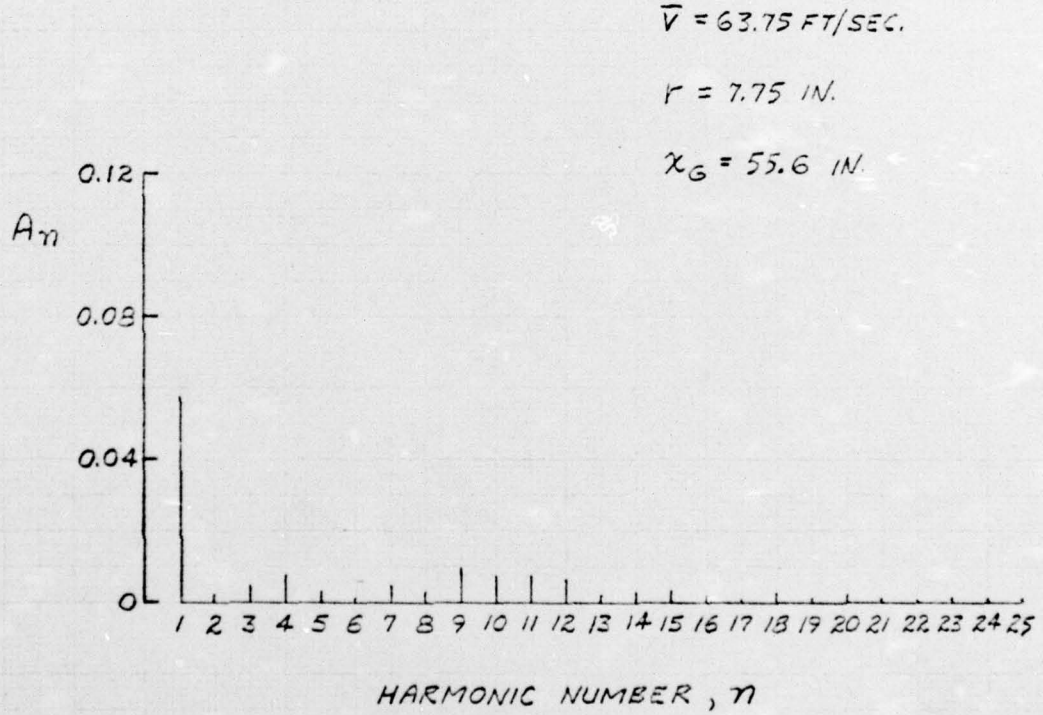

January 8, 1974
EPB:vcb

FIGURE 33. TWELVE-CYCLE SCREEN OVERLAY SEGMENT CHARACTERISTICS

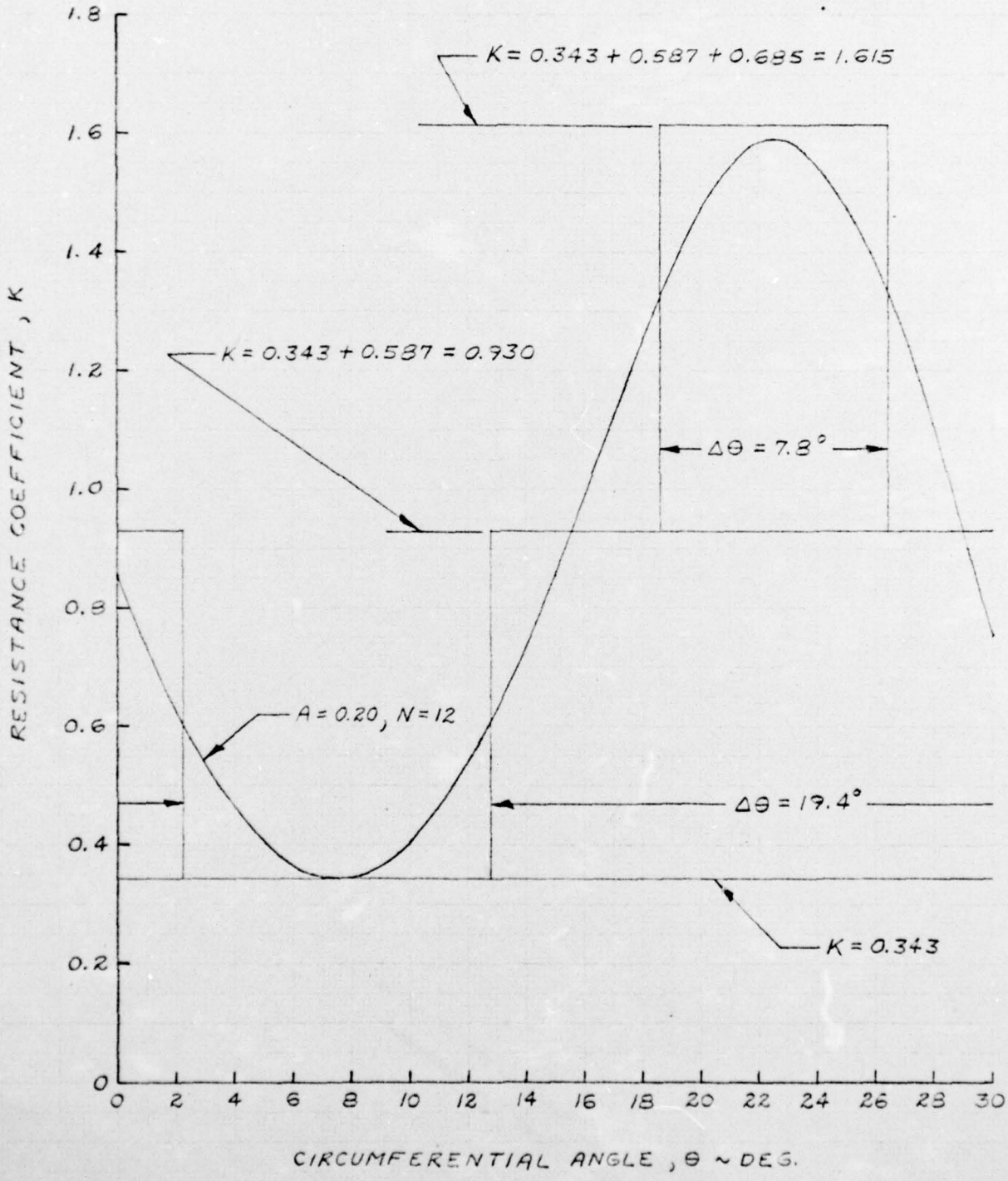

January 8, 1974
EPB:vcb

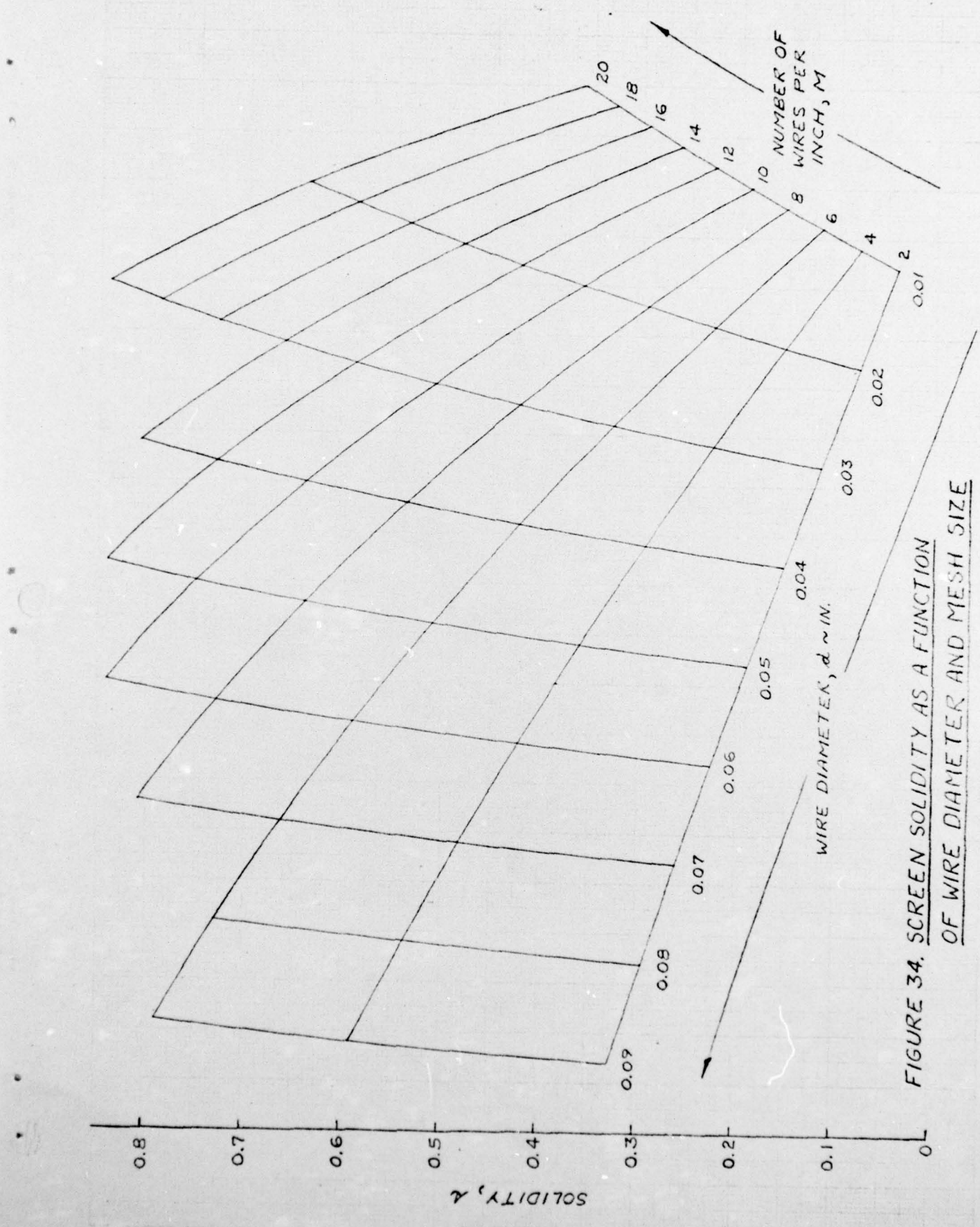

FIGURE 34. SCREEN SOLIDITY AS A FUNCTION OF WIRE DIAMETER AND MESH SIZE

January 8, 1974
EPB:vcb

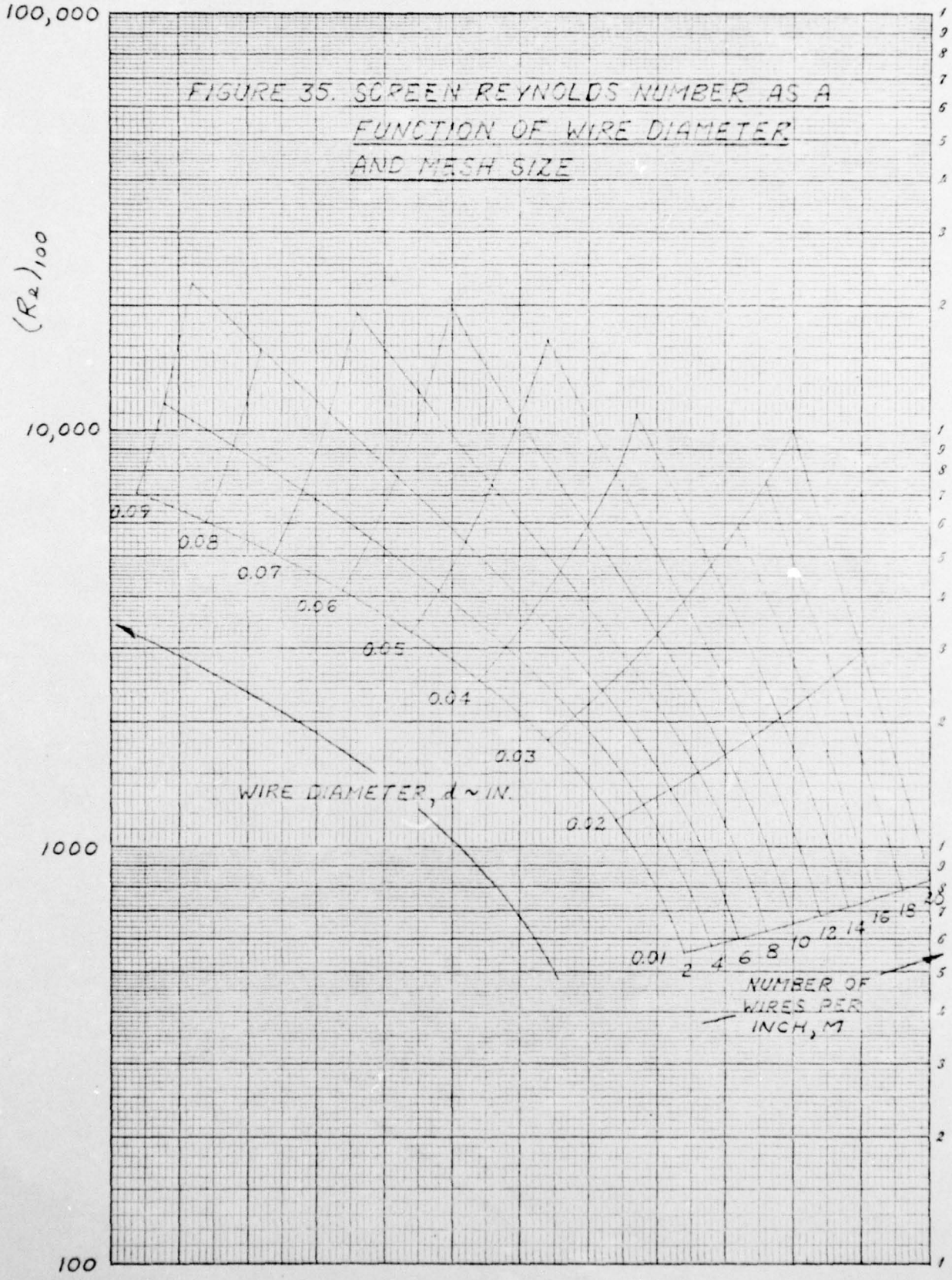

FIGURE 35. SCREEN REYNOLDS NUMBER AS A FUNCTION OF WIRE DIAMETER AND MESH SIZE

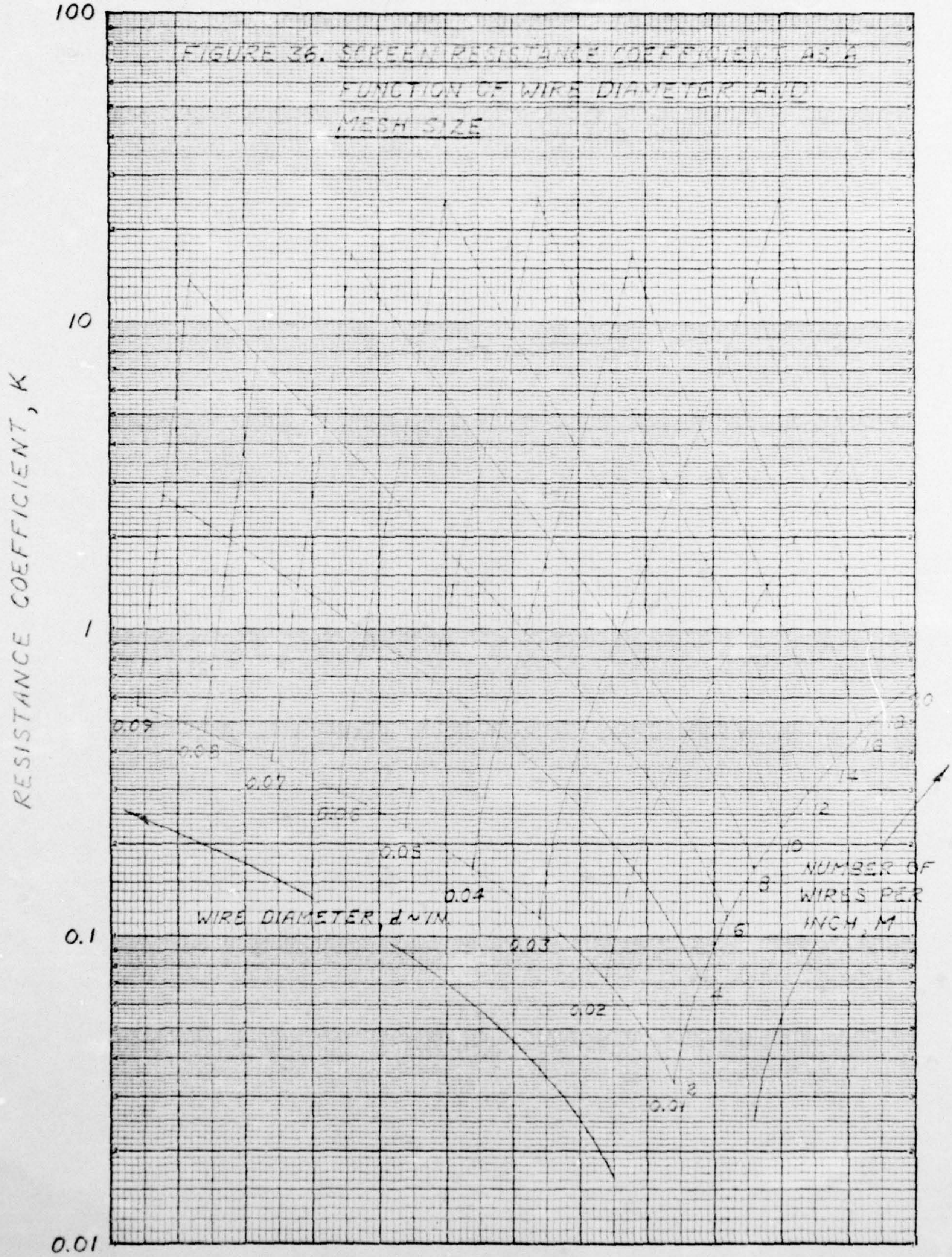

FIGURE 36. SCREEN RESISTANCE COEFFICIENT AS A FUNCTION OF WIRE DIAMETER AND MESH SIZE

Security Classification

DOCUMENT CONTROL DATA - R & D

(Security classification of title, body of abstract and indexing annotation must be entered when the overall report is classified)

1. ORIGINATING ACTIVITY (Corporate author)	2a. REPORT SECURITY CLASSIFICATION
Applied Research Laboratory State College, PA 16801	Unclassified
	2b. GROUP

3. REPORT TITLE

The Design and Evaluation of Screens to Provide Multi-Cycle 20% Amplitude Sinusoidal Variations in the AFRF Rotor Inlet Axial Velocity Component

4. DESCRIPTIVE NOTES (Type of report and inclusive dates)

ARL Technical Memorandum, January 8, 1974

5. AUTHOR(S) (First name, middle initial, last name)

Edgar P. Bruce

6. REPORT DATE	7a. TOTAL NO. OF PAGES	7b. NO. OF REFS
January 8, 1974	75	7

8a. CONTRACT OR GRANT NO.	9a. ORIGINATOR'S REPORT NUMBER(S)
N00017-73-C-1418	TM 74-16
b. PROJECT NO.	
c.	9b. OTHER REPORT NO(S) (Any other numbers that may be assigned this report)
d.	

10. DISTRIBUTION STATEMENT

Approved for public release. Distribution unlimited.
Per NAVORD - April 12, 1974

11. SUPPLEMENTARY NOTES	12. SPONSORING MILITARY ACTIVITY

13. ABSTRACT

This memorandum describes the results of an effort initiated in April 1973, whose objective was to provide new disturbance-producing screens for use in the Axial Flow Research Fan (AFRF). The performance of the screens originally developed for use in this facility was characterized by the generation of axial velocity profiles whose maximum and minimum values differed from the mean value by approximately 6% and by the presence of harmonics whose amplitude was on the order of 20% of the amplitude of the fundamental. The new screens were designed to produce axial velocity profiles with variations about the mean value of ± 20%, and care was exercised in the selection of materials and in the assembly of the screens in an attempt to reduce the amplitude of the other harmonics relative to the amplitude of the fundamental. Results are presented for one-, two-, four-, six-, nine-, and fifteen-cycle screens which show that the design objectives were met to within a few percent. In addition, appendices are included which: 1) describe the performance characteristics of the original one-cycle screen, 2) define a modified approach and the design characteristics adopted to permit fabrication of twelve- and fifteen-cycle screens, and 3) contain design charts that are useful in the selection of the screening materials required in a development program of this type.

DD FORM 1 NOV 65 1473 (PAGE 1) PLATE NO. 21056

S/N 0102-014-6600

Security Classification

14 KEY WORDS	LINK A		LINK B		LINK C	
	ROLE	WT	ROLE	WT	ROLE	WT
Incompressible Flow	8					
Screen Resistance	8					
Inlet Velocity Maldistribution	8					

DISTRIBUTION LIST FOR UNCLASSIFIED TM 74-16

Commander
Naval Ordnance Systems Command
Department of the Navy
Washington, D. C. 20360
Attn: Library
Code ORD-632
(Copies 1 and 2)

Naval Ordnance Systems Command
Attn: S. R. Marcus
Code ORD-03A
(Copy No. 3)

Naval Ordnance Systems Command
Attn: Code ORD-034B
(Copy No. 4)

Naval Ordnance Systems Command
Attn: T. E. Peirce
Code ORD-035B
(Copy No. 5)

Naval Ordnance Systems Command
Attn: PMO-402
(Copy No. 6)

Naval Ordnance Systems Command
Attn: G. R. Moltrup
Code ORD-54
(Copy No. 7)

Naval Ordnance Systems Command
Attn: O. Seidman
Code ORD-035
(Copy No. 8)

Naval Ordnance Systems Command
Attn: Chief Technical Analyst
Code ORD-05121
(Copy No. 9)

Naval Ordnance Systems Command
Attn: Chief Analyst, J. J. Bellaschi
Code ORD-03B
(Copy No. 10)

Commander
Naval Ship Systems Command
Department of the Navy
Washington, D. C. 20360
Attn: A. R. Paladino
DIV 037
(Copy No. 11)

Naval Ship Systems Command
Attn: R. Sherwood
DIV 037
(Copy No. 12)

Naval Ship Systems Command
Attn: Library
Code 2052
(Copy No. 13)

Commander
Naval Ship Engineering Center
Department of the Navy
Washington, D. C. 20360
Attn: W. L. Louis
Code 6136B
(Copy No. 14)

Naval Ship Engineering Center
Attn: R. M. Petros
Code 6148
(Copy No. 15)

Commanding Officer
Naval Underwater Systems Center
Newport, Rhode Island 02840
Attn: J. Brady
(Copy No. 16)

Naval Underwater Systems Center
Attn: J. D. Powers
(Copy No. 17)

Officer-in-Charge
Naval Undersea Center
San Diego Laboratory
San Diego, California 92132

Attn: J. W. Hoyt
(Copy No. 18)

Naval Undersea Center
Attn: J. Green
(Copy No. 19)

Commander
Naval Ordnance Laboratory
Silver Spring, Maryland 20910
Attn: S. A. Humphrey
Code 054
(Copy No. 20)

DISTRIBUTION LIST FOR UNCLASSIFIED TM 74-16 (continued)

Naval Ordnance Laboratory
Attn: Library
(Copy No. 21)

Commanding Officer & Director
Naval Ship Res. & Dev. Center
Department of the Navy
Bethesda, Maryland 20034
Attn: W. Morgan
Code 526
(Copy No. 22)

Naval Ship Res. & Dev. Center
Attn: M. Strasberg
Code 901
(Copy No. 23)

Naval Ship Res. & Dev. Center
Attn: J. B. Hadler
Code 520
(Copy No. 24)

Naval Ship Res. & Dev. Center
Attn: M. Sevik
Code 019
(Copy No. 25)

Dr. Hsuan Yeh, Director
Towne School of Civil & Mech. Engrg.
University of Pennsylvania
Room 113 Towne, 220 South 33rd Street
Philadelphia, Pennsylvania 19104
(Copy No. 26)

Dr. Frank Carta
Supervisor, Aeroelastics
United Aircraft Corporation
400 Main Street
East Hartford, Connecticut 06108
(Copy No. 27)

U. S. Naval Post Graduate School
Monterey, California
Attn: Library
(Copy No. 28)

Dr. A. J. Acosta
Professor of Mechanical Engineering
Div. of Engineering & Applied Science
California Institute of Technology
Pasadena, California 91109
(Copy No. 29)

Mr. M. J. Hartmann
NASA Lewis Research Center
21000 Brookpark Road
Cleveland, Ohio 44135
(Copy No. 30)

Dr. C. L. Morfey
Lecturer in Noise Research
University of Southampton
ISVR
Southampton, England
(Copy No. 31)

Professor J. H. Horlock
SRC Turbomachinery Laboratory
Madingley Road
Cambridge, England
(Copy No. 32)

Dr. J. D. Van Manen
Haagsteeg 2
Postbox 28
Wageningen, Netherlands
(Copy No. 33)

National Physical Laboratory
Teddington, Middlesex
Feltham, England
Attn: Dr. H. Ritter
(Copy No. 34)

Mr. A. Mitchell
Admiralty Research Laboratory
Teddington, Middlesex
England
(Copy No. 35)

Dr. P. Leehey
Department of Naval Architecture
Massachusetts Institute of Technology
77 Massachusetts Avenue
Cambridge, Massachusetts 02139
(Copy No. 36)

Dr. W. R. Sears
Cornell University
Graduate School of Aerospace Engineering
Grumman Hall
Ithaca, New York 14850
(Copy No. 37)

DISTRIBUTION LIST FOR UNCLASSIFIED TM 74-16 (continued)

Von-Karman Institute for Fluid Dynamics
Turbomachinery Laboratory
Rhode-Saint-Genese
Belgium
Attn: Library
(Copy No. 38)

Dr. C. Feiler
NASA Lewis Research Center
21000 Brookpark Road
Cleveland, Ohio
(Copy No. 39)

Dr. G. K. Serovy
Professor
Mechanical Engineering Department
Iowa State University
Ames, Iowa 50010
(Copy No. 40)

Wright Patterson Air Force Base
Dayton, Ohio 45433
Attn: Dr. William H. Heiser
(Copy No. 41)

Dr. Robert Goulard
Director
Project Squid
Purdue University
Jet Propulsion Center
W. Lafayette, Indiana 47907
(Copy No. 42)

Dr. R. C. Dean, Jr., President
Creare, Inc.
Box 226
Hanover, New Hampshire 03755
(Copy No. 43)

Professor H. Marsh
Durham University
Durham, England
(Copy No. 44)

Dr. L. H. Smith
Compressor & Fan Design Tech. Oper.
DTO, Mail Drop H-43
Cincinnati, Ohio 45215
(Copy No. 45)

SRC Turbomachinery Laboratory
Madingley Road
Cambridge
England
Attn: Library
(Copy No. 46)

Defense Documentation Center
5010 Duke Street
Cameron Station
Alexandria, Virginia 22314

Via: Commander (ORD 632)
Naval Ordnance Systems Command
Department of the Navy
Washington, D. C. 20360
(Copies 47 through 58)